Technische Universität München
Fakultät für Elektrotechnik und Informationstechnik
Lehrstuhl für Energiewirtschaft und Anwendungstechnik

Comparison of optimization methods for model predictive control: An application to a compressed air energy storage system

Dipl.-Ing. Dennis Atabay

Vollständiger Abdruck der von der Fakultät für Elektrotechnik und Informationstechnik der Technischen Universität München zur Erlangung des akademischen Grades eines

Doktor-Ingenieurs (Dr.-Ing.)

genehmigten Dissertation.

Vorsitzender:

Prof. Dr. rer. nat. Thomas Hamacher

Prüfer der Dissertation:

1. Prof. Dr.-Ing. Ulrich Wagner
2. Prof. Dr.-Ing. Gunther Reinhart

Die Dissertation wurde am 27.07.2017 bei der Technischen Universität München eingereicht und durch die Fakultät für Elektrotechnik und Informationstechnik am 13.04.2018 angenommen.

Für Motte

Abstract

In energy systems with a high share of renewable energy sources, electrical energy storage plays an important role in balancing energy production and demand. The optimal operation times of a storage can depend on locally available energy production (e.g. distributed solar battery storage) or external signals such as a time-sensitive electricity price (e.g. pumped hydroelectric energy storage). Model Predictive Control (MPC) is a modern control strategy that allows one to consider forecasts of future parameters, such as power production or electricity prices, and therefore has been widely applied to energy systems and storages in the last years. A model of the energy storage system is used to define and solve an optimization problem and find the optimal charging and discharging times. Since MPC is not a unique technique but rather a set of methodologies, different models and optimization methods can be used to solve the optimal control problem.

In this thesis, a compressed air energy storage system is used to compare different optimization methods for MPC. Based on experimental investigations, the system parameters, such as the electrical round-trip efficiency, are calculated. A linear, a mixed-integer-linear and a nonlinear model of the system are developed and used for MPC. To compare the different optimization methods, MPC is used to minimize operational costs covering a given 24-hour air demand using a time-sensitive electricity price as an incentive. The experiments are performed for several scenarios with variations in air demand, electricity price, optimization timestep size and forecast quality.

The results indicate that dynamic programming demonstrates the most cost savings throughout all performed experiments. For this application, it shows better results than the other two nonlinear optimization methods used in this thesis, genetic algorithms and mixed-integer nonlinear programming. Due to its detailed model, dynamic programming also clearly outperforms the linear programming method. The results using mixed-integer linear programming are only slightly different than with dynamic programming and even better in some specific cases.

Zusammenfassung

In Energiesystemen mit einem hohen Anteil fluktuierender erneuerbarer Energien spielen Energiespeicher eine wichtige Rolle zum Ausgleich von Angebot und Nachfrage. Der optimale Einsatz von einzelnen Speichern kann dabei von vorhandenen lokalen Erzeugungsprofilen und Lasten (z.B. dezentrale PV Speicher) sowie variablen Strompreissignalen (z.B. Pumpspeicher) abhängen. Prädiktive Regelstrategien erlauben es zukünftige Ereignisse, wie die Vorhersage von Verbrauch und Erzeugung oder Strompreisverläufe, mit einzubeziehen und sind somit für die Regelung von Energiespeichern prädestiniert. Die modellprädiktive Regelung (Model Predictive Control, MPC) verwendet hierbei ein Modell zur Vorhersage des zukünftigen Verhaltens des Systems. Durch Lösen eines Optimierungsproblems basierend auf diesem Modell, können die zu wählenden Lade- und Entladezeitpunkte für den Speicher für die nächsten Minuten, Stunden oder Tage ermittelt werden. MPC beschreibt keinen exakten Algorithmus, sondern ein generelles Verfahren zur prädiktiven Regelung von Systemen. Dabei wurden im Rahmen einer modellprädiktiven Regelung von Energiespeichern bereits eine Vielzahl verschiedener Optimierungsmethoden angewendet.

Diese Arbeit vergleicht verschiedene Optimierungsmethoden zur modellprädiktiven Regelung am Anwendungsbeispiel eines Druckluftspeichers. Auf Basis von messtechnischen Untersuchungen und der Bestimmung von verschiedenen Systemparametern, wie dem elektrischen Speichernutzungsgrad, wird ein lineares, ein gemischt-ganzzahlig lineares und ein nichtlineares Modell der Anlage entwickelt. Mit Hilfe dieser Modelle wird eine modellprädiktive Regelung des Speichers für einen Zeitraum von 24 Stunden durchgeführt. Ziel ist dabei die Deckung eines vorgegebenen Bedarfs mit minimalen Stromkosten. Für die drei Methoden werden jeweils mehrere Szenarien mit verschiedenen Verbrauchs- und Strompreisprofilen betrachtet. Zudem wird auch der Einfluss der Optimierungsschrittweite sowie der Genauigkeit der Verbrauchsprognose auf die Ergebnisse untersucht.

Die Ergebnisse zeigen, dass bei Betrachtung aller durchgeführten Experimente mit Hilfe der dynamischen Programmierung die größten Kosteneinsparungen erreicht werden können. Für den untersuchten Anwendungsfall zeigt sich, dass die dynamische Programmierung besser geeignet ist als die beiden anderen untersuchten nichtlinearen Optimierungsmethoden, der genetische Algorithmus und die gemischt-ganzzahlige nichtlineare Programmierung. Aufgrund der genaueren Modellierung des System können auch im Vergleich zur linearen Programmierung deutlich bessere Ergebnisse erzielt werden. Die Kosteneinsparungen, die mit Hilfe der gemischt-ganzzahligen linearen Programmierung erreicht werden können, sind im Vergleich zur dynamischen Programmierung nur geringfügig schlechter. Für bestimmte Szenarien werden hier sogar bessere Ergebnisse erzielt.

Danksagung

Die vorliegende Arbeit entstand im Rahmen meiner Tätigkeit als wissenschaftlicher Mitarbeiter am Lehrstuhl für Energiewirtschaft und Anwendungstechnik der Technischen Universität München. Ich habe diese Zeit sehr genossen und durfte viele Erfahrungen sammeln. Daher möchte ich mich an dieser Stelle bei allen bedanken, die mich in den letzten Jahren während meiner Promotion begleitet haben.

Mein Dank gilt Herrn Prof. Dr.-Ing. Ulrich Wagner für das jederzeit sehr angenehme Betreuungsverhältnis und die große Freiheit in der Umsetzung meiner eigenen Ideen. Bei Herrn Prof. Dr.-Ing. Gunther Reinhart möchte ich mich für die Übernahme des Korreferats bedanken. Mein besonderer Dank gilt Herrn Prof. Dr. rer. nat. Thomas Hamacher für die lehrreiche gemeinsame Zeit am Lehrstuhl sowie für die Übernahme des Prüfungsvorsitzes.

Ich bedanke mich bei allen Kollegen, mit denen ich während meiner Zeit an der TUM zusammenarbeiten durfte. Vielen Dank für die große Unterstützung in allen Bereichen, die zahlreichen Diskussionen und Gespräche sowie die sehr angenehme Atmosphäre am Lehrstuhl.

Mein besonderer Dank gilt meiner Familie und meinen Freunden. Ich danke meinen Eltern für die große Unterstützung in allen Lebenssituationen, für die Möglichkeiten die sie mir dadurch in meinem Leben eröffnet haben und das in mich gesetzte Vertrauen. Ganz besonders danke ich meiner Frau, Verena Atabay, für ihr großes Verständnis und ihre Unterstützung während des gesamten Zeitraums meiner Arbeit.

Hamburg im Mai 2018

Dennis Atabay

Contents

Chapter 1

Introduction

Reducing the worldwide greenhouse gas emissions in order to mitigate global warming is one of the biggest challenges of today's generation. To achieve its goal to reduce CO_2 emissions by 80 % compared to 1990 [14], one main part of Germany's concept is to increase the share of renewable energies in the electricity sector to 80 % by 2050 [12].

In 2015, wind turbines and photovoltaic (PV) systems provided more than half of the renewable electric energy in Germany [15]. Subsidized by the government, both have already shown tremendous growth in the last years. Because of the fluctuation of wind and solar generation, which cannot be accurately predicted, the need for flexibility in the power system increases with their installation. Energy storages are one approach to provide this flexibility.

There are different concepts and subsidy programs to integrate energy storages in Germany's energy system. Large-scale electric energy storages that are directly connected to the grid, such as pumped hydro storages, are exempt from demand charges and EEG surcharges [12]. In May 2016, a subsidy program for small-scale battery storages combined with a PV system, which are mainly installed in the residential sector, was launched [17]. Also, for heat storages in combination with a combined heat and power (CHP) unit [13] or a heat pump [16], subsidy programs were initiated. Heat storages can provide flexibility to the electric power sector by decoupling electricity production (CHP) or consumption (heat pump) and heat supply.

The optimal operation to maximize revenues or minimize costs of such storage (and generation) systems over a certain time horizon can depend on the given demand that has to be covered, the availability of a variable energy resource and the electricity price curve. Model Predictive Control (MPC) is an advanced method of system control that allows one to consider these future parameters when calculating the next control action. MPC has been widely used for the control of energy systems including storages in many recent publications.

1.1 Introduction to Model Predictive Control

Model Predictive Control (MPC), also known as model-based predictive control or receding-horizon control, is a modern control strategy for the operation of systems. While this section provides a short introduction to MPC, a detailed overview of the topic and its applications can be found in the books [89, 19, 87, 36, 55] and survey papers [72, 67, 26].

The general idea of MPC is to use an internal model of a system to predict its future behavior over a given time horizon. The output of the system for each time sample $t = 1...N$ in this horizon is calculated based on previous system inputs, outputs, states, and the proposed optimal future control actions. This control sequence is calculated by solving an optimization problem taking into account the objective function (e.g. minimizing costs) as well as constraints for the system operation (e.g. covering the demand). At each instant, the first control signal of the sequence is applied to the system and the new outputs and states are measured. Then the horizon is displaced one timestep towards the future and the optimization problem is solved again using the new information (receding strategy). The general structure of MPC is shown in Figure 1.1 [19].

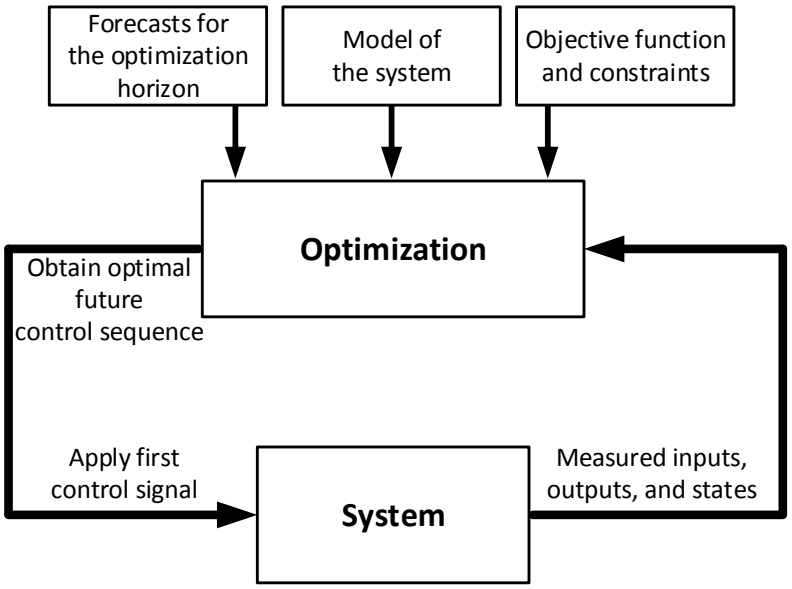

Figure 1.1: General structure of MPC

In contrast to classical control methods, such as PID controllers, in which the next control action is calculated only based on previous measured inputs and outputs, MPC additionally allows one to consider predicted or already known future parameters. Because of its systematic account for constraints and its feed-forward design, MPC shows better performance than non-predictive control methods [89, p. 5-6]. Therefore, it has become the most widely accepted modern control strategy [55, p. 2] and the MPC technology can be found in a wide variety of industrial application areas [84].

1.2 Motivation

Model Predictive Control is a control strategy in which an optimal operation problem is repeatedly solved over a rolling horizon in real time with updated information. Thus, MPC is not a unique technique, but rather a set of different methodologies that can be applied to control a system [19, p. 4]. Thereby, the model, which describes the dynamic behavior of the system, is the cornerstone of MPC. The chosen model defines not only the accuracy of the prediction of the system behavior, but also the optimization method that can be used to calculate the control sequence. While linear or quadratic (convex) models are limited in their accuracy of predicting the system outputs, fast and reliable solvers are available to solve the optimization problem. In contrast, nonlinear models are able to predict the system outputs more accurately, but the implied optimization is computationally more intensive and, moreover, the convergence to a global optimum cannot be assured [72].

In the last years, several reviews of optimization methods for the (model predictive) control of energy systems containing storages, such as electric power systems [5, 34, 102, 4, 41], microgrids [77, 31, 69, 37], tri-generation systems [99], heating, ventilation, and air conditioning (HVAC) systems [1], and thermal energy storages [79] have been published. The commonly used optimization methods in these studies are linear programming (LP), mixed-integer linear programming (MILP), mixed-integer nonlinear programming (MINLP), dynamic programming (DP) and evolutionary computation algorithms[1].

All of these methods have already been applied to energy storage systems for experimental investigations. So far, however, there are no studies comparing the performance of the model predictive control of an energy storage using different optimization methods.

1.3 Objective and outline of this thesis

The objective of this thesis is to evaluate the influence of the model's accuracy versus the computational effort and reliability of the optimization problem's solution for the model predictive control of an energy storage. Therefore, different optimization methods for the MPC of an energy storage system are evaluated. They are applied to a compressed air energy storage (CAES) system to compare their performance under different scenarios.

In **chapter 2** the optimization methods used in this thesis are introduced. For each method an overview of publications where they were used for the model predictive control of energy storage systems is given.

Chapter 3 describes the design and operation of the compressed air energy storage (CAES) system. As for typical compressed air systems in the industry, the CAES system consists of compressors, air treatment devices, and an air receiver tank. An additional booster is used to raise the pressure of the compressed air delivered by the compressors and store it in a high pressure storage tank. In this way, the electricity consumption and air supply can be decoupled. Based on experimental results a method for calculating the electrical round-trip efficiency of

[1] There exist various different evolutionary computation algorithms that have been used for optimal control of energy system, such as particle swarm optimization or ant colony optimization. In this thesis the genetic algorithm (GA) is applied because it is the most commonly used method.

the storage system is presented. Additionally, the specific storage costs of the CAES system are calculated and compared to battery storage systems.

In **chapter 4** the mathematical descriptions of the CAES system models for each optimization method used in this thesis are given. Simulation results of the models are used to validate and compare them to measured data.

In **chapter 5** these optimization models are used for the model predictive control of the CAES system, with the objective to cover a given air demand over 24 hours with minimal costs. The experiments are performed with different air demand and electricity price scenarios. Additionally, the influences of the optimization timestep size and the quality of the air demand forecast are investigated.

Chapter 6 concludes the thesis.

Chapter 2

Optimization methods for Model Predictive Control

In this chapter the optimization methods used in this thesis are introduced. For each method a literature overview of their application to Model Predictive Control (MPC) of energy systems including storage is given.

2.1 Linear programming

Linear programming (LP) problems are a subclass of convex optimization problems, where the objective function and all constraints are linear. As for all convex optimization problems, a local minimum of the objective functions is also a global minimum. In the last decades several effective methods for solving linear programming (LP) problems where developed, such as the simplex method and the interior point method. They can easily solve very big problems with hundreds of variables and thousands of constraints. The main drawback of LP is that the behavior of many real-world systems can only be approximated, since all variables have to be real-numbered and all constraints and the objective function have to be linear. A general linear program, where the vector x is the optimization variable and the matrices A, G and the vectors b, c, d, h are problem parameters that specify the objective and constraint functions, can be stated as follows. A detailed insight into the theory and practice of linear programming is given in [8] and [86].

$$\begin{aligned} \text{minimize} \quad & c^T x + d \\ \text{subject to} \quad & Gx \leq h \\ & Ax = b \end{aligned} \tag{2.1}$$

In the last years various articles using LP for MPC or optimal control of energy systems including storages have been published. Xie and Ilic [103] used LP for model predictive control of a small electric energy system containing intermittent renewable resources. An application of LP for optimal scheduling of a CHP system with a battery unit and a thermal energy storage unit is presented by Majic et al. [63]. Ma et al. [61] propose a MPC technique using LP to reduce costs for the operation of a HVAC system. Further examples can be found in [85, 20, 60, 78].

2.2 Mixed-integer linear programming

Mixed-integer linear programming (MILP) is a special case of the more general mixed-integer programming. In MILP the objective function and constraints are linear. Some of the decision variables are integers whereas others are continuous variables. Using integer or binary variables allow a more detailed representation of energy systems than with LP by considering e.g. start-up costs and part-load performance. State-of-the-art MILP solvers use a combination of algorithms, such as branch-and-bound, cutting plane and heuristics. Although, they are able to solve large problems with regard to the number of variables and constraints, the computational effort compared to LP rises significantly due to the addition of integers to the problem. An imporant advantage of these algorithms is that they provide an assessment of the current solution. The time for solving a MILP depends upon the specific structure of the problem and is thus hard to be estimated in general terms. Equation 2.2 states the general formulation of a MILP with the integer variable vector y and the real variable vector x. The matrices G, A, M, N and the vectors c, w, d, h, b are problem parameters that specify the objective and constraint functions. Detailed mathematical foundations of integer programming are presented in the textbook of Conforti [22].

$$\begin{aligned} \text{minimize} \quad & c^T x + w^T y + d \\ \text{subject to} \quad & Gx + My \leq h \\ & Ax + Ny = b \\ & x \in \mathbb{R}, y \in \mathbb{Z} \end{aligned} \tag{2.2}$$

Recently, MILP models have been used widely for the optimal control of energy systems containing energy storages. They were used for the model predictive control of microgrids including battery storage systems by Parisio et al. [81, 82], Palma-Behnke et al. [80], Bracco et al. [11], and Kriett et al. [56]. An application of MPC using a MILP model for active load management in a distributed power system containing a battery storage is presented by Zong et al. [107]. Zhang et al. used MILP for model predictive control of industrial loads and energy storage for demand response [106]. Stadler et al. used a MILP model for MPC of an energy system in a building including heat and electric storages [95]. A MILP approach for model predictive control of a residential HVAC system with a thermal energy storage is presented by Fiorentini et al. [28, 29]. Further applications of MPC to energy systems with energy storages using MILP can be found in [70, 68, 10, 65, 66, 101]

2.3 Mixed-integer nonlinear programming

Mixed-integer nonlinear programming (MINLP) covers a wide range of mathematical optimization problems. In this thesis, MINLP refers to exact methods for solving problems where the objective and constraint functions include non-convexities and the decision variables are integers and continuous. There are some exact approaches to solve non-convex MINLP problems, such as spatial branch-and-bound, branch-and-reduce and α-branch-and-bound. Although there are software packages available that can solve non-convex MINLPs to proven optimality, relative small problems can still cause existing methods to run into serious difficulties.

Compared to MILP, solving MINLP problems requires a much higher computational effort and are much more time consuming. The survey paper by Burer and Letchford gives a good overview of non-convex MINLP [18]. The general formulation of a MINLP is given in equation 2.3, where the objective function $f(x, y)$ is to be minimized finding the optimal values of the integer variable vector y and the real variable vector x. The constraints are defined by a number of inequality functions c_i and equality functions c_j. Here, I and E are two disjoint sets of integers defining the number of constraints.

$$\begin{aligned} \text{minimize} \quad & f(x, y) \\ \text{subject to} \quad & c_i(x, y) \leq 0 \qquad \forall i \in I \\ & c_j(x, y) = 0 \qquad \forall j \in E \\ & x \in \mathbb{R}, y \in \mathbb{Z} \end{aligned} \tag{2.3}$$

Compared to other optimization methods, mixed-integer nonlinear programming is rarely used for MPC of energy systems. Sachs et al. used MINLP for model predictive control of island energy systems including a battery storage [90]. A MINLP model for MPC of an energy storage system in the smart grid environment is used by Nojavan et al. [76]. Shirazi et al. [92] used a MINLP model for optimal scheduling of residential HVAC system including a battery system. Ma et al. [62, 105] used a nonlinear programming for model predictive control of a thermal energy storage in building cooling systems.

2.4 Genetic algorithm

A genetic algorithm (GA) is a meta-heuristic optimization method inspired by biological evolution and the most popular technique within the more general class of evolutionary algorithms. The basic idea of GA is to create a population of candidate solutions (individuals) for the optimization problem. Each candidate solution is evaluated based on the value of the objective function (fitness). The best candidates are selected and used to create a new generation by crossover (creating a new child candidate by combining two or more parent candidates) and mutation (small random changes to an individual to explore the whole search space). The new generation population is then again evaluated and the loop continues until the last population meets a certain stopping criteria. GA can be applied to almost every optimization problem, such as non-convex, discrete, mixed-integer and black-box problems and only needs rough information of the objective function. Major disadvantages of GA are that solving big problems requires tremendously high time and that it gives no information about the quality of a solution. A detailed introduction to genetic algorithms is given in [93].

Because of its easy implementation, the genetic algorithm is often used for optimal control of energy systems. Jungwirth applied MPC with a GA to control heating and cooling of buildings, using the thermal building mass as heat storage [42]. Lipp used a GA for model predictive control of a micro CHP unit with a thermal energy storage [43]. Lujano-Rojas et al. used GA for optimizing the daily operation of battery energy storage systems under real-time pricing schemes. A MPC approach using GA for the operation of an energy smart home lab including an energy storage system is presented by Kochanneck et al. [54]. Further examples of using genetic algorithm for MPC can be found in [3, 64, 73]

2.5 Dynamic programming

Dynamic programming (DP) is an optimization technique introduced by Richard Bellman [6], that can be applied to multistage decision problems requiring a sequence of interrelated decisions. It is based on Bellman's principle of optimality which states that a sub-policy of an optimal policy for a given problem must itself be an optimal policy of the sub-problem. For a given discrete-time dynamic system

$$x_{t+1} = f_t(x_t, u_t), \qquad t = 0, 1, ..., N-1 \tag{2.4}$$

where x_t represents the state of the system and u_t the control (decision) at time period t, DP is able to find the optimal policy $\pi^* = \{u_0^{\pi^*}, u_1^{\pi^*}, ..., u_{N-1}^{\pi^*}\}$ that minimizes the total costs given by

$$J_\pi(x_0) = g_N(x_N) + \sum_{t=0}^{N-1} g_t(x_t, u_t^\pi) \tag{2.5}$$

for the given starting state x_0 and the given cost functions g_t.
To calculate the optimal policy π^*, the DP algorithm proceeds backward[1] in time (from $t = N-1$ to $t = 0$) and calculates the optimal decision u_t^* to minimize the current (g_t) and following (J_{t+1}) costs for each possible state x_t.

$$J_N(x_N) = g_N(x_N) \tag{2.6}$$

$$J_t(x_t) = \min_{u_t} g_t(x_t, u_t) + J_{t+1}\left(f_t(x_t, u_t)\right) \tag{2.7}$$

The optimal cost $J_\pi^*(x_0)$ and decisions π^* are then given for every initial state x_0 after the last step of this algorithm.
DP can deal with every problem given in this form, including non-convex, non-continuous, non-differentiable and black-box functions and is able to find the global optimal solution of a problem. If the state space is not already a finite set, it has to be discretized, which may lead to suboptimal solutions. The computational requirements are depending on the number of possible values of x and the number of possible decisions u as well as on the number of time periods t. Therefore, DP can become quite time-consuming for very big problems (known as Bellman's curse of dimensionality). A detailed insight into the theory and practice of dynamic programming is given by Bertsekas in [7].
DP has been widely used for model predictive and optimal control of energy storage systems. Henze et al. used DP for MPC of a building thermal storage [38, 35]. A DP approach for scheduling of residential energy storage systems under dynamic pricing was presented by Yoon et al. [104] and Wang et al. [100]. Zhang et al. [59] and Nguyen et al. [75] used DP for optimal control of a battery combined with a wind power system. Further applications of dynamic programming for optimal control of energy storages are presented in [21, 88, 58, 27, 30]

[1] A forward in time implementation of the DP algorithm is also possible

2.6 Overview of the optimization methods used in this thesis

Table 2.1 summarizes the optimization methods used for MPC in this thesis with their advantages and disadvantages. Linear programming is very limited in the available expression to model the system, but is able to solve the optimization problem fast and reliable. With mixed-integer linear programming the accuracy of the model, as well as the computational effort of solving the problem, increases. The nonlinear optimization models, MINLP, GA and DP, are able to represent complex interactions of the system very detailed, but require a very high computational effort to solve the problem.

Table 2.1: Optimization methods used in this thesis with their advantages and disadvantages (based on [57, 25, 86])

Method	**Advantages**	**Disadvantages**
Linear programming (LP)	– Scales well to big problems – Globally optimal solution attainable	– Very limited expressions available – Complex interactions difficult or impossible to represent
Mixed-integer linear programming (MILP)	– Can scale well to big problems – Complex interactions representable – Quality of solutions can be assessed	– Bad worst-case complexity – Global optimum often not attainable
Mixed-integer nonlinear programming (MINLP)	– Complex interactions fully representable – High freedom of expression	– Scales horribly to big problems
Dynamic programming (DP)	– Full freedom of expression (can also be used with "black box" models) – Globally optimal solution of the discretized system attainable	– Scales horribly to big problems (Bellman's "curse of dimensionality") – Continuous variables must be discretized which may lead to a suboptimal solution
Genetic algorithm (GA)	– Full freedom of expression (can also be used with "black box" models)	– Scales horribly to big problems – Quality of solutions impossible to assess

Chapter 3

Compressed air energy storage system

To evaluate the different methods of control optimization, they are applied to a real energy storage test system. Therefore, a small-scale compressed air energy storage system is used. It represents a typical compressed air system in the industry that is used to cover a given air demand. An additional booster allows one to store compressed air in high-pressure storage tanks. The air from these tanks can then be used to cover the air demand without the compressors running. Thereby, the electricity consumption of the system can be influenced and adapted to a given incentive.

In this chapter at first the design and the operation modes of the compressed air energy storage (CAES) system are introduced. Then the results for different experimental investigations are shown. These results are used to calculated the specific costs of the CAES system and compare them with battery storage systems.

3.1 Compressed air constants and definitions

Pressure is defined as force per unit area. There are three different categories for pressure measurement. The *absolute pressure* p_a is zero referenced to a complete vacuum, while the *gauge pressure* p_g is defined as the pressure referenced against the atmospheric pressure. The *differential pressure* p_d measures the difference between two unknown pressures [9, p. 145].

Although the SI unit of pressure is Pascal (Pa), in the compressed air industry the pressure is usually depicted in bar gauge pressure. The pressure sensors used in the compressed air system also have bar gauge pressure as output. In this thesis p_a indicates the absolute pressure and is given in $\mathrm{Pa_a}$ or $\mathrm{bar_a}$, while p_g given in the units $\mathrm{Pa_g}$ or $\mathrm{bar_g}$ shall indicate the gauge pressure.

Compressed air flow, like the free air delivery (FAD) of the compressors or the compressed air demand represent the mass flow $\dot{m}$ of the air with the SI unit $\frac{\mathrm{kg}}{\mathrm{s}}$. In the compressed air industry air flow is usually given as normal (or standard) volumetric flow $\dot{V}_n$ with the unit standard (or normal) cubic meters per minute ($\frac{\mathrm{m^3_n}}{\mathrm{min}}$). This represents a volumetric flow of the air converted to standardized conditions of temperature T_n and pressure p_n, often referred as

normal temperature and pressure or standard temperature and pressure. Using the ideal gas equation of state (3.2) [71, p.127], where p is the pressure, V the Volume, m the mass, R_s the specific gas constant and T the temperature of the gas, the mass flow $\dot{m}$ can be converted to the normal volumetric flow $\dot{V}_n$ (and vice versa) given the standard conditions p_n and T_n.

$$p \cdot V = m \cdot R_s \cdot T \tag{3.1}$$

$$\dot{V}_n = \dot{m} \cdot \frac{R_s \cdot T_n}{p_n} \tag{3.2}$$

There are a variety of normal or standard conditions for temperature and pressure established by different organizations. In this thesis these reference values are defined to $p_n = 1.0\,\mathrm{bar_a}$ and $T_n = 273.15\,\mathrm{K}$ as per ISO 8778:2003. The specific gas constant of air is defined as $R_{s,air} = 287.0\,\frac{\mathrm{J}}{\mathrm{kg \cdot K}}$ [71, p.123]. All constants used for compressed air calculations are shown in table 3.1

Table 3.1: Constants used for compressed air calculations

Symbol	Value	Unit	Description
p_n	1.0	$\mathrm{bar_a}$	Normal condition for pressure
T_n	273.15	K	Normal condition for temperature
$R_{s,air}$	287.0	$\frac{\mathrm{J}}{\mathrm{kg \cdot K}}$	Specific gas constant of air

3.2 Design of the compressed air energy storage system

The compressed air energy storage system is located at the Technical University of Munich and represents a typical compressed air system in the industry with an additional high-pressure compressed air storage. Figure 3.1 shows the structure of the test system. The compressed air is produced by three rotary screw compressors with a total maximum free air delivery (FAD) of 2.53 $\frac{\mathrm{m^3_n}}{\mathrm{min}}$ and a maximum output pressure of 11 bar. The air treatment consists of two dryers and two filters. The air receiver tank, with a volume of $2\,\mathrm{m^3}$, is used to reduce compressor cycling. To simulate an arbitrary compressed air demand, a control valve is used, through which the air is released into the ambient. A reciprocating compressor (booster) that is able to boost the compressed air from the rotary screw compressors up to a pressure of 38 bar allows one to store the air in two high-pressure storage tanks with a volume of $2\,\mathrm{m^3}$, each. The air from these tanks can be fed back into the system by opening the outlet valve. To prevent a pressure increase in the low-pressure part of the system when the the outlet valve is open, a pressure regulator is used.

The electric power consumption of the compressors and the booster as well as the temperature and the gauge pressure at three different positions is measured and stored with a time resolution of one second. Table 3.2 provides an overview of all measured and calculated values of the CAES system.

The technical data of the compressors are shown in table 3.3, information about the other components can be found in appendix A.

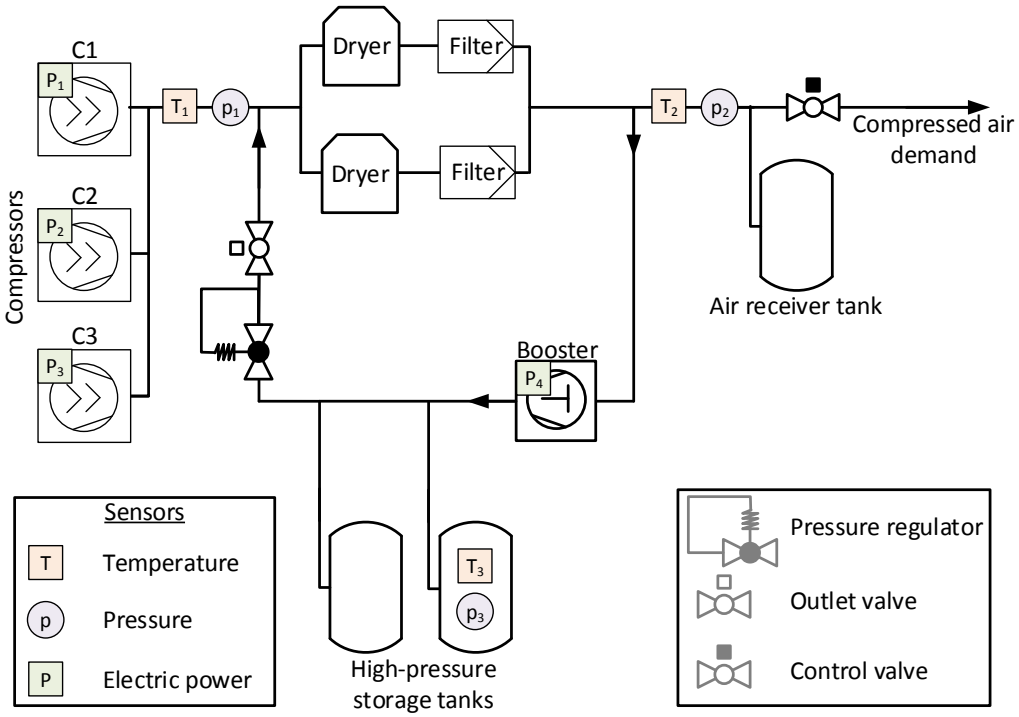

Figure 3.1: Schematic representation of the compressed air energy storage test system

Table 3.2: Measured and calculated values of the CAES system

Symbol	Unit	Description
p_1	bar_g	Gauge pressure at compressors output
$p_2 = p_{sys}$	bar_g	System gauge pressure (after dryer and filter)
$p_3 = p_{sto}$	bar_g	Gauge pressure in high-pressure storage
T_1	K	Temperature at compressors output
T_2	K	Temperature after dryer and filter
T_3	K	Temperature in high-pressure storage
P_1	kW	Electric power consumption of compressor C1
P_2	kW	Electric power consumption of compressor C2
P_3	kW	Electric power consumption of compressor C3
$P_4 = P_{bo}$	kW	Electric power consumption of booster
P_{co}	kW	Sum of electric power consumption of compressors C1, C2 and C3
P_{tot}	kW	Sum of electric power consumption of compressors and booster
E_{tot}	kWh	Sum of electric energy consumption of compressors and booster

Table 3.3: Technical specifications of the compressors from manufacturer KAESER

Compressor	Model	FAD or flow rate ($\frac{m^3_n}{min}$)	Max. output pressure (bar_g)	Data sheet
C1	SM12 SFC 10 bar	0.34 - 1.04	11	[51]
C2	SM12 10 bar	1.01	11	[51]
C3	SX6 10 bar	0.48	11	[52]
Booster	N153-g 10 bar	0.89	40	[48]

3.3 Operation of the compressed air energy storage system

As shown in figure 3.2, the compressed air energy storage system is controlled by two different components. The Sigma Air Manager (SAM) from KAESER Compressors controls the three screw compressors, such that the system pressure p_{sys} stays above the setpoint of the system pressure $\hat{p}_{sys}$ within a given pressure range $\Delta\hat{p}_{sys}$ ($\hat{p}_{sys} \leq p_{sys} \leq \hat{p}_{sys} + \Delta\hat{p}_{sys}$). It decides which compressors are running to cover the actual air demand. The control software implemented in LabVIEW directly controls the outlet valve, the control valve and the booster. Additionally, it communicates with the SAM and is able to specify the setpoint of the system pressure $\hat{p}_{sys}$ and to turn off all compressors.

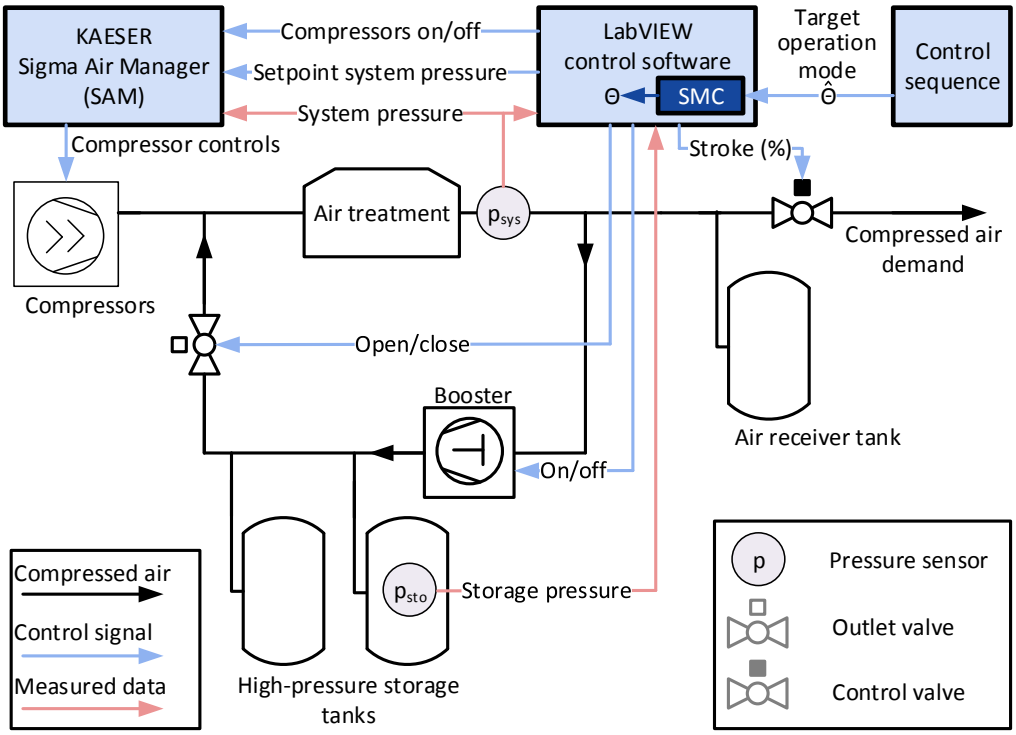

Figure 3.2: Control of the compressed air energy storage test system

The CAES system has three operation modes: *normal*, *charge* and *discharge*. The target operation mode of the system $\hat{\Theta}$ is given by a control sequence that contains control signals for each timestep. A superior mode controller (SMC) implemented in the LabVIEW control software intervenes if the target operation mode $\hat{\Theta}$ is invalid (e.g. when the storage is already full and should be charged) and assigns a valid concrete operation mode Θ.

Figure 3.3 shows an example of the system behavior of all three operation modes, based on the time curves of measured system pressure p_{sys} and storage pressure p_{sto} as well as power consumption of the compressors P_{co}, of the booster P_{bo} and the total power consumption P_{tot}. Additionally, the target operation mode $\hat{\Theta}$ applied by the control schedule and the concrete operation mode Θ assigned by the superior mode controller are shown. For this example, the compressed air demand is kept constant at 0.9 $\frac{m^3_n}{min}$.

In **normal** operation mode ($t < t_1$, $t_2 \leq t < t_3$ and $t > t_4$), the complete air demand $\dot{V}_d$ is

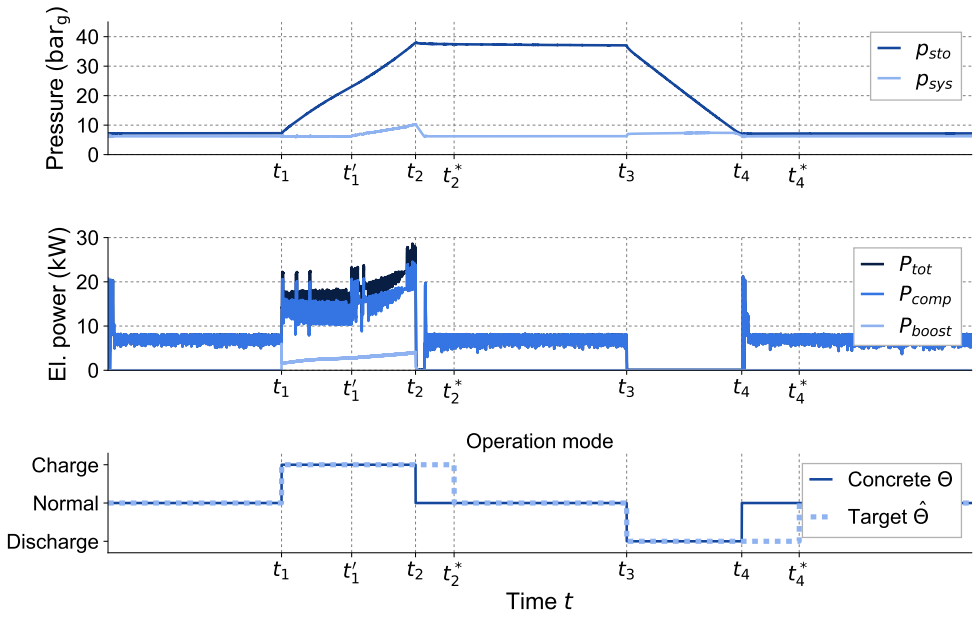

Figure 3.3: Storage pressure, electric power consumption and operation modes of the CAES system for one full cycle

covered by the compressors that are controlled by the SAM. The booster is switched off and the outlet valve of the storage is closed. The setpoint of the system pressure $\hat{p}_{sys}$ is set to the normal setpoint pressure $\hat{p}_{sys}^{norm}$.

During the operation mode **charge** ($t_1 \leq t < t_2$), the booster is running and the high-pressure storage is filled. The compressors are controlled by the SAM and have to cover the complete air demand $\dot{V}_d$ and the air consumption of the booster. If the sum of the air demand and the flow rate of the booster exceeds the maximum free air delivery (FAD) of the compressors, this will lead to a pressure decrease in the system. To avoid this, a system-pressure-dependent hysteresis is implemented in the superior mode controller (SMC). If the system pressure drops under the value of the lower bound of the hysteresis $\underline{p}_{sys}^{ch}$, the concrete operation mode Θ is set to *normal* by the SMC. The CAES system stays in this mode until the upper bound of the hysteresis $\bar{p}_{sys}^{ch}$ is reached or a new target operation mode is applied.

When the storage pressure reaches the maximum pressure level $\bar{p}_{sto}$, the concrete operation mode Θ is set to *normal*. The state of the storage is set to *full* until the operation mode *discharge* is applied, even if the pressure drops below the maximum pressure $\bar{p}_{sto}$ because of a temperature decrease or leakage losses. When the target operation mode $\hat{\Theta} = \textit{charge}$ is applied while the storage is in the *full* state, the concrete operation mode Θ is set to *normal* by the SMC ($t_2 \leq t < t_2^*$).

Since the booster has a maximum compression ratio of $r_{bo} = 4$, the input pressure of the booster (which is the system pressure p_{sys}) has to be adapted during charge mode. If the storage pressure p_{sto} is greater than the system pressure p_{sys} multiplied by the compression ratio r_{bo} minus an offset of 1 bar for safety, the setpoint of the system pressure $\hat{p}_{sys}$ is calculated by dividing the actual storage pressure p_{sto} by the compression ratio r_{bo} and adding an offset

of 0.5 bar ($t_1 \leq t < t_2'$). Otherwise the setpoint of the system pressure is set to the normal system pressure $\hat{p}_{sys}^{norm}$ ($t_1 \leq t < t_2'$). For a maximum compression ratio of $r_{bo} = 4$ the system pressure has to be adapted for storage pressures $p_{sys} > 23\,\text{bar}$.

$$\hat{p}_{sys} = \begin{cases} p_{sto}/r_{bo} + 0.5\,\text{bar} & \text{if} \quad p_{sto} > p_{sys} \cdot r_{bo} - 1\,\text{bar}, \\ \hat{p}_{sys}^{norm} & \text{else.} \end{cases} \tag{3.3}$$

Depending on which value is higher, the setpoint of the system pressure is either set to the normal system pressure $\hat{p}_{sys} = \hat{p}_{sys}^{norm}$ ($t_1 \leq t < t_2'$) or calculated depending on the actual storage pressure $\hat{p}_{sys} = p_{sto}/r_{bo} + 0.5\,\text{bar}$ ($t_2' \leq t < t_2$).

In **discharge** operation mode ($t_3 \leq t < t_4$), all compressors and the booster are turned off. The outlet valve is opened and the complete air demand $\dot{V}_d$ is covered by the air in the high-pressure storage. When the storage pressure reaches the minimum pressure level $\underline{p}_{sto}$, the outlet valve is closed and the CAES system is set to *normal* operation mode. The state of the storage is set to *empty* until the operation mode *charge* is applied, even if the pressure exceeds the minimum pressure again because of a temperature increase. When the storage is in the *empty* state and the target operation mode $\hat{\Theta}$ is set to *discharge*, the SMC assigns the concrete operation mode $\Theta = \textit{normal}$ and prevents the system from being discharged ($t_4 \leq t < t_4^*$).

Table 3.4 shows the control parameters of the CAES system used for all experiments in this thesis.

Table 3.4: Control parameters of the CAES system used in this thesis

Symbol	Value	Unit	Description
$\hat{p}_{sys}^{norm}$	6	bar_g	Normal setpoint pressure
$\Delta\hat{p}_{sys}$	0.5	bar	Pressure range of the SAM
$\overline{p}_{sto}$	38	bar_g	Maximum storage pressure
$\underline{p}_{sto}$	7	bar_g	Minimum storage pressure
$\underline{p}_{sys}^{ch}$	5.9	bar_g	Lower bound of the SMC system pressure hysteresis during *charge*
$\overline{p}_{sys}^{ch}$	6.4	bar_g	Upper bound of the SMC system pressure hysteresis during *charge*

3.4 Experimental investigations

To investigate the behavior of the compressed air energy storage (CAES) system, several experiments measuring the power consumption of the compressors and the booster for different operating conditions were performed. The obtained results are used for the calculation of the parameters needed to identify different models of the CAES system (see chapter 4) as well as for an economic evaluation of the system (see section 3.5).

3.4.1 Power consumption of the compressors

The electric power consumption of the compressors was measured during normal operation mode for different air flows and system pressures. For each measurement the operating state was kept constant for three hours and the mean power consumption was calculated. Each measurement was performed three times and the mean value was calculated to reduce the influence of measurement errors. As shown in figure 3.4 the power consumption of the compressors increases monotonically with the air flow. The compressors also consume more power for higher system pressures. The influence of the system pressure depends on the air flow. For very small air flows, there is only little difference of the power consumption between the different system pressures, while for high air flows the influence of the system pressure increases.
The results also show that the maximum free air delivery (FAD) of the compressors decreases for higher output pressures [45, 46, 47]. For a setpoint pressure of 8 $\mathrm{bar_g}$ and higher, the compressors are not capable of covering an air demand over 2.5 $\frac{\mathrm{m^3_n}}{\mathrm{min}}$.

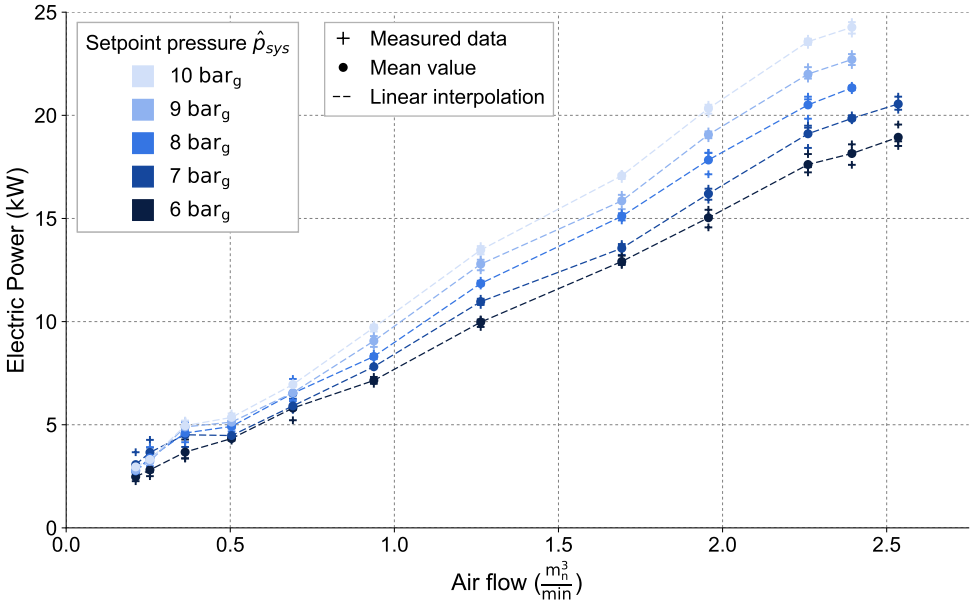

Figure 3.4: Power consumption of the compressors for different air flows and system pressures

In figure 3.5 the specific power consumption of the compressors is illustrated. The specific power consumption can be calculated by dividing the electric power consumption of the compressors by the air flow.

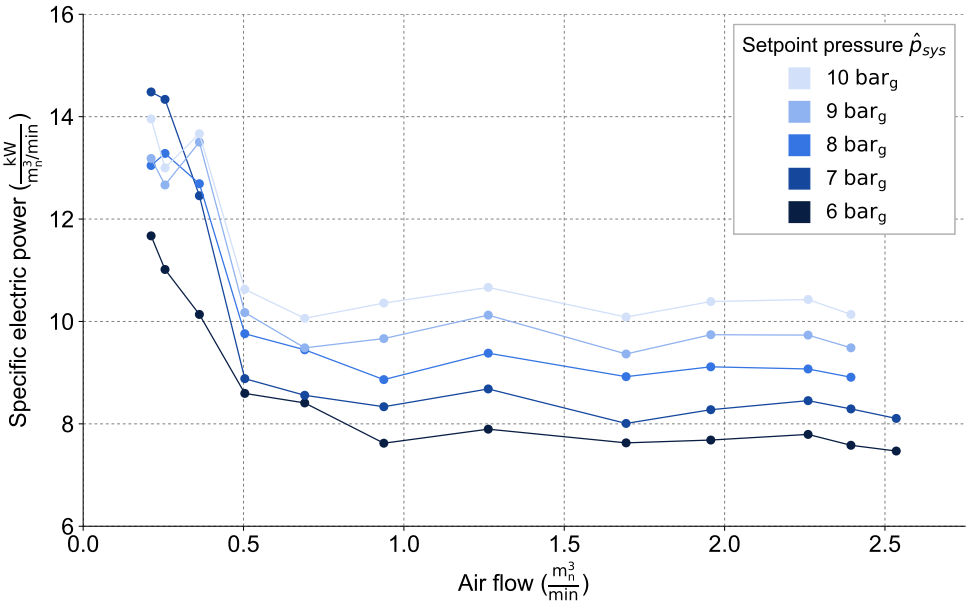

Figure 3.5: Specific power consumption of the compressors for different air flows and pressures

For very small air flows, the system has a high specific power consumption. The reason is that for an air demand which is lower than the minimum FAD of each compressor, one or more compressors are repeatedly switched on and off to cover the demand. This generates additional losses during start-up and shut-down. As shown in figure 3.6, for a constant air demand of $\dot{V}_d = 0.2\,\frac{m^3_n}{min}$ the SAM controller regulates the compressors differently depending on the setpoint pressure. While for setpoint pressures of $\hat{p}_{sys} = 6\,bar_g$ and $\hat{p}_{sys} = 10\,bar_g$ mostly just the smallest compressor SX6 is used, for a setpoint pressure of $\hat{p}_{sys} = 7\,bar_g$ always the compressors SX6 and SM12 SFC are switched on and off together. Because of this, the specific power consumption for $\hat{p}_{sys} = 10\,bar_g$ is lower than for $\hat{p}_{sys} = 7\,bar_g$.
For increasing air flows, the specific electric power consumption of the system generally decreases. But as shown in figure 3.5, this descent is not monotonic. For a constant setpoint pressure of $\hat{p}_{sys} = 6\,bar_g$ and an air flow of 0.9 $\frac{m^3_n}{min}$ the specific power is lower than for an air flow of 1.3 $\frac{m^3_n}{min}$. The reason is the part-load efficiency curve of the variable frequency drive compressor SM12 SFC. The SM12 SFC is constructed to have its best efficiency at a frequency of 50 Hz, which corresponds to a FAD of about 0.9 $\frac{m^3_n}{min}$ at a system pressure of $\hat{p}_{sys} = 6\,bar_g$ [53]. If the FAD differs from this value, the specific power consumption of the SM12 SFC increases. As shown in figure 3.6, for $\hat{p}_{sys} = 6\,bar_g$ the SM12 SFC delivers less than 0.9 $\frac{m^3_n}{min}$ air for the operation points $\dot{V}_d$=0.7 $\frac{m^3_n}{min}$ and $\dot{V}_d = 1.3\,\frac{m^3_n}{min}$. The efficiency decrease of the SM12 SFC compared to its best operation point leads to an increase of the specific electric power of the system.

For a system pressure of $\hat{p}_{sys} = 10\,\mathrm{bar_g}$ the best efficiency at a frequency of 50 Hz of the SM12 SFC corresponds to a FAD of about 0.8 $\frac{\mathrm{m^3_n}}{\mathrm{min}}$ [53]. Together with a reduced maximum air delivery for higher system pressures this causes a different operation of the compressors by the SAM controller as for lower system pressure (see figure 3.6). Therefore, in contrast to $\hat{p}_{sys} = 6\,\mathrm{bar_g}$, the specific electrical power consumption increases with the air flow for values between 0.7 $\frac{\mathrm{m^3_n}}{\mathrm{min}}$ and 1.3 $\frac{\mathrm{m^3_n}}{\mathrm{min}}$ for a system pressure of $\hat{p}_{sys} = 10\,\mathrm{bar_g}$, as shown in figure 3.5. Thus the specific electrical power consumption of the system for a certain operation point depends on how the three compressors are controlled by the SAM. The combination of three different compressor models and the part-load dependent efficiency of the variable frequency drive compressor SM12 SFC causes a nonlinear dependence of the electrical power consumption on the air demand and the system pressure.

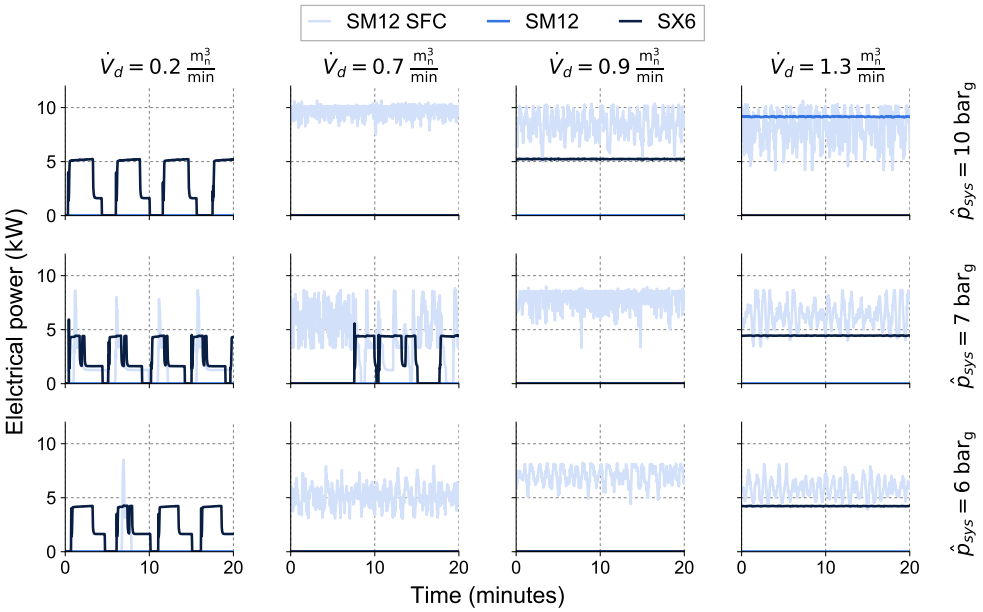

Figure 3.6: Measured power consumption of the individual compressors for different exemplary air flows and system pressures

3.4.2 Power consumption of the booster

The electric power consumption of the booster was measured with a resolution of one second, while the high pressure storage was completely charged from an empty state ($p_{sto} = 7\,\mathrm{bar_g}$) to the maximum pressure of $p_{sto} = 38\,\mathrm{bar_g}$. To reduce the influence of measurement errors, the experiment was performed five times. Figure 3.7 shows the power consumption of the booster in relation to the storage pressure. The illustrated mean value was calculated for linear discretized pressure ranges of 0.1 bar. The increase of the system pressure at a storage pressure of 23 bar (see eq. 3.3) results in a change of the power curve. The few points with a higher power consumption at a storage pressure of 7 bar are caused by the start-up of the booster.

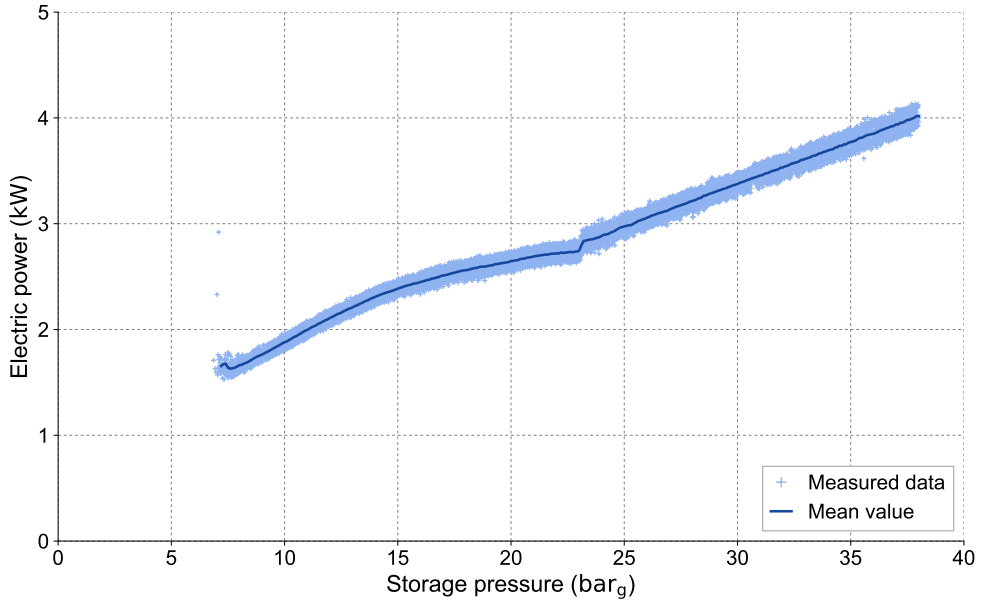

Figure 3.7: Power consumption of the booster

3.4.3 Round-trip efficiency

The round-trip efficiency η of an energy storage is described by the ratio of energy a full energy storage can deliver until it is empty (discharge energy E_{dch}) to the energy needed to completely charge an empty storage (charge energy E_{ch}).

$$\eta = \frac{E_{dch}}{E_{ch}} \tag{3.4}$$

The compressed air energy storage system described in this chapter, is used to shift the electrical energy demand. To describe the CAES system as an electrical energy storage, the electrical efficiency η_{el} has to be calculated.

The electrical power consumed by the compressed air system during charging, is used to deliver the air needed to charge the storage as well as to cover the air demand $\dot{V}_d$. To calculate the power that is used only for charging the storage, the reference power P_{ref} needed to deliver the air demand has to be subtracted from the measured power P_{tot} of the system. Thereby P_{ref} is the power the compressors would consume in *normal* operation mode to cover the air demand $\dot{V}_d$, which corresponds to the power consumption of the compressors for $\hat{p}_{sys} = \hat{p}_{sys}^{norm} = 6\,\mathrm{bar_g}$ (see figure 3.4). The charge energy E_{ch} can be calculated by integrating the difference of P_{tot} and P_{ref} over the charging time (t_0^{ch} to t_1^{ch}), as shown in figure 3.8.

$$E_{ch} = \int_{t_0^{ch}}^{t_1^{ch}} \left(P_{tot}(t) - P_{ref}(t)\right) dt \tag{3.5}$$

The CAES system is not able to deliver electrical energy during discharging. But because the air demand $\dot{V}_d$ is covered by the air out of the storage, the compressors are turned off, which leads to a reduction of the power consumption of the CAES system by P_{ref}. The reference power P_{ref} here again is the power the compressors would consume in *normal* operation mode to cover the air demand. When the compressors are turned off, they still consume electrical power because of their stand-by losses which correspond to the measured total electrical power P_{tot}. Thus the charge energy E_{dch} can be calculated by integrating the difference of P_{ref} and P_{tot} over the discharging time (t_0^{dch} to t_1^{dch}, see figure 3.8).

$$E_{dch} = \int_{t_0^{dch}}^{t_1^{dch}} \left(P_{ref}\left(t\right) - P_{tot}\left(t\right)\right) dt \tag{3.6}$$

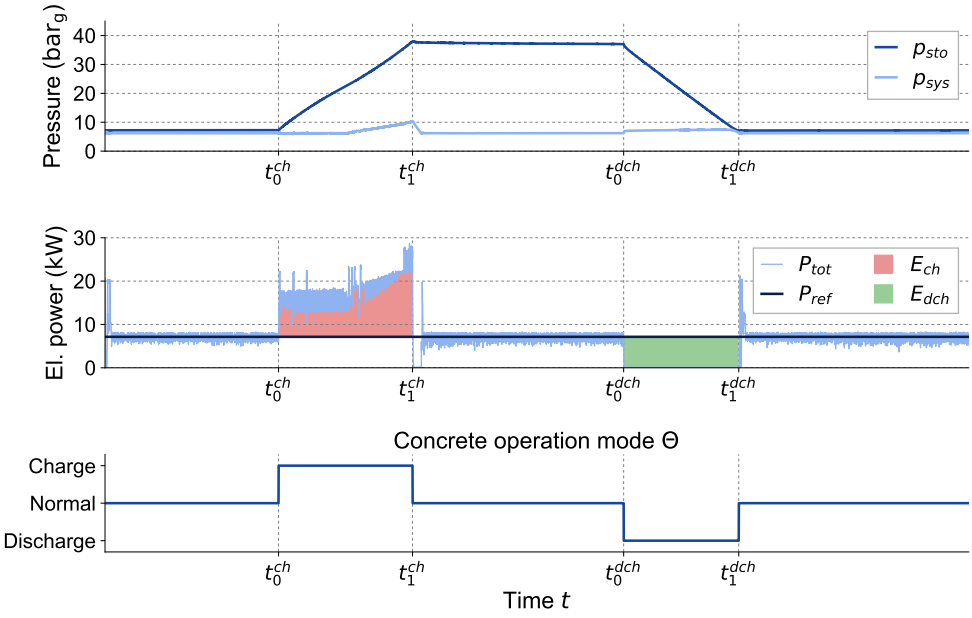

Figure 3.8: Charge and discharge energy for one full cycle of the storage with a constant air demand

When the CAES system is charged, the setpoint of the system pressure $\hat{p}_{sys}$ has to be increased for high storage pressures (see section 3.3). As shown in figure 3.4, an increased system pressure leads to a higher electrical power consumption of the compressors, depending on the air flow. During charging, the compressors have to cover the air flow into the storage as well as the air demand $\dot{V}_d$. Therefore, the CAES system cannot be charged for high air demands. Since the air flow into the storage is constant when the booster is running, the power consumption of the compressors during charging and therefore the charge energy E_{ch} of the CAES system depends on the air demand. To determine the influence of $\dot{V}_d$ on the charge energy E_{ch}, measurements for different air demands where performed. Therefore, $\dot{V}_d$ was kept constant while the empty storage was completely charged. For each air demand the mean value of at least three measurements were calculated to reduce the influence of measurement errors. The results are shown in figure 3.9. As expected, the charge energy generally increases

for higher air demands. The deviation for an air demand of 0.7 $\frac{m^3_n}{min}$ is a consequence of the nonlinear dependence of the electrical power consumption on the air demand and the system pressure (see section 3.4.1).

The experiments to determine the discharge energy E_{dch} were performed in the same way as for the charge energy. When a full high-pressure storage is completely discharged, approximately the same amount of air can be retrieved from the storage, independent from the actual air demand. But the reference power P_{ref} used to calculate the discharge energy E_{dch}, which is the power the compressors would consume in normal operation mode to cover the air demand, does depend on the air demand of the system. Therefore, the dependence of the discharge energy E_{dch} on the air demand is related to the specific power consumption of the compressors for $\hat{p}_{sys} = \hat{p}^{norm}_{sys} = 6\,\text{bar}_g$ as shown in figure 3.5. The discharge energy E_{dch} of the CAES for different air demands during discharging is also illustrated in figure 3.9.

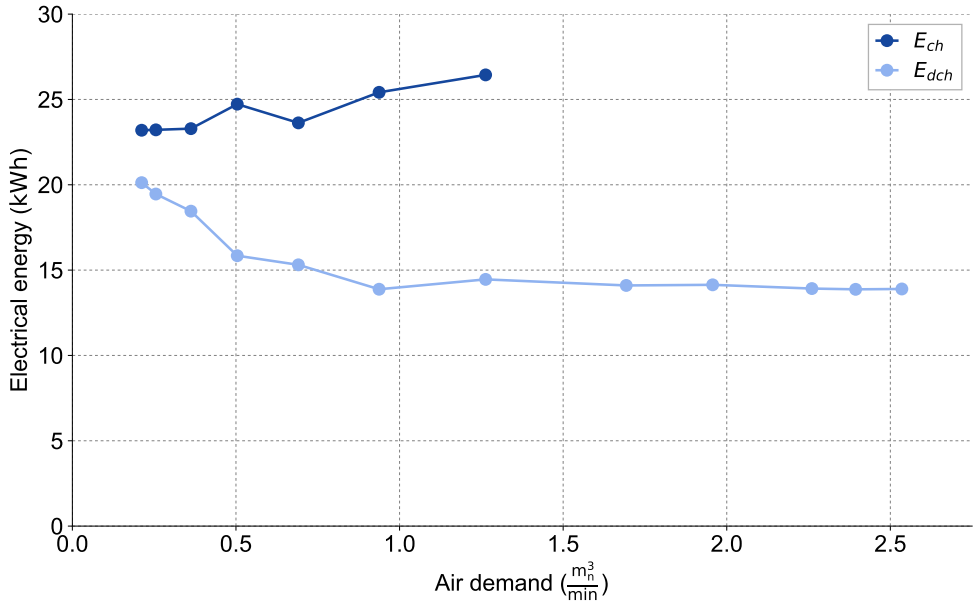

Figure 3.9: Charge and discharge energy for different air demands during charging and discharging

Using the values for the charging energy E_{ch} and the discharging energy E_{dch} of figure 3.9, the electrical round-trip efficiency η_{el} of the compressed air energy storage can be calculated with equation 3.4. As shown in figure 3.10, the round-trip efficiency has its maximum value of 86.76 % for an air demand of $\dot{V}_d = 0.2\,\frac{m^3_n}{min}$ during charging and discharging. The minimum round-trip efficiency of 52.47 % occurs for an air demand of $\dot{V}_d = 1.3\,\frac{m^3_n}{min}$ during charging and $\dot{V}_d = 2.4\,\frac{m^3_n}{min}$ during discharging.

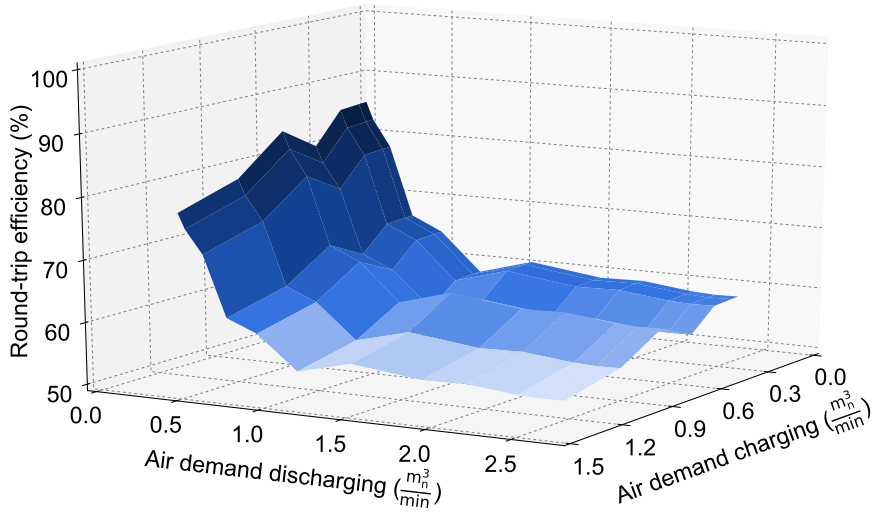

Figure 3.10: Round-trip efficiency of the CAES for different air demands during charging and discharging

3.5 Economic evaluation of the compressed air energy storage system

For an economic evaluation of the CAES system, the specific energy costs c_{sto} are calculated and compared with battery storages. The specific energy costs c_{sto} represent the costs for the energy that is retrieved from the storage. They can be calculated by dividing the investment costs C_{inv} by the product of the discharge energy E_{dch} that can be retrieved from the storage for one full discharge cycle and the number of full charge and discharge cycles Z within a certain observation period. If the number of full cycles Z within the observation period exceeds the number of maximum full cycles Z_{max}, a new storage has to be used. This is considered by using the round up operator $\lceil x \rceil$ in equation 3.7. Additionally, costs for charging the storage have to be considered. To take the losses during charging and discharging into account, the energy costs c_{en} (in $\frac{€}{\text{kWh}}$) are divided by the round-trip efficiency η of the storage.

$$c_{sto} = \frac{C_{inv}}{Z \cdot E_{dch}} \cdot \left\lceil \frac{Z}{Z_{max}} \right\rceil + \frac{c_{en}}{\eta} \tag{3.7}$$

For the CAES system three different cases are considered for the specific energy cost calculations. For the best and worst case the parameters with the resulting best and worst round-trip efficiencies are used (see section 3.4.3). For the mean case, the air demand during charging and discharging is considered to be the mean value of measured air demand data used for the experiments in this thesis (see chapter 5.1.1, table 5.2). The round-trip efficiency is linearly interpolated using the data shown in figure 3.9. For the investment costs of the CAES only the components needed in addition to a typical compressed air energy storage system are considered (see appendix A.2).

For the economic evaluation of the compressed air energy storage system, the costs are compared with battery storage systems with a similar energy capacity. The cost and technical data needed for the specific energy cost calculation of the CAES system and the battery storages are summarized in table 3.5. In addition to the parameters needed for the cost calculation, the duration of one full charge and discharge cycle Δt_Z is given.

Table 3.5: Costs and technical data of the storages for the specific energy cost calculations

Storage	C_{inv} (€)	E_{dch} (kWh)	Z_{max} (1)	η (%)	Δt_Z (h)	**Source**
CAES mean	55,200	15.7	∞	64.3	5.7	
CAES best	55,200	20.1	∞	86.7	10.8	
CAES worst	55,200	13.9	∞	52.5	3.1	
Sonnenbatterie eco	21,224	14.0	10,000	94.1	8.5	[94]
Tesla Powerwall [1]	4,200	5.6	10,000	88.8	4	[97]

Figure 3.11 shows the specific energy cost of the CAES system cases and the battery storage depending on the number of full cycles per day. Here the observation period is defined to be 10 years and the electricity costs during charging are set to 0.10 $\frac{€}{\text{kWh}}$. The different maximum cycles per day of the curves are a result of the individual duration of one full charge and discharge cycle Δt_Z. Each storage can only be charged and discharged with a certain number of full cycles within the 24 hours of a day. The step in the specific costs of the battery storages are caused by exceeding the maximum number of 10,000 cycles (2.74 cycles per day for 10 years). The results show, that the specific energy costs of the CAES system for all three considered cases are higher than the costs of the battery storages.

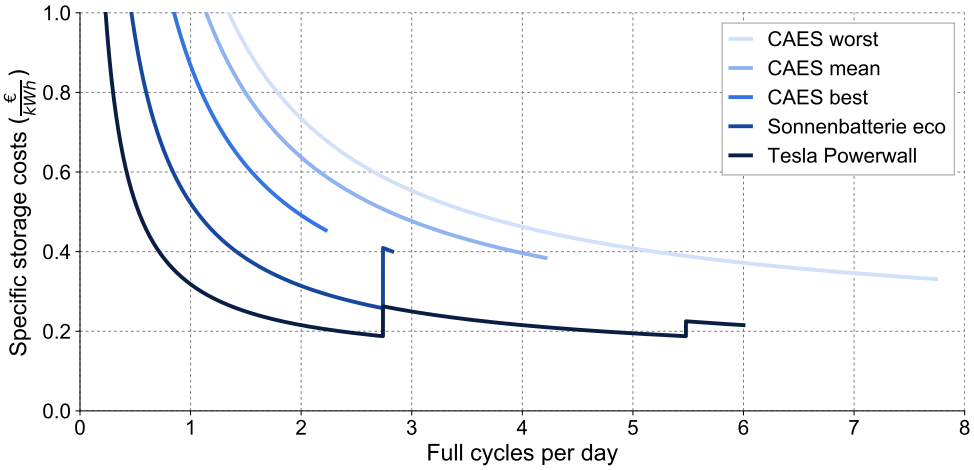

Figure 3.11: Specific storage costs depending on the number of full cycles per day for an observation period of 10 years and electricity costs during charging of 0.10 $\frac{€}{\text{kWh}}$

[1] The costs and the round-trip efficiency are given including an inverter with investment costs of 2.000 € and an efficiency of 96 %.

Chapter 4

Optimization Models

In this chapter, a linear, a mixed-integer linear, and a nonlinear mathematical model used for the different optimization methods are described and validated. While the sections of this chapter present the general structure of the models and the most important equations, a detailed mathematical description of each model is given in appendix B.

4.1 Objective function, sets, parameters, and variables

The objective of all optimization models described in this chapter is to minimize the total costs c_{tot} over the optimization horizon. The optimization horizon is described by the set of timesteps $\mathcal{T} = \{t_1, ..., t_N\}$, where ΔT is the duration of the optimization horizon, Δt is the duration of each timestep, and N is the number of timesteps $t \in \mathcal{T}$ (see table 4.1).

Table 4.1: Time set and parameters

Name	Unit	Description
$\mathcal{T}$		Set of all timesteps $\mathcal{T} = \{t_1, ..., t_N\}$
ΔT	h	Duration of the optimization horizon
Δt	s	Timebase of the optimization (duration of one time period)
N	1	Number of timesteps $N = \frac{\Delta T}{\Delta t / 3600}$

The total costs c_{tot} are calculated by the product of the electricity price C^t_{el} and the total electrical energy consumption E^t_{tot} at each timestep t, summed up for all timesteps. The total electrical energy consumption E^t_{tot} of the CAES system at each timestep is defined by the total electrical power consumption P^t_{tot} and the timestep duration Δt.

$$\min c_{tot} = \min \left(\sum_{t \in \mathcal{T}} C^t_{el} \cdot E^t_{tot} \right) = \min \left(\sum_{t \in \mathcal{T}} C^t_{el} \cdot P^t_{tot} \cdot \frac{\Delta t}{3600 \, \frac{\mathrm{s}}{\mathrm{h}}} \right) \tag{4.1}$$

To describe a mathematical optimization problem, the parameters used are distinguished into constant model parameters (usually referred to as *parameters*) and variable parameters (usually referred to as *variables*). The model parameters and variables are used to specify the optimization problem. The values of the parameters are constant, which means they do not

change while the optimization problem is solved. In contrast, the values of the variables are unknown until the model has been solved. Solving an optimization model means finding the values for the variables, that lead to an optimal result of the objective function, satisfying all given constraints.

The parameters and variables used to describe the optimization problems in this chapter are summarized in tables within the model description section for each model. The values of the parameters for each model can be found in appendix C.

4.2 Linear programming model

The CAES system has three operation modes defining its behavior, *normal*, *charge* and *discharge* (see section 3.3). Modeling these modes within an optimization problem requires integer variables and, thus, is not possible using linear programming. Also, the behavior of the booster, which has only an on/off mode, and the pressure dependency of the electric power consumption of the compressors and the booster (see figure 3.4 and 3.7) can only be modeled using integer variables. Therefore, instead of modeling the booster and high-pressure storage tanks separately, they are summarized and treated as an electrical energy storage system using the parameters calculated in section 3.4.3. Additionally, the three screw compressors are summarized as well and modeled as one single component covering the whole air demand. Figure 4.1 shows the structure of the LP model of the CAES system. The parameters and variables used to describe the LP model are summarized in table 4.2 and 4.3.

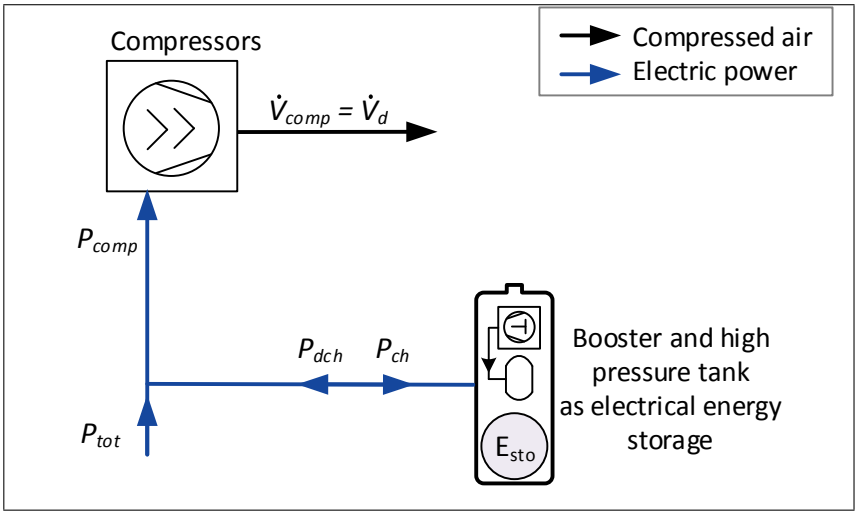

Figure 4.1: Structure of the LP model of the CAES system

The objective of the LP model is to minimize the total costs over the optimization horizon. The costs depend on the electricity price C^t_{el} and the total power consumption of the system P^t_{tot} at each timestep (see eq. 4.1). The total power consumption of the system P^t_{tot} is comprised of the power consumption of the compressors P^t_{co} and the charge power P^t_{ch} or discharge power P^t_{dch} of the electrical energy storage.

$$P^t_{tot} = P^t_{co} + P^t_{ch} - P^t_{dch} \tag{4.2}$$

Table 4.2: Parameters of the LP model

Name	Unit	Description
$\overline{E}_{sto}$	kWh	Maximum electrical energy capacity of the storage
ς_1	$\frac{\text{kW}}{\text{m}^3_\text{n}/\text{min}}$	Slope of the linear function used to model the electrical power consumption of the compressors
η^t_{ch}	1	Storage electrical charge efficiency at timestep t
η^t_{dch}	1	Storage electrical discharge efficiency at timestep t
$\dot{V}^t_d$	$\frac{\text{m}^3_\text{n}}{\text{min}}$	Air demand at timestep t
$\overline{P}^t_{ch}$	kW	Upper limit of the electrical charge power at timestep t dependent on $\dot{V}^t_d$
C^t_{el}	$\frac{€}{\text{kWh}}$	Electricity price at timestep t
Δt	s	Timebase of the optimization (duration of one time period)

Table 4.3: Variables of the LP model

Name	$\in$	Unit	Description
$\dot{V}^t_{co}$	$\mathbb{R}^+_0$	$\frac{\text{m}^3_\text{n}}{\text{min}}$	Compressed air produced by the compressors at timestep t
P^t_{co}	$\mathbb{R}^+_0$	kW	Electrical power consumed by the compressors at timestep t
P^t_{tot}	$\mathbb{R}^+_0$	kW	Total electrical power consumed by the CAES system at timestep t
P^t_{ch}	$\mathbb{R}^+_0$	kW	Electrical charge power of the storage at timestep t
P^t_{dch}	$\mathbb{R}^+_0$	kW	Electrical discharge power of the storage at timestep t
E^t_{sto}	$\mathbb{R}^+_0$	kWh	Electrical energy content of the storage at timestep t

Compressors

For the LP model, the system pressure is assumed to be constant. Therefore, the power consumption of the compressors P^t_{co} only depends on the air demand $\dot{V}^t_d$ and is modeled as a linear function with the slope ς_1. Figure 4.2 shows the modeled compressor power in comparison with measured values. The LP formulation does not allow to use an offset in this function, which leads to an inaccurate representation of the model, especially for low and high air demands.

$$P^t_{co} = \varsigma_1 \cdot \dot{V}^t_d \tag{4.3}$$

Storage

When the CAES system is in *discharge* mode, the compressors are switched off and the air demand is covered by the air stored in the high-pressure storage tank. The power consumption of the CAES system then becomes zero. In the LP model, this is represented by discharging the electrical storage system. When the discharge power of the storage P^t_{dch} equals the power consumption of the compressors P^t_{co}, the air demand is "covered" by the storage. The CAES system is not able to generate electricity, so the discharge power of the storage is limited by the power consumption of the compressors. The LP implementation does not allow one to use a binary variable b^t_{dch} representing the *discharge* mode of the system, thus, it is not possible to define P^t_{dch} to be either 0 or P^t_{co} dependent on the mode (e.g. $P^t_{dch} = b^t_{dch} \cdot P^t_{co}$), as can

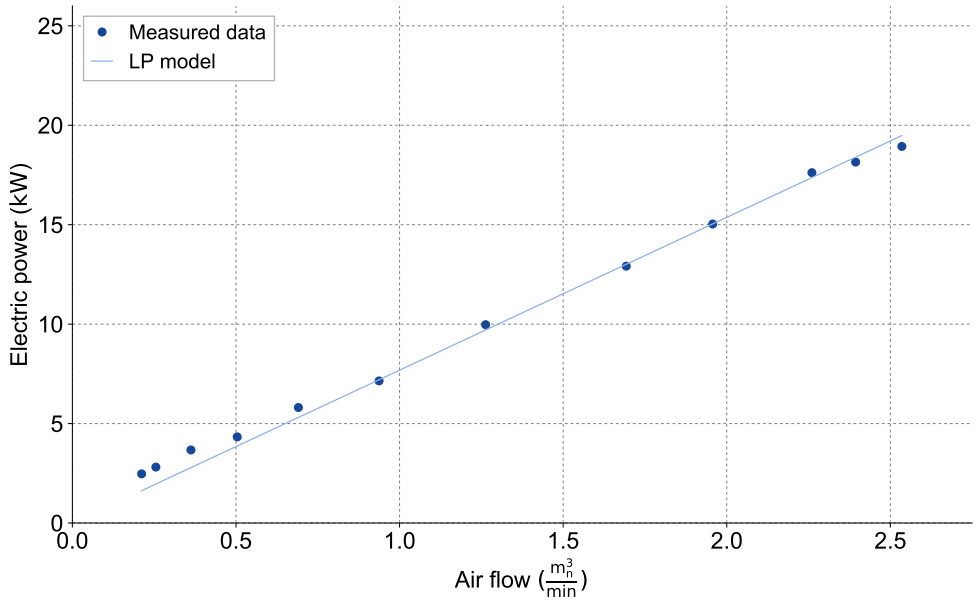

Figure 4.2: LP function of compressor electric power consumption

be done for the MILP and the nonlinear model. This allows the LP model to obtain states in which the air demand is partly covered by the compressors, while the rest is covered by the storage. Because these states are not possible for the real CAES system, this could lead to inaccurate optimization results.

$$P^t_{dch} \leq P^t_{co} \tag{4.4}$$

When the CAES system is in *charge* mode, the booster is switched on and the high-pressure storage tank is filled. The compressors have to cover the additional air demand of the booster. In the LP model, this is modeled by charging the electrical storage system. The charge energy and, therefore, the mean charge power $\overline{P}^t_{ch}$ of the electrical storage representation of the CAES system is dependent on the air demand $\dot{V}^t_d$ (see chapter 3.4.3, figure 3.9). Therefore, for each timestep and its (predicted) air demand $\dot{V}^t_d$, the mean charge power $\overline{P}^t_{ch}$ is calculated as explained in appendix C.1.1 and used as an upper limit of the charge power P^t_{ch}. As explained before for the discharge power, it is not possible to to define P^t_{ch} to be either 0 or $\overline{P}^t_{ch}$ dependent on the system mode using a LP model, which might lead to inaccurate modeling results.

$$P^t_{ch} \leq \overline{P}^t_{ch} \tag{4.5}$$

The energy content E^{t+1}_{sto} of the electrical energy storage for the timestep t+1 is calculated based on the energy content E^t_{sto}, the charge power P^t_{ch}, and the discharge power P^t_{dch} at timestep t. The losses during charging and discharging are represented by the charge efficiency η^t_{ch} and the discharge efficiency η^t_{dch}. The electrical round-trip efficiency of the CAES system is dependent on the air demand during charging and discharging (see chapter

3.4.3, figure 3.10). The charge efficiency and the discharge efficiency for each timestep are calculated depending on the corresponding air demand as explained in appendix C.1.2.

$$E_{sto}^{t+1} = E_{sto}^{t} + \eta_{ch}^{t} \cdot P_{ch}^{t} - \frac{1}{\eta_{dch}^{t}} \cdot P_{dch}^{t} \tag{4.6}$$

The energy storage content E_{sto}^{t} is limited by the maximum energy capacity of the storage $\overline{E}_{sto}$. The value of $\overline{E}_{sto}$ is the maximum measured discharge energy of the CAES system as described in chapter 3.4.3 ($\overline{E}_{sto} = 20.12\,\mathrm{kWh}$).

$$E_{sto}^{t} \leq \overline{E}_{sto} \tag{4.7}$$

For visualization and comparison of the optimization and simulation results with measured data, the energy content of the storage can be converted to pressure values by a linear interpolation between the minimum ($\underline{p}_{sto}$) and maximum ($\bar{p}_{sto}$) values of the storage pressure.

$$p_{sto}^{t} = \frac{E_{sto}^{t}}{\overline{E}_{sto}} \cdot (\bar{p}_{sto} - \underline{p}_{sto}) + \underline{p}_{sto} \tag{4.8}$$

Figure 4.3 shows the storage pressure profile for a charge and three discharging processes calculated with equations 4.6 and 4.8 in comparison to measured values. The significant difference for the discharge process with an air demand of 0.2 $\frac{\mathrm{m_n^3}}{\mathrm{min}}$ results from the underestimation of the electric power consumption P_{co}^{t} (which limits the discharge energy, see eq. 4.4) in this operation point, as shown in figure 4.2.

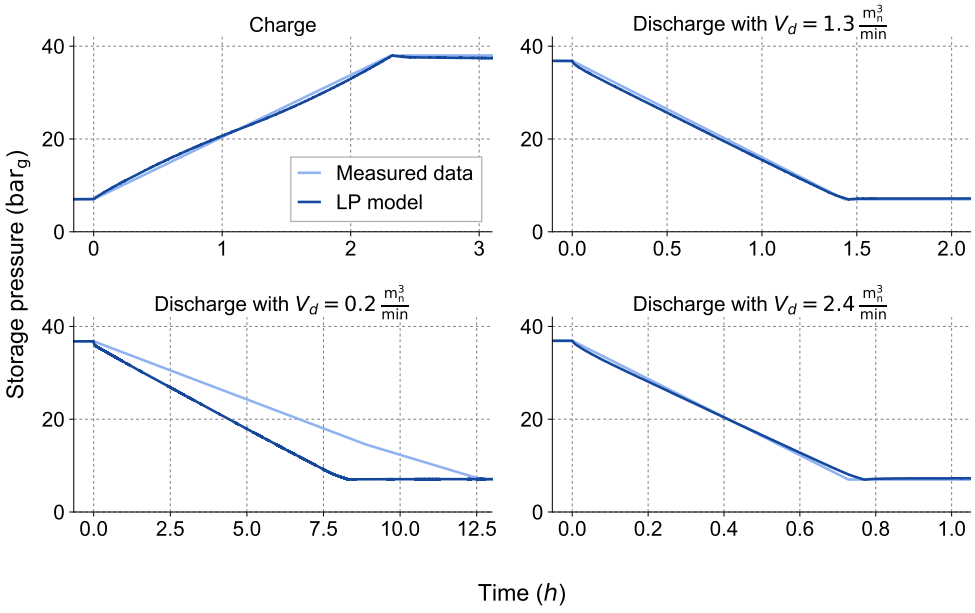

Figure 4.3: Calculated storage pressure for exemplary charging and discharging processes using the LP model compared to measured data

4.3 Mixed-integer linear programming model

In the mixed-integer linear programming (MILP) formulation of the optimization problem, binary variables representing the operation mode of the CAES system can be used. Thus, the CAES system can be modeled in more detail than with the LP model described in chapter 4.2. Figure 4.4 shows the structure of the MILP model. Here the booster and the high-pressure tank are modeled separately. The three screw compressors are summarized and modeled as one single component. The demand that has to be covered by the compressors depends on the air demand and the operation mode of the system. The parameters and variables of the MILP model are summarized in table 4.4 and 4.5.

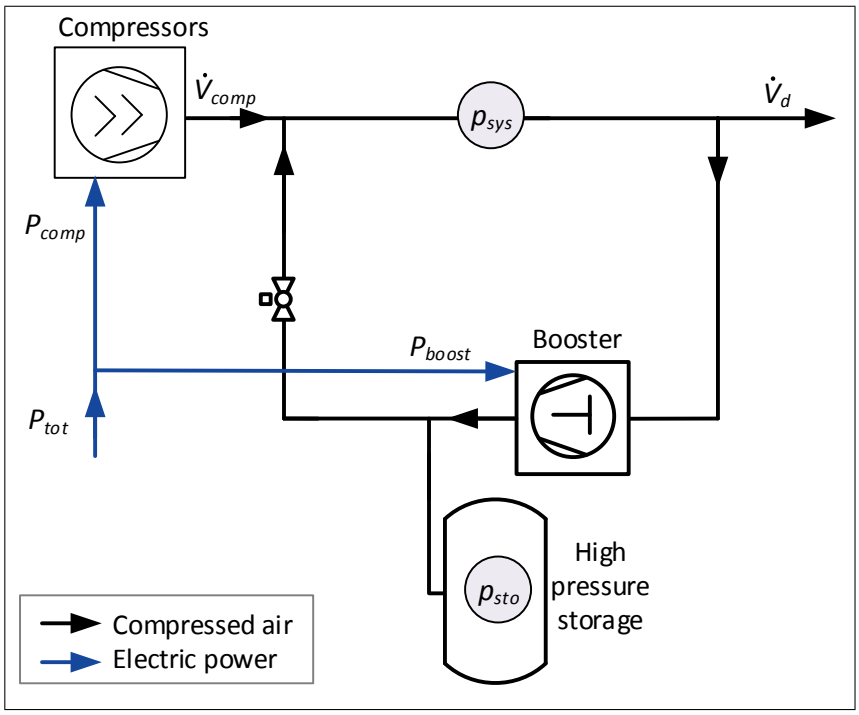

Figure 4.4: Structure of the MILP model of the CAES system

Table 4.4: Parameters of the MILP model

Name	Unit	Description
$\hat{p}_{sys}^{norm}$	bar_g	Setpoint pressure in normal mode (normal system pressure)
ς_i		Parameters used to model the electrical power consumption of the compressors
β_i		Parameters used to model the electrical power consumption of the booster
δ_i		Parameters used to model the storage pressure state equation
$\dot{V}_d^t$	$\frac{m_n^3}{min}$	Air demand at timestep t
C_{el}^t	$\frac{€}{kWh}$	Electricity price at timestep t
Δt	s	Timebase of the optimization (duration of one time period)

Table 4.5: Variables of the MILP model

Name	$\in$	Unit	Description
p_{sys}^t	$\mathbb{R}_0^+$	bar_g	System pressure at timestep t
p_{sto}^t	$\mathbb{R}_0^+$	bar_g	Storage pressure at timestep t
$\Delta p_{sto,ch}^t$	$\mathbb{R}_0^+$	bar_g	Pressure difference at timestep t when charging
$\Delta p_{sto,dch}^t$	$\mathbb{R}_0^+$	bar_g	Pressure difference at timestep t when discharging
P_{co}^t	$\mathbb{R}_0^+$	kW	Electrical power consumed by the compressors at timestep t
P_{bo}^t	$\mathbb{R}_0^+$	kW	Electrical power consumed by the booster at timestep t
P_{tot}^t	$\mathbb{R}_0^+$	kW	Total electrical power consumed by the CAES system at timestep t

The objective of the MILP model is to minimize the total costs over the optimization horizon. The costs depend on the electricity price C_{el}^t and the total power consumption of the system P_{tot}^t at each timestep (see eq. 4.1). In the MILP model, the total power consumption of the system P_{tot}^t is comprised of the power consumptions of the compressors P_{co}^t and of the booster P_{bo}^t.

$$P_{tot}^t = P_{co}^t + P_{bo}^t \tag{4.9}$$

Compressors

In the MILP model, the power consumption of the compressors can be formulated depending on the operation mode. When the system is in *normal* mode, the compressors have to cover the complete air demand $\dot{V}_d^t$. The system pressure is defined to be constant ($p_{sys}^t = \hat{p}_{sys}^{norm}$) and, thus, has no influence on the consumed power. In the operation mode *charge*, in addition to the air demand of the system $\dot{V}_d^t$, the air demand of the booster $\dot{V}_{bo}$ has to be covered. Furthermore, the system pressure p_{sys}^t during charging is not constant, which affects the power consumption of the compressors. This is taken into account with a linear dependence of the power consumption on the difference of the system pressure and the normal system pressure ($p_{sys}^t - \hat{p}_{sys}^{norm}$) and the product of the air demand ($\dot{V}_d^t + \dot{V}_{bo}$) and the system pressure increase ($p_{sys}^t - \hat{p}_{sys}^{norm}$). In *discharge* mode, the air demand is covered by the air out of the high-pressure storage and the compressors are switched off.

$$P_{co}^t = \begin{cases} \varsigma_1 \cdot (\dot{V}_d^t + \dot{V}_{bo}) + \varsigma_2 \cdot (p_{sys}^t - \hat{p}_{sys}^{norm}) \\ \quad + \varsigma_3 \cdot (\dot{V}_d^t + \dot{V}_{bo}) \cdot (p_{sys}^t - \hat{p}_{sys}^{norm}) + \varsigma_4 & \text{in } \textit{charge} \text{ mode,} \\ \varsigma_1 \cdot \dot{V}_d^t + \varsigma_4 & \text{in } \textit{normal} \text{ mode,} \\ 0 & \text{in } \textit{discharge} \text{ mode.} \end{cases} \tag{4.10}$$

During charging, the system pressure p_{sys}^t of the CAES system depends on the storage pressure p_{sto}^t (see chapter 3.3). The system pressure has to be increased during charging, when the storage pressure is above a certain value ($p_{sys}^t \cdot r_{bo} - 1\,\text{bar} = 23\,\text{bar}$), because of the limited compression ratio r_{bo} of the booster. If the storage pressure is below this value, or the

system is in *normal* or *discharge* operation mode, the system pressure p_{sys}^t corresponds to the normal system pressure $\hat{p}_{sys}^{norm}$. Figure 4.5 shows the modeled system pressure dependent on the storage pressure in *charge* mode, as defined in equation 4.11.

$$p_{sys}^t = \begin{cases} (p_{sto}^t + 2\,\text{bar})/r_{bo} & \text{if} \quad p_{sto}^t > p_{sys}^t \cdot r_{bo} - 1\,\text{bar} \quad \text{in } \textit{charge} \text{ mode,} \\ \hat{p}_{sys}^{norm} & \text{else.} \end{cases} \tag{4.11}$$

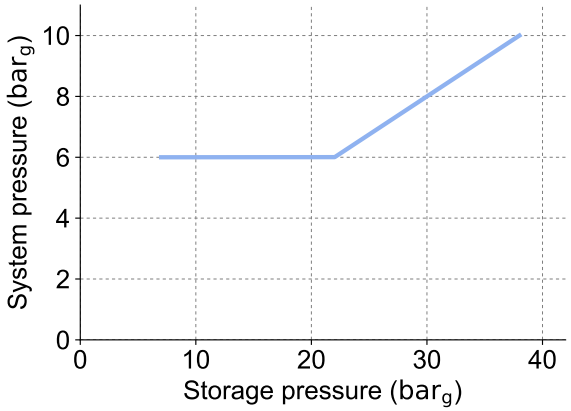

Figure 4.5: System pressure as a function of the storage pressure in *charge* mode

Figure 4.6 shows the modeled compressor power using the MILP formulation in comparison with measured values. The possibility to use an offset (ς_4) in the linear function results in a more accurate representation of the power consumption in comparison to the LP model (see figure 4.2). In contrast to the LP model, the MILP model considers energy losses during start-up and shut-down of the compressors, as described in appendix B.2.

Booster

The power consumption of the booster depends mainly on its output pressure, which corresponds to the pressure in the high-pressure storage. Therefore, the power consumption of the booster is defined as a linear function of the storage pressure with an offset β_2. The booster only consumes power in *charge* mode. Figure 4.7 shows the modeled power consumption of the booster compared to measured values. For the booster as well, losses for start-up and shut-down are considered, as described in appendix B.2.

$$P_{bo}^t = \begin{cases} \beta_1 \cdot p_{sto}^t + \beta_2 & \text{in } \textit{charge} \text{ mode,} \\ 0 & \text{else.} \end{cases} \tag{4.12}$$

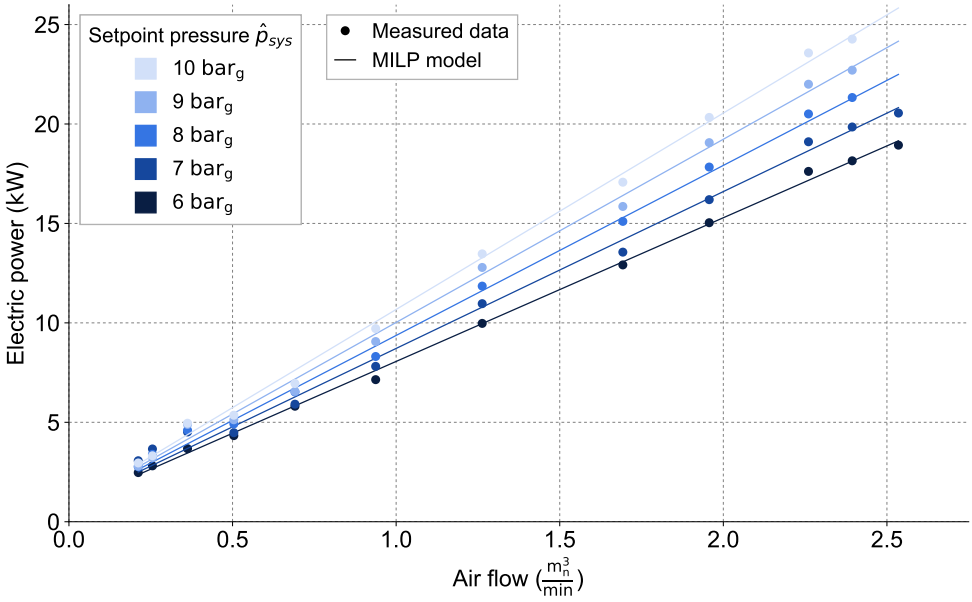

Figure 4.6: MILP model for the electric power consumption of the compressors

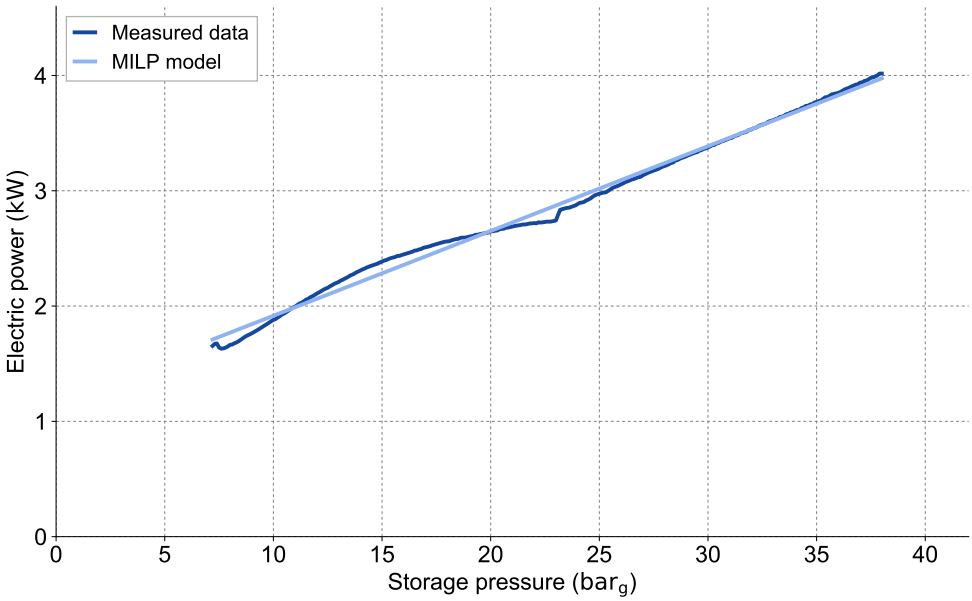

Figure 4.7: MILP model for the electric power consumption of the booster

Storage

The pressure in the high-pressure storage tank at the beginning of the next timestep p_{sto}^{t+1} depends on the storage pressure p_{sto}^{t} at timestep t and the operation mode of the system. In *charge* mode, the pressure difference $\Delta p_{sto,ch}^{t}$ is added. In *discharge* mode, the pressure is reduced by $\Delta p_{sto,dch}^{t}$.

$$p_{sto}^{t+1} = \begin{cases} p_{sto}^{t} + \Delta p_{sto,ch}^{t} & \text{in } \textit{charge} \text{ mode,} \\ p_{sto}^{t} & \text{in } \textit{normal} \text{ mode,} \\ p_{sto}^{t} - \Delta p_{sto,dch}^{t} & \text{in } \textit{discharge} \text{ mode.} \end{cases} \tag{4.13}$$

The pressure increase during charging is formulated as a linear function dependent on the previous storage pressure p_{sto}^{t}.

$$\Delta p_{sto,ch}^{t} = \Delta t \cdot \left(\delta_{ch,1} \cdot p_{sto}^{t} + \delta_{ch,2}\right) \tag{4.14}$$

The pressure decrease during discharging is modeled as a linear function dependent on the air demand of the system $\dot{V}_d$ and the previous storage pressure p_{sto}^{t}.

$$\Delta p_{sto,dch}^{t} = \Delta t \cdot \left(\delta_{dch,1} \cdot \dot{V}_d + \delta_{dch,2} \cdot p_{sto}^{t} + \delta_{dch,3}\right) \tag{4.15}$$

Figure 4.8 shows the storage pressure profile for a charge and three discharging processes calculated with equations 4.13 - 4.15 in comparison with measured values. The calculated values show only a slight deviation from the measured data for all four cases. Compared to LP (see figure 4.3), the MILP model shows a better representation of the pressure characteristics for charge and discharge, especially for discharge with a low air demand ($\dot{V}_d = 0.2\ \frac{m_n^3}{min}$).

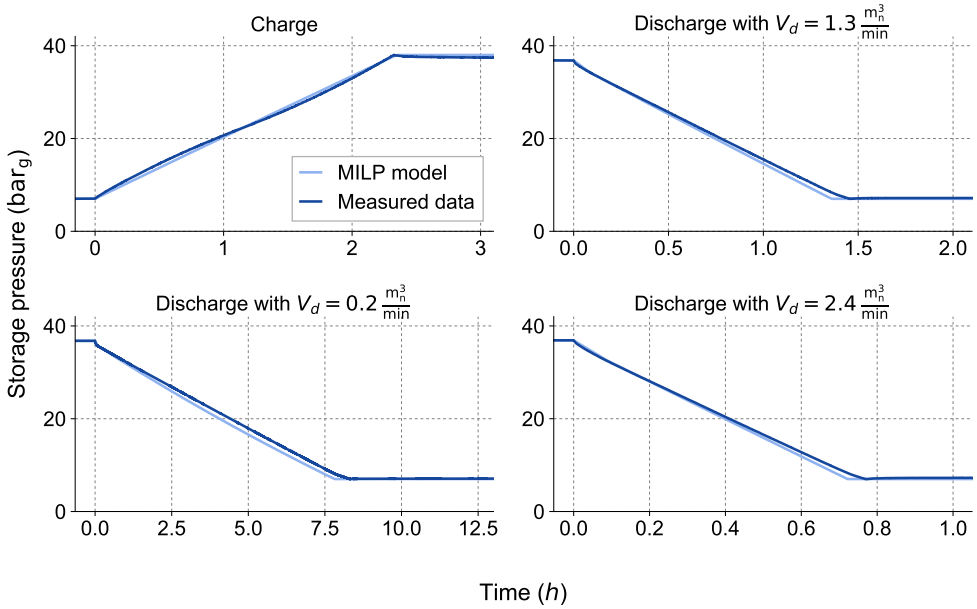

Figure 4.8: Calculated storage pressure for exemplary charging and discharging processes using the MILP model compared to measured data

4.4 Nonlinear model

The nonlinear (and non-convex) formulation of the optimization problem allows for very high freedom of expression to describe the CAES system. Thus, the system can be modeled in much more detail than with a LP or MILP formulation. The optimization methods dynamic programming (DP) and genetic algorithm (GA) use the nonlinear description of the CAES system implemented as a simulation model, as described detailed in appendix B.3. To use the mixed-integer nonlinear programming (MINLP) method a simplified version of the nonlinear model is formulated using equality and inequality functions, as describe in appendix B.4.

The structure of the nonlinear CAES system model is shown in figure 4.9. As in the MILP formulation, the booster and the high-pressure tank are modeled separately. The three screw compressors are summarized and modeled as one single component. Here, the air receiver tank, which is used to reduce compressor cycling, is also taken into account. The parameters and variables used to describe the nonlinear model are summarized in table 4.6 and 4.7.

Table 4.6: Parameters of the nonlinear model

Name	Unit	Description
$\hat{p}_{sys}^{norm}$	$\mathrm{bar_g}$	Setpoint pressure in normal mode (normal system pressure)
p_n	$\mathrm{bar_a}$	Normal pressure
V_{rec}	$\mathrm{m^3}$	Volume of air receiver tank
ς_i		Parameters used to model the electrical power consumption of the compressors
β_i		Parameters used to model the electrical power and air consumption of the booster
δ_i		Parameters used to model the storage pressure state equation
r_{bo}	1	Maximum compression ratio of the booster
$\dot{V}_d^t$	$\frac{\mathrm{m_n^3}}{\mathrm{min}}$	Air demand at timestep t
C_{el}^t	$\frac{€}{\mathrm{kWh}}$	Electricity price at timestep t
Δt	s	Timebase of the optimization (duration of one time period)

Table 4.7: Variables of the nonlinear model

Name	$\in$	Unit	Description
p_{sys}^t	$\mathbb{R}_0^+$	$\mathrm{bar_g}$	System pressure at timestep t
p_{sto}^t	$\mathbb{R}_0^+$	$\mathrm{bar_g}$	Storage pressure at timestep t
$\Delta p_{sto,ch}^t$	$\mathbb{R}_0^+$	$\mathrm{bar_g}$	Pressure difference at timestep t when charging
$\Delta p_{sto,dch}^t$	$\mathbb{R}_0^+$	$\mathrm{bar_g}$	Pressure difference at timestep t when discharging
$\Delta p_{th,de}^t$	$\mathbb{R}_0^+$	bar	Pressure decrease caused by temperature decrease after charging
$\Delta p_{th,in}^t$	$\mathbb{R}_0^+$	bar	Pressure increase caused by temperature increase after discharging
$\dot{V}_{rec}^t$	$\mathbb{R}$	$\frac{\mathrm{m_n^3}}{\mathrm{min}}$	Compressed air into (positive) or out of (negative) the air receiver tank
$\dot{V}_{bo}^t$	$\mathbb{R}_0^+$	$\frac{\mathrm{m_n^3}}{\mathrm{min}}$	Compressed air consumption of the booster at timestep t
P_{co}^t	$\mathbb{R}_0^+$	kW	Electrical power consumed by the compressors at timestep t
P_{bo}^t	$\mathbb{R}_0^+$	kW	Electrical power consumed by the booster at timestep t
P_{tot}^t	$\mathbb{R}_0^+$	kW	Total electrical power consumed by the CAES system at timestep t

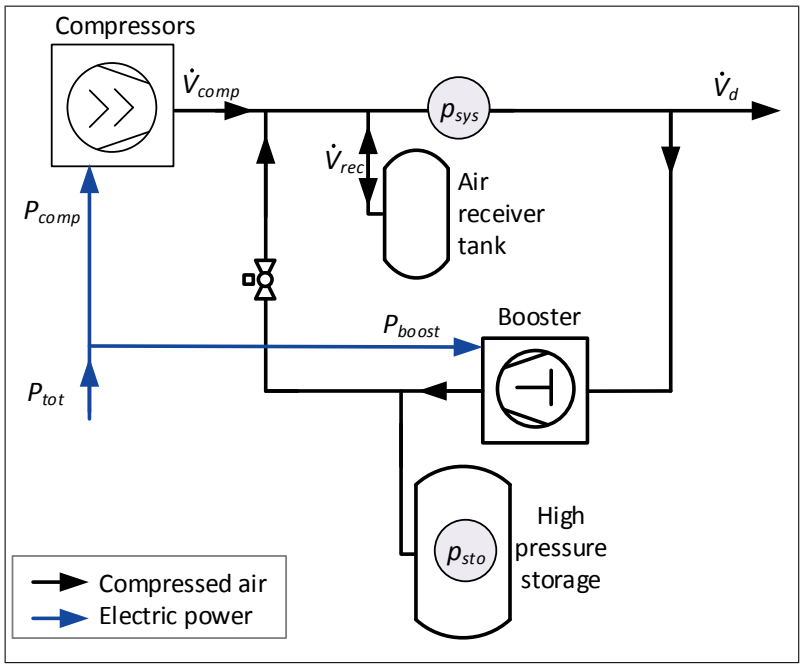

Figure 4.9: Structure of the nonlinear model of the CAES system

The total power consumption of the system P^t_{tot}, which is used to calculate the total costs (see eq. 4.1), is comprised of the power consumptions of the compressors P^t_{co} and of the booster P^t_{bo}.

$$P^t_{tot} = P^t_{co} + P^t_{bo} \tag{4.16}$$

Air receiver tank

The air receiver tank is used in compressed air systems to reduce compressor cycling by smoothing high-frequent variations of the air demand. The pressure in the air receiver tank is equal to the system pressure. When the CAES system is charged, the system pressure has to be increased for high storage pressures. To increase the pressure in the air receiver tank, additional air $\dot{V}_{rec}$ is needed, that has to be covered by the compressors. Figure 4.10 shows the increase of the system pressure during charging from time t_1 to t_2. When the CAES system switches to *normal* or *discharge* mode after charging, and the system pressure p^{t-1}_{sys} is higher than the normal system pressure $\hat{p}^{norm}_{sys}$, the receiver tank releases air $\dot{V}_{rec}$ to reduce its pressure. This air covers the air demand $\dot{V}_d$ as long as the pressure in the tank is greater than the normal system pressure $\hat{p}^{norm}_{sys}$. As shown in figure 4.10, the power consumption of the system becomes zero during this period (between t_2 and t_3).

Using the ideal gas equation of state (see eq. 3.1) the additional air to raise the pressure (positive $\dot{V}_{rec}$) or the released air to decrease it (negative $\dot{V}_{rec}$), can be calculated by the pressure difference from p^{t-1}_{sys} to p^t_{sys} as follows[1].

[1] It is assumed, that the air temperature is constant. The parameters of this equation have to be converted to SI units. The absolute pressure value has to be used.

$$\dot{V}_{rec} = \frac{60\ \frac{s}{min}}{\Delta t} \cdot (p_{sys}^{t} - p_{sys}^{t-1}) \cdot \frac{V_{rec}}{p_n} \tag{4.17}$$

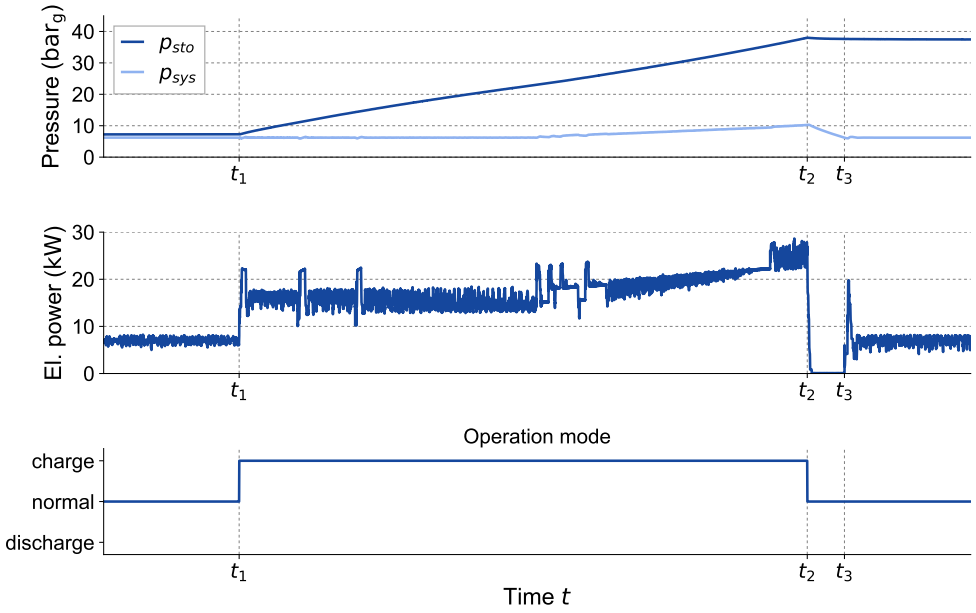

Figure 4.10: Storage and system pressure and total power consumption of the CAES system during a charging process

Compressors

In the nonlinear model, the dependence of the power consumption of the compressors on the system pressure and the air demand can be modeled in more detail than in the MILP model, using a polynomial function of degree 3.

When the system is in *normal* mode, the compressors have to cover the air demand $\dot{V}_d^t$. If the system was charging one timestep before and the system pressure was increased, the air out of the receiver tank $\dot{V}_{rec}$ covers a part of this demand.

In the operation mode *charge*, in addition to the air demand of the system $\dot{V}_d^t$, the air demand of the booster $\dot{V}_{bo}$ and the air needed to increase the pressure in the receiver tank $\dot{V}_{rec}$ has to be covered. Thereby the air demand of the booster $\dot{V}_{bo}$ is not constant during the charging process and depends on the storage pressure p_{sto}^t. In contrast to the LP and MILP model, this relation is taken into account in the nonlinear model (see eq. 4.19). The increase of the system pressure related to normal system pressure ($p_{sys}^t - \hat{p}_{sys}^{norm}$) also affects the power consumption of the compressors. The relation between the system pressure p_{sys}^t and the storage pressure p_{sto}^t during charging is formulated in the same way as in the MILP model (see eq 4.11 and figure 4.6).

In *discharge* mode, the air demand is covered by the high-pressure storage and the air delivered by the compressors is zero.

$$P_{co}^{t} = \begin{cases} \varsigma_1 \cdot (\dot{V}_d^t + \dot{V}_{bo} + \dot{V}_{rec}) + \varsigma_2 \\ + (p_{sys}^t - \hat{p}_{sys}^{norm}) \\ \quad \cdot (\varsigma_3 \cdot (\dot{V}_d^t + \dot{V}_{bo} + \dot{V}_{rec})^3 \\ \quad\quad + \varsigma_4 \cdot (\dot{V}_d^t + \dot{V}_{bo} + \dot{V}_{rec})^2 \\ \quad\quad + \varsigma_5 \cdot (\dot{V}_d^t + \dot{V}_{bo} + \dot{V}_{rec}) \\ \quad\quad + \varsigma_6) & \text{in } \textit{charge} \text{ mode,} \\ \varsigma_1 \cdot (\dot{V}_d^t + \dot{V}_{rec}) + \varsigma_2 & \text{in } \textit{normal} \text{ mode,} \\ 0 & \text{in } \textit{discharge} \text{ mode.} \end{cases} \tag{4.18}$$

$$\dot{V}_{bo}^{t} = \beta_7 \cdot {p_{sto}^t}^2 + \beta_8 \cdot p_{sto}^t + \beta_9 \tag{4.19}$$

Figure 4.11 shows the modeled compressor power in comparison with measured values. Especially the power consumption for an increased system pressure is represented in more detail than with the MILP model (see figure 4.6). As in the MILP model, energy losses during start-up and shut-down of the compressors are considered in the nonlinear model (see appendix B.3).

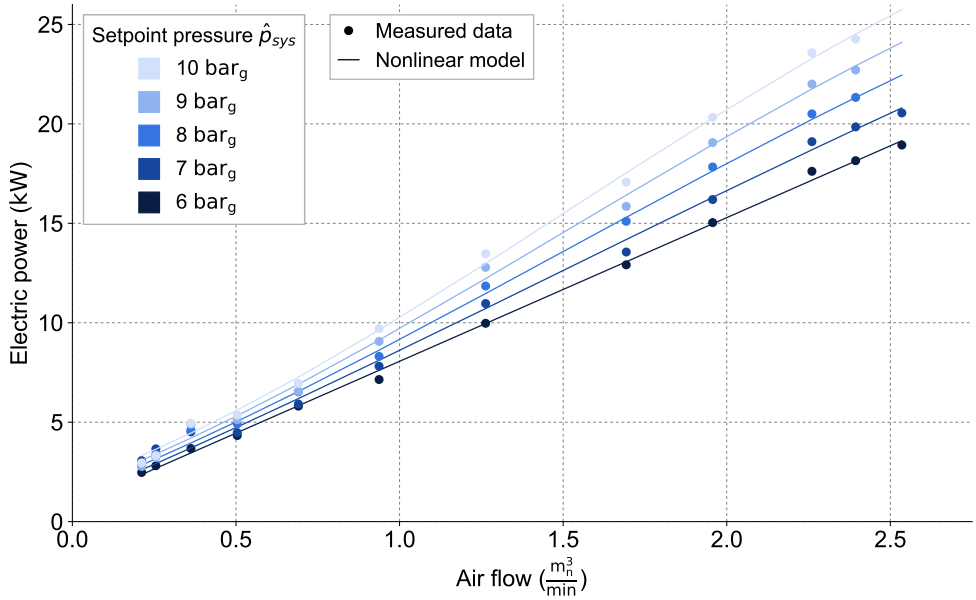

Figure 4.11: Nonlinear model for the electric power consumption of the compressors

Booster

In the nonlinear model, the dependency of the power consumption of the booster on the storage pressure p_{sto}^t is defined as a polynomial function of degree 5. Figure 4.12 shows the modeled power consumption of the booster compared to measured values. The nonlinear formulation results in a better representation of the power consumption, in comparison with the MILP model (see figure 4.7). For the booster as well, losses for start-up and shut-down are considered, as described in appendix B.3.

$$P_{bo}^t = \begin{cases} \beta_1 \cdot (p_{sto}^t)^5 + \beta_2 \cdot (p_{sto}^t)^4 + \beta_3 \cdot (p_{sto}^t)^3 \\ + \beta_4 \cdot (p_{sto}^t)^2 + \beta_5 \cdot (p_{sto}^t) + \beta_6 & \text{in } \textit{charge} \text{ mode,} \\ \\ 0 & \text{else.} \end{cases} \tag{4.20}$$

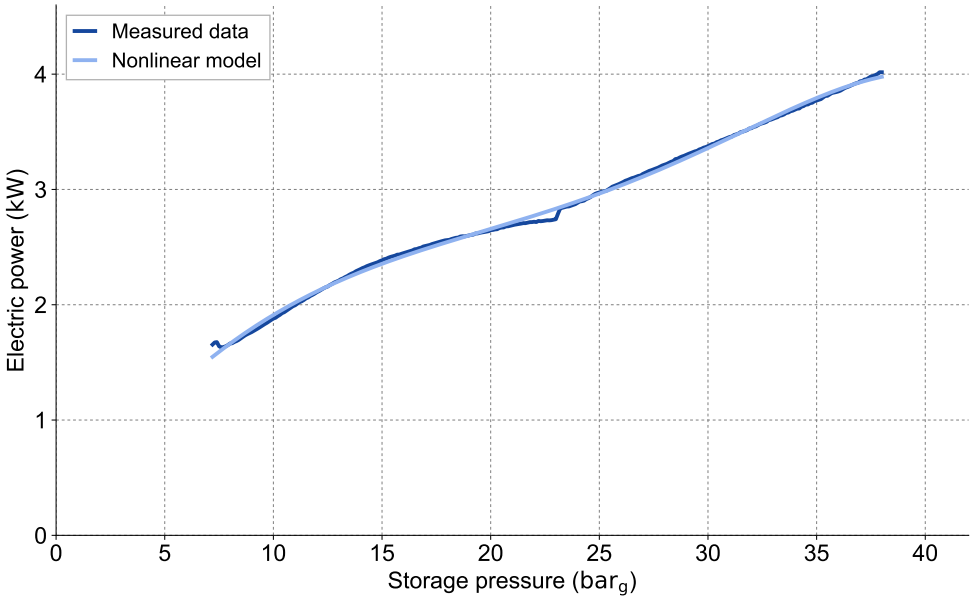

Figure 4.12: Nonlinear model for the electric power consumption of the booster

Storage

The pressure in the high-pressure storage tank at the beginning of the next timestep p_{sto}^{t+1} depends on the storage pressure p_{sto}^{t} at timestep t and the operation mode of the system. In addition to the pressure increase $\Delta p_{sto,ch}^{t}$ and decrease $\Delta p_{sto,dch}^{t}$ during charging and discharging, pressure changes $\Delta p_{th,in}^{t}$ or $\Delta p_{th,de}^{t}$ because of variations of the air temperature, are taken into account in the nonlinear model.

$$p_{sto}^{t+1} = \begin{cases} p_{sto}^{t} + \Delta p_{sto,ch}^{t} & \text{in } \textit{charge} \text{ mode,} \\ p_{sto}^{t} + \Delta p_{th,in}^{t} - \Delta p_{th,de}^{t} & \text{in } \textit{normal} \text{ mode,} \\ p_{sto}^{t} - \Delta p_{sto,dch}^{t} & \text{in } \textit{discharge} \text{ mode.} \end{cases} \tag{4.21}$$

The pressure increase during charging is described as a polynomial function of degree 3, dependent on the previous storage pressure p_{sto}^{t}.

$$\Delta p_{sto,ch}^{t} = \Delta t \cdot \left(\delta_{ch,1} \cdot (p_{sto}^{t})^3 + \delta_{ch,2} \cdot (p_{sto}^{t})^2 + \delta_{ch,3} \cdot p_{sto}^{t} + \delta_{ch,4} \right) \tag{4.22}$$

The pressure decrease during discharging depends on the air demand of the system $\dot{V}_{d}^{t}$ (taking into account the air provided by the air receiver tank $\dot{V}_{rec}^{t}$) and the previous storage pressure p_{sto}^{t} and is modeled as follows.

$$\Delta p_{sto,dch}^{t} = \Delta t \cdot \left(\frac{\delta_{dch,1} \cdot (\dot{V}_{d}^{t} + \dot{V}_{rec}^{t})}{\delta_{dch,2} + (\dot{V}_{d}^{t} + \dot{V}_{rec}^{t})} + \delta_{dch,3} \cdot p_{sto}^{t} + \delta_{dch,4} \right) \tag{4.23}$$

In *normal* mode, the pressure storage is neither charged nor discharged. Nevertheless, changes in the storage pressure caused by temperature variation have to be taken into account. During charging, the air in the storage is heated up. After switching from *charge* to *normal* mode, the air in the storage slowly cools down, which leads to a pressure decrease $\Delta p_{th,de}^{t}$ (see figure 4.13). Analogous to the up-heating during charging, the air in the storage cools down when the CAES system is discharged. After switching from *discharge* to *normal* mode, the air in the storage slowly heats up, which leads to a pressure increase $\Delta p_{th,in}^{t}$. The pressure decrease and increase are modeled by an exponential function of the storage pressure of the form $\Delta p = \Delta p_0 \cdot e^{-kt}$. The mathematical formulation is described in appendix B.3.1, eq. B.47 and B.48.

As for the LP and the MILP model, the equations of the nonlinear model are used to calculate the storage pressure profile for a charge and three discharging processes, as shown in figure 4.14. Compared to the other models (see figures 4.3 and 4.8), the nonlinear model shows the best representation of pressure characteristics for charge and discharge. Here, only when discharging with $\dot{V}_{d}$=1.3 $\frac{\mathrm{m_n^3}}{\mathrm{min}}$, differences between the simulated and measured values can be seen.

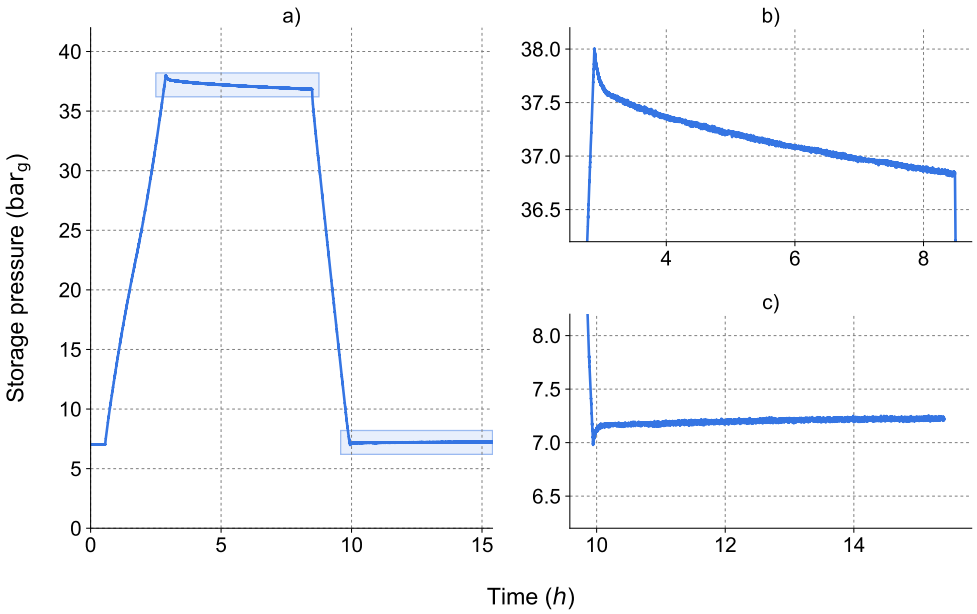

Figure 4.13: Pressure profile of an exemplary charge and discharge cycle of the CAES system (a) with magnified pressure decrease after charging (b) and pressure increase after discharging (c)

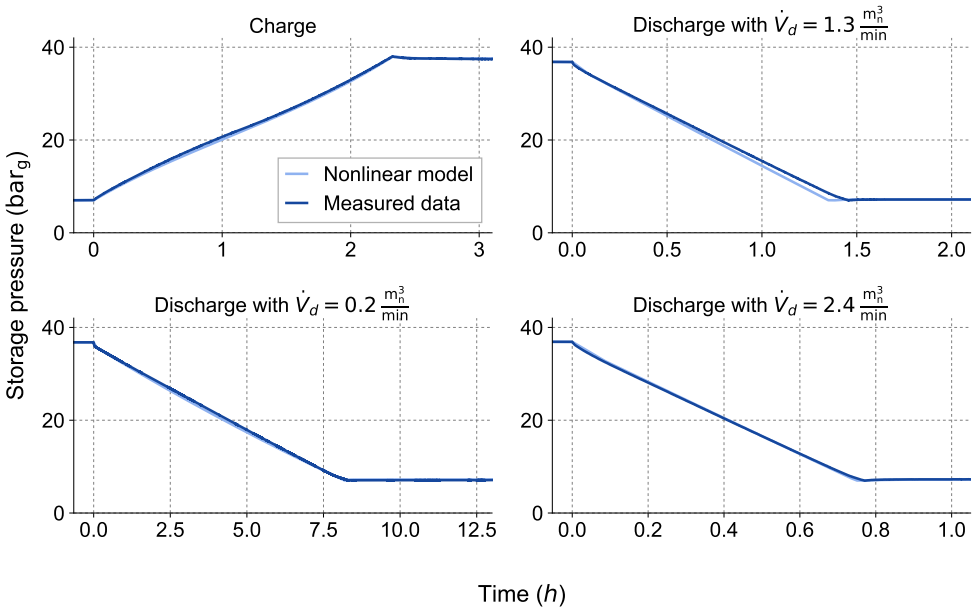

Figure 4.14: Calculated storage pressure for exemplary charging and discharging processes using the nonlinear model compared to measured data

4.5 Validation of the models

To validate the different models of the CAES system, simulation results for the storage pressure and total electrical power are compared to measured values.

4.5.1 Validation data

To obtain the validation data, three different control sequences with a time horizon of 24 hours are applied to the CAES system. In control sequence "normal", the system is in *normal* operation mode the whole time, so that the compressors cover the complete air demand. In control sequence "random", a randomly chosen sequence of the operation modes *normal*, *charge* and *discharge* is used. The third sequence "2 cycles" is chosen to result in two full charge and discharge cycles of the system. For each control sequence two measurements with a different air demand profile are performed.

Figure 4.15 shows the measured storage pressure and total electrical power consumption of the CAES system for the three control sequences with the *typical working day* air demand profile, as described in chapter 5.1.1. The same data for the air demand profile *typical non-working day* is shown in figure 4.16. Because of the lower air demand in the non-working day profile, the pressure decreases slower during discharging, which leads to different pressure profiles. Also the power consumption of the system is lower because of the lower air demand.

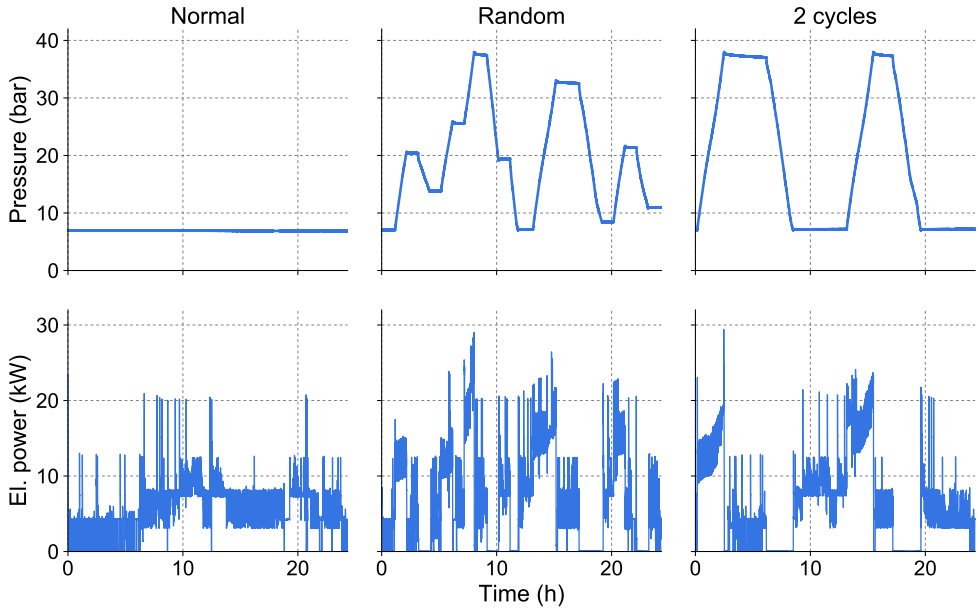

Figure 4.15: Validation data for air demand *working day*

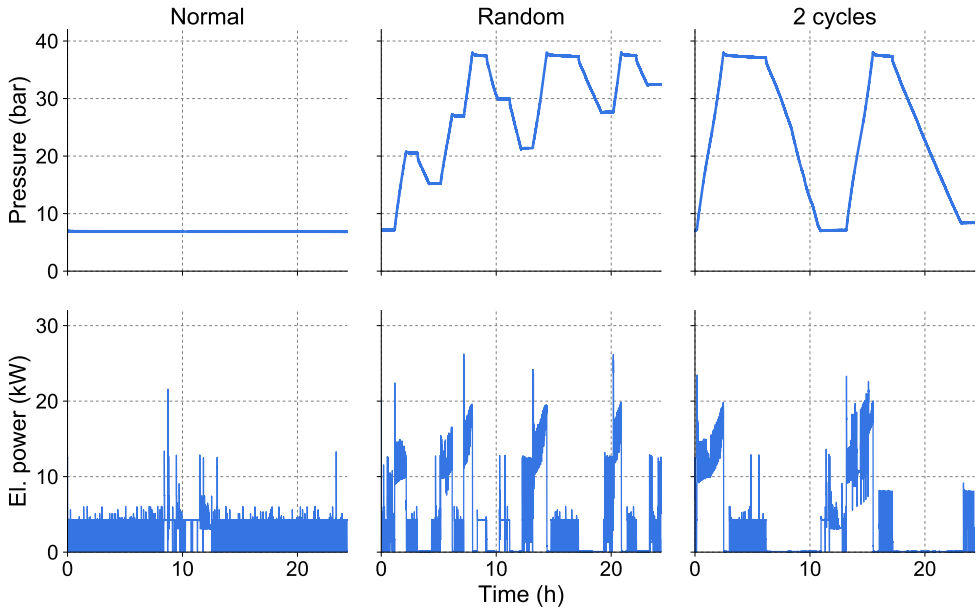

Figure 4.16: Validation data for air demand *non-working day*

4.5.2 Results

For each model, the equations described in this chapter are used to simulate the operation of the CAES system. The operation mode for each timestep is given by the measured validation data. Figure 4.17 shows the resulting pressure storage and power consumption of the CAES system using the linear (LP), the mixed-integer (MILP) and the nonlinear (NL) model for the "random" control sequence with air demand *typical working day*. The models are simulated using a timestep size of 5 minutes. The results are compared to the measured data, which is aggregated to 5 minute average values for better visualization. Looking at the pressure profiles, it can be seen that the results of LP model show the largest deviation, while the NL model shows the best result.

To compare the results of the models, the mean absolute error of the pressure and the power consumption for each model and validation data set was calculated. The results are shown in figure 4.18. The LP model shows the poorest results for all cases regarding pressure and electric power. For the "random" and "2 cycle" cases, the NL model outperforms the MILP model in both, pressure and electric power simulation. In the "normal" cases, both models show the same results for the electrical power consumption.

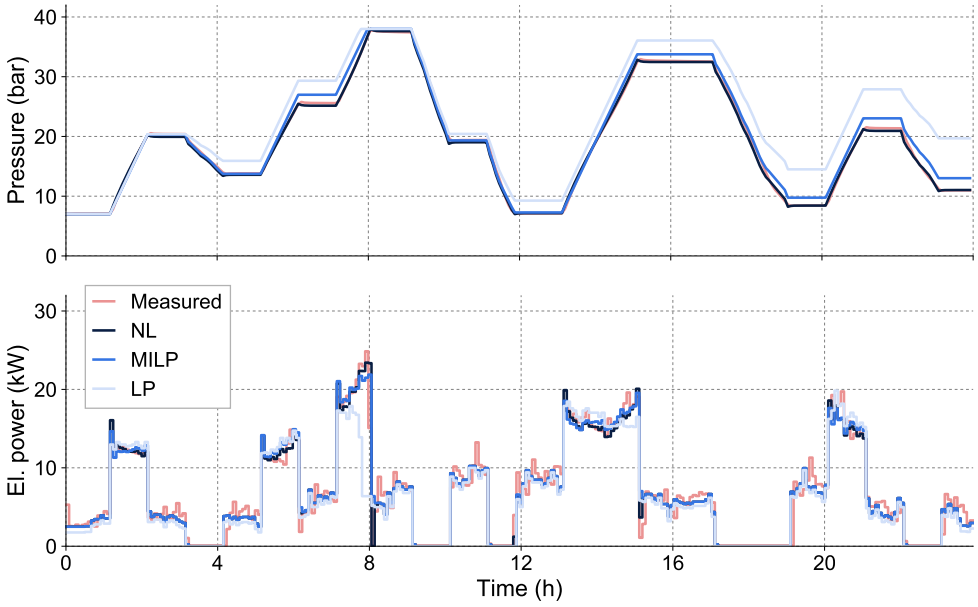

Figure 4.17: Simulated results using the equations of the linear (LP), the mixed-integer (MILP) and the nonliner (NL) model for the "random" control sequence with air demand "typical working day"

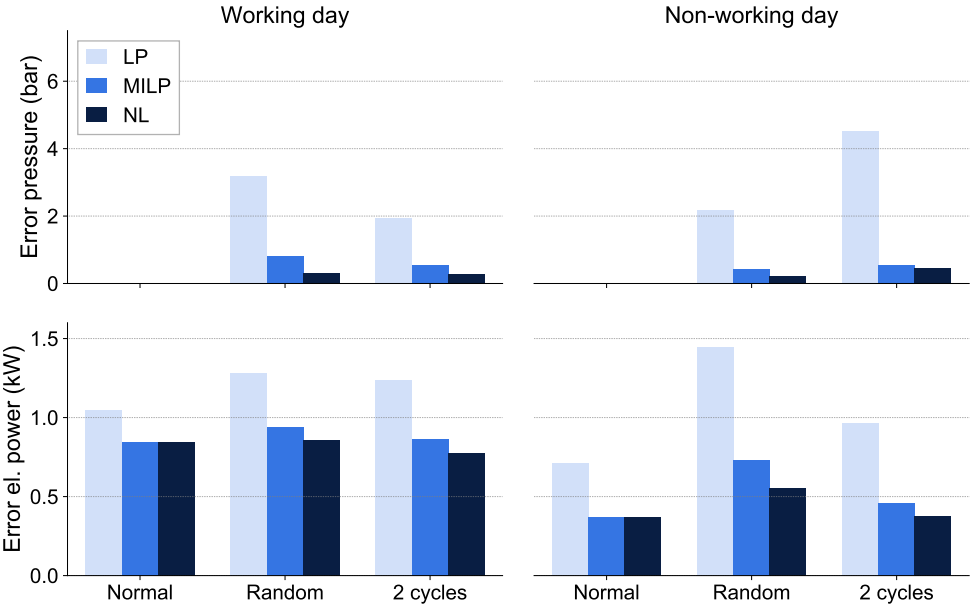

Figure 4.18: Mean absolute error of pressure and electric power of the linear model (LP), the mixed-integer linear model (MILP) and the nonlinear model (NL)

Chapter 5

Model Predictive Control of the compressed air energy storage system

In this chapter, the optimization models are used for the Model Predictive Control (MPC) of the compressed air energy storage (CAES) system, with the objective to cover a given air demand over 24 hours with minimal costs. In the first part of this chapter, the general implementation of MPC for the CAES system is described and the scenarios are defined. The experiments are performed with different air demand and electricity price scenarios. Additionally, the influences of the optimization timestep size and the quality of the air demand forecast are investigated. Then, preliminary investigations and the optimization parameters are described. In the third part of this chapter, the results of the comparison between the optimization methods are presented.

5.1 Implementation

Figure 5.1 shows an overview of the implementation of MPC for the CAES system. The CAES system always starts with an empty storage ($p_{sto} = 7\,\text{bar}$) and in *normal* operation mode. For each experiment, a given air demand for one day (24 hours) has to be covered. A time-sensitive electricity price is applied as an incentive to make sure that the storage system is used. Forecasts for the air demand and the electricity price are used as inputs to the optimization. Depending on the chosen model and optimization method, the optimal future control sequence for the 24-hour time horizon is calculated, so that the electricity costs are minimized. The first control signal, which represents one of the possible operation modes, *normal*, *charge* or *discharge*, is then applied to the CAES system. The superior controller prevents the applied target operation mode from being invalid by setting the concrete operation mode to *normal* if necessary (see chapter 3.3). After every multiple of the timestep size, the storage pressure, the system pressure and the concrete operation mode are measured and used to start a new optimization for the remaining time horizon. To make sure that the results of the different experiments can be compared, the end of the optimization horizon is not shifted towards the future, but stays at the end of the 24-hour time horizon of the experiment.

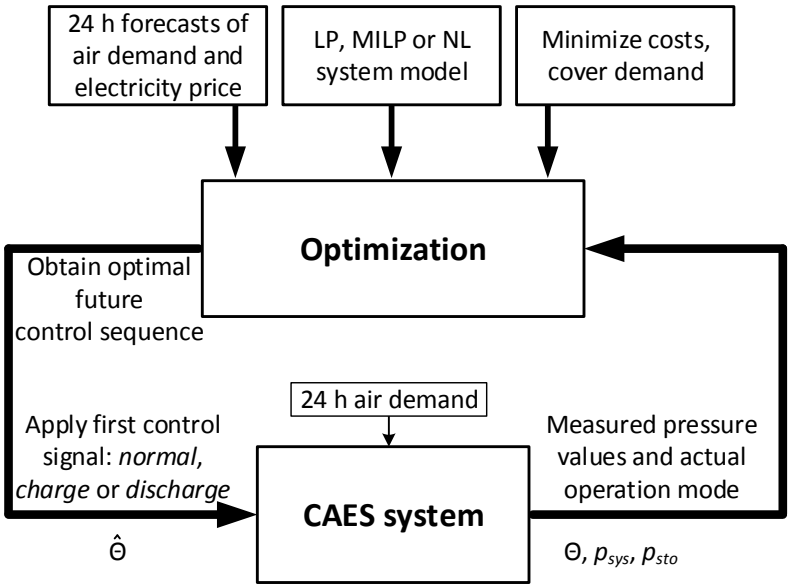

Figure 5.1: Implementation of MPC for the CAES system

To compare the results of the different optimization methods, various experiment scenarios varying the air demand, the forecast quality and the electricity price are used. Additionally, two different values for the timestep size of the optimization are used to investigate their influence on the results. Table 5.1 provides an overview of all experiment scenarios used in this thesis to compare the different optimization methods. A detailed description of the respective differences is given in the following sections.

5.1.1 Air demand time-series and forecast scenarios

In order to apply realistic values of the air demand of an industrial compressed air system for the experiments within this thesis, real measured air demand time-series data is used. Therefore, the compressed air demand of the toolmaking department of an automotive manufacturer was measured for one year with a time resolution of one minute. Since the compressed air system of this department has a maximum free air delivery of about 20 $\frac{m^3_n}{min}$ and a maximum measured air demand of 18 $\frac{m^3_n}{min}$, the values have to be scaled down to be used for the compressed air system introduced in this chapter. The scaling factor is fixed to 8 based on the relation of the maximum free air delivery of the two systems. All following values for the air demand are already scaled by the factor of 8. Table 5.2 shows the minimum, mean and maximum values for the measured and scaled air demand data.

To compare different methods of Model Predictive Control, in the performed experiments in this thesis air demand time-series for one day (24 hours) are used. To find typical days for the air demand, they are separated into *working days* and *non-working days*. Therefore, the weekends and the official holidays of Bavaria are defined as non-working days. This may differ from the real working and non-working days of the department because of some days of weekend work or company holidays.

Table 5.1: Scenarios used in this thesis to compare the different optimization methods

Forecast	Air demand	Electricity price	Timestep size
Perfect	Working day	Typical	5 minutes
			15 minutes
		Untypical	5 minutes
			15 minutes
	Non-working day	Typical	5 minutes
			15 minutes
		Untypical	5 minutes
			15 minutes
Inaccurate	Working day	Typical	5 minutes
			15 minutes
	Non-working day	Typical	5 minutes
			15 minutes
Worst-case	Working day	Typical	5 minutes
			15 minutes
	Non-working day	Typical	5 minutes
			15 minutes

Table 5.2: Scaled minimum, mean and maximum values of the measured air demand

Days	Minimum	Mean	Maximum
All days	$0\ \frac{m_n^3}{min}$	$0.57\ \frac{m_n^3}{min}$	$2.25\ \frac{m_n^3}{min}$
Working days	$0\ \frac{m_n^3}{min}$	$0.69\ \frac{m_n^3}{min}$	$2.25\ \frac{m_n^3}{min}$
Non-working days	$0\ \frac{m_n^3}{min}$	$0.33\ \frac{m_n^3}{min}$	$2.25\ \frac{m_n^3}{min}$

For the working and non-working days, the typical and the untypical day of air demand time-series were respectively determined. Therefore, the absolute difference of every minute of one day to the mean demand of the same minute of all considered days was calculated and summed up for the whole day. The day with the smallest error was chosen as the typical day and the day with the biggest error as the untypical day. These demand time-series are used to simulate a *perfect* and a *worst-case* air demand forecast scenario for the experiments. Thereby, the air demand forecast used for the optimization always corresponds to the typical air demand. In the case of a *perfect* forecast, the same typical air demand is applied to the CAES system, whereas for the *worst-case* forecast, the untypical air demand is applied.

Additionally, an *inaccurate* forecast scenario is defined, where the difference of the applied air demand to the typical air demand used for the optimization is less than in the worst case scenario. Therefore, for the working and the non-working day, respectively, the day 7 days after the typical day is chosen. Since this is the same day of the week and in the same period of the year, this is considered to represent a realistic relation between forecast and actual demand.

Figure 5.2 shows the air demand for the typical and untypical working day as well as for the

day seven days after the typical one. Figure 5.3 shows the same graphs for the non-working day. Table 5.3 summarizes the definitions for the different forecast scenarios.

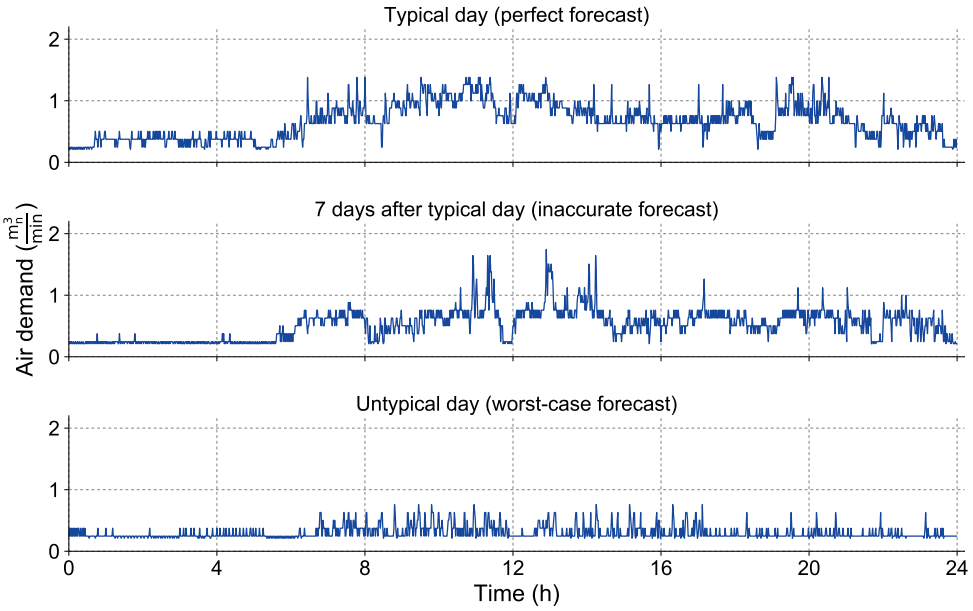

Figure 5.2: Working day air demands (used for the respective forecast scenario)

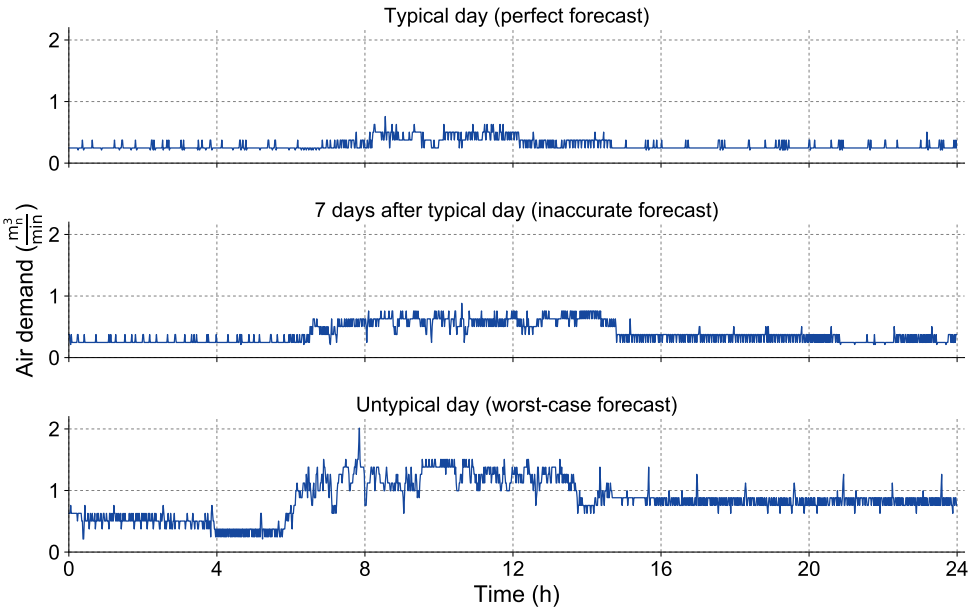

Figure 5.3: Non-working day air demands (used for the respective forecast scenario)

The available air demand was measured in a one minute resolution and this data is directly applied to the control valve of the CAES system. The timestep size of the optimization used in this thesis is either 5 or 15 minutes, as described in section 5.1.3. Therefore, the mean value of

Table 5.3: Definition of forecast scenarios

Forecast scenario	Air demand for the optimization	Air demand applied to CAES system
Perfect	Typical day	Typical day
Inaccurate	Typical day	7 days after typical day
Worst-case	Typical day	Untypical day

the air demand over one time period has to be aggregated and used for the optimization. This averaging over the optimization timestep size leads to a difference between the air demand used for the MPC and the air demand applied to the CAES system, even in the *perfect* forecast scenarios.

5.1.2 Electricity price scenarios

The variation over time of the electricity price provides the incentive to use the compressed air energy storage system. For the experiments to compare the optimization methods for MPC in this thesis, two different electricity price time-series are used. Based on the EPEX SPOT day-ahead auction prices for Germany (Phelix) in 2015, the days with the *typical* and *untypical* price curve were identified. To use them for this thesis, an offset was added to both curves, so that their mean values over the day result in 0.13 $\frac{€}{kWh}$, which is a typical electricity price for industrial customers in Germany. Additionally, for both curves, the difference to the mean value in each hour was scaled by a factor so that the difference between the maximum and minimum price of the day results in 0.15 $\frac{€}{kWh}$. This ensures a big enough incentive to use the storage system and prevents that the cheapest operation to cover the demand is staying in *normal* mode for the whole day.

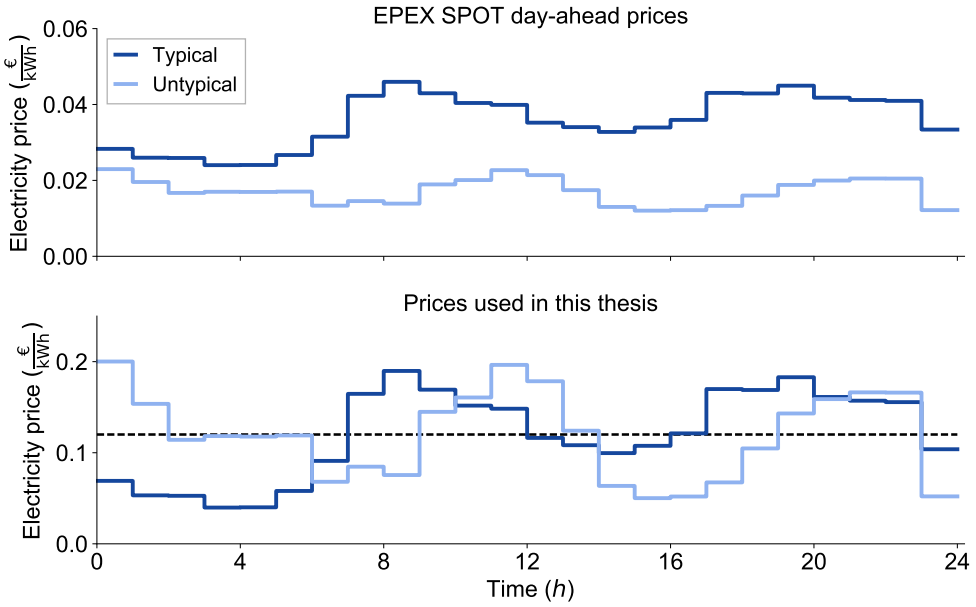

Figure 5.4: Electricity prices

5.1.3 Optimization timestep size

The timestep size of the optimization is an important parameter for Model Predictive Control. A large timestep size may result in poor accuracy of the model and the reduced possibilities to change the control signal based on measured parameters can lead to higher total costs. On the other hand, a small timestep size leads to a larger optimization problem that takes more time to be solved. This can result in an inexact solution either because the algorithm has to be aborted before finding the optimal solution or the parameters of the algorithm have to be adapted.

According to Müller [73] and Mauser [64], for the optimization of device operation, the timestep size is usually between 15 and 60 minutes. In the German power sector, a 15 minutes time period is currently the shortest temporal resolution of trading (EPEX SPOT intra day market) or measuring (industrial customers). Therefore, in this thesis, a timestep size of 15 minutes is used for optimization. To investigate the influence of a decrease in the timestep size, every experiment is additionally performed with a 5 minute timestep size, as shown in table 5.1.

5.2 Preliminary investigations and optimization parameters

5.2.1 Reference values

The results of the experiments using MPC for the CAES system are evaluated based on cost savings compared to the *normal* operation of the system in which the booster and high-pressure storage tank are not used and the air demand is always covered by the compressors. Therefore, reference measurements for each demand (see figures 5.2 and 5.3) were performed. Based on these measurements, the reference energy costs for each scenario defined in section 5.1 were calculated. The energy consumption and total costs for each reference measurement are summarized in table 5.4.

Table 5.4: Energy consumption and costs of the reference measurements

Air demand	**Electricity price**	**Energy consumption** (kWh)	**Costs** (€)
Working day (typical)	Typical	139.22	18.21
Working day (typical)	Untypical	139.22	17.08
Working day (7 days after typical)	Typical	109.73	14.17
Working day (untypical)	Typical	73.51	9.05
Non-working day (typical)	Typical	70.32	8.66
Non-working day (typical)	Untypical	70.32	8.56
Non-working day (7 days after typical)	Typical	86.49	10.84
Non-working day (untypical)	Typical	173.19	22.60

5.2.2 Influence of measurement inaccuracy and operation

When the CAES system is controlled using MPC, different parameters can influence the power consumption and thereby the resulting costs of one experiment. On the one hand, the power consumption of the compressors and the pressure of the storage tank depend on ambient

Table 5.5: Energy consumption, costs and cost savings of 4 experiments for the same scenario

Measurement	Energy consumption (kWh)	Costs (€)	Cost savings (€)
1	155.05	16.82	1.39
2	154.70	16.75	1.46
3	154.04	16.65	1.56
4	155.11	16.85	1.36
Maximum difference	2.17	0.20	0.20

conditions like temperature and humidity of the air. On the other hand, all measurement devices, such as the pressure transmitters and the power meters, have a certain measurement inaccuracy. Additionally, the compressors are not controlled directly. The MPC only gives the current operation mode to the SAM (as described in section 3.3), which decides which compressors are running based on internal calculations. Another influence that can affect the results is the initial storage pressure. Before every experiment, the storage is completely discharged to a pressure of 7 bar. As explained in section 4.4, temperature variations can lead to a small pressure increase after discharging the storage. Because the level of the pressure increase depends on the discharge time and the ambient temperature, the initial storage pressure is not exactly the same for every experiment.

To estimate the total possible deviation caused by the described influences, the same experiment is performed four times and compared regarding the cost savings. Therefore, MPC using LP as the optimization method[1] is applied to the scenario with *perfect* forecast, air demand *working day*, the *typical* electricity price and a timestep size of 5 minutes. Table 5.5 shows the energy consumption, costs and cost savings of these 4 experiments as well as the maximum difference of each parameter. These values can be used to assess and interpret the results, when the different optimization methods are compared.

5.2.3 Optimization parameters

Each optimization method is defined by various parameters that influence the solution quality and solving time. Since it is crucial for MPC that the problem is solved within the time period of one timestep, the optimization parameters have to be adjusted to ensure this. All optimization problems are solved using an Intel Core i7-3930K CPU 3.20 GHz, 64 GB RAM.

The linear programming (LP) and the mixed-integer linear programming (MILP) model are formulated with Pyomo [83] and solved using the state of the art solver CPLEX [40]. The solver allows one to set a time limit, that stops the solving process when the limit is exceeded and returns the best current solution. To ensure that the solution can be used for the MPC within one timestep period of 5 or 15 minutes, considering time for pre and post-processing, the time limit is set to 4 minutes and 30 seconds or 14 minutes and 30 seconds, respectively[2]. The maximum number of CPU threads to be used by the solver is set to 8. For the MILP problem,

[1] LP is used as the optimization method, because it finds the global optimum within the given time limit, so that the measured deviations are not caused by imperfect solutions of the optimization problem

[2] For all experiments performed within this thesis, the LP problem was always solved in under 1 minute so that the time limit was never exceeded. For the MILP problem with a 5 minute timestep size, in some cases the time limit was exceeded before the absolute or relative MIP gap was reached.

the relative MIP gap is set to 0.0001 and the absolute MIP gap is set to 0.001. For all other parameters, the default values are used.

The mixed integer nonlinear problem is also formulated with Pyomo but solved using the state of the art solver BARON [98]. BARON also allows to set a time limit and the maximum number of CPU threads. For both parameters the same values as for the LP and MILP settings are used. CPLEX is set as the LP solver, which is used by BARON to solve linear sub-problems. For all other parameters the default values are used.

For the implementation of the genetic algorithm (GA) the evolutionary computation framework DEAP [23] is used. DEAP does not allow to set a time limit to stop the solving process. Therefore, the number of individuals within one generation (population) and the number of generations which are evaluated define the solving time of this algorithm. Based on investigations of Jungwirth [42], the number of individuals of one generation is set to 10, the mutation probability to 1/N (where N is the number of timestep) and the crossover probability to 0.7. Given this parameters, the number of generations has to be chosen such that the time limit of 5 minutes or 15 minutes, respectively, is not exceeded. Based on empirical experiments, the number of generations is set to 7 or 90, respectively. For all other parameters the default values are used.

To implement dynamic programming as an optimization method for MPC in this thesis, a new open-source toolbox prodyn was developed and published online [24]. prodyn is a generic implementation of the dynamic programming algorithm for optimal system control written in Python. The time for solving a DP problem using prodyn can not be limited to a maximum value. Therefore the number of discretization steps for the state variable, which is the storage pressure in this case, has to be adjusted to ensure that the problem is solved within the given time limits. Empirical experiments showed that, with 621 discretization steps, the time for solving the problem does not exceed the time limit for the 5 minute optimization timestep. For the storage pressure, which is limited by its minimum value of 7 bar and its maximum value of 38 bar, this results in a discretization step size of 0.05 bar. For the 15 minute optimization timestep size, the discretization steps can be increased to 3101, which results in a discretization step size of 0.01 bar for the storage pressure.

The software and solvers with the parameters used for the different optimization methods are summarized in table 5.6.

5.2.4 Comparison of the nonlinear optimization methods

Before the differences of the linear, mixed-integer and nonlinear models for MPC are investigated, one of the nonlinear optimization methods is chosen. Therefore, all three nonlinear optimization methods, MINLP, DP and GA, are used for MPC of the CAES system for the scenario with the air demand *working day*, a *perfect* forecast and a *typical* electricity price. For each method, the experiment is performed using an optimization timestep size of 5 and 15 minutes. Figure 5.5 shows the resulting costs for the different methods. Additionally, the reference costs (Ref) for normal operation of the CAES system without using the storage are shown (see section 5.2.1).

For both scenarios, the DP method shows the best result, leading to the lowest costs. Since the resulting costs are almost the same for both scenarios, it seems that the error made because

Table 5.6: Parameter settings of the used software and solvers for the different optimization methods

Method	Software/solver	Optimization parameters
Linear programming (LP)	Pyomo/CPLEX	– Maximum threads = 8 – Time limit = 870 s (15 minute timestep size) – Time limit = 270 s (5 minute timestep size)
Mixed-integer linear programming (MILP)	Pyomo/CPLEX	– Maximum threads = 8 – Relative MIP gap = 0.0001 – Absolute MIP gap = 0.001 – Time limit = 870 s (15 minute timestep size) – Time limit = 270 s (5 minute timestep size)
Mixed integer nonlinear programming (MINLP)	Pyomo/BARON	– Maximum threads = 8 – LP solver = CPLEX – Time limit = 870 s (15 minute timestep size) – Time limit = 270 s (5 minute timestep size)
Dynamic programming (DP)	prodyn	– Discretization steps = 3101 (15 minute timestep size) – Discretization steps = 621 (5 minute timestep size)
Genetic algorithm (GA)	DEAP	– Population = 10 – Crossover probability = 0.7 – Mutation probability = 1/N – Generations = 90 (15 minute timestep size) – Generations = 7 (5 minute timestep size)

of the discretization of the storage pressure in order to ensure the problem is solved within one time period has only minor affects on the results. Using the MINLP and the GA method to solve the optimization problem, the costs using the MPC correspond to the reference costs (the small deviations are caused by measurement inaccuracy, as explained in section 5.2.2). This is the case, because both methods were not able to find a control schedule leading to lower costs than the normal operation mode of the system.

To analyze how much the limited solving time influences the optimization result of the different methods, the respective limiting parameters[3] are increased and the first optimization problem of the MPC for the 15 minute scenario (from the first timestep until the end of the horizon) is solved. The solution is then used as an input for the nonlinear simulation model (as used for the validation of the nonlinear model in chapter 4.5, the results are not applied to the real CAES system in this case). The resulting costs calculated by the simulation over the solving time are shown in figure 5.6. The results show, that using the DP method, the solution found within the required 15 minutes already is very close to the optimal solution and an increase of discretization steps does not bring a benefit. For the MINLP method the resulting costs decrease with the increase of the allowed solving time. It seems that the best solution is still not found after 12 hours. This shows, that the MINLP method, which is able to solve a wide range of general optimization problems, is not suited to solve the given problems in the time required to implement MPC. The results of the GA show, that this method is not able to find a

[3]The following values are used for the increase of the limiting parameters (see section 5.2.3):
Discretization steps for DP: 3101, 12401, 31001, 62001, 310001, 496001
Time limits for MINLP: 15 min, 1 h, 2 h, 4 h, 12 h
Number of generations for GA: 90, 360, 720, 1440, 4320

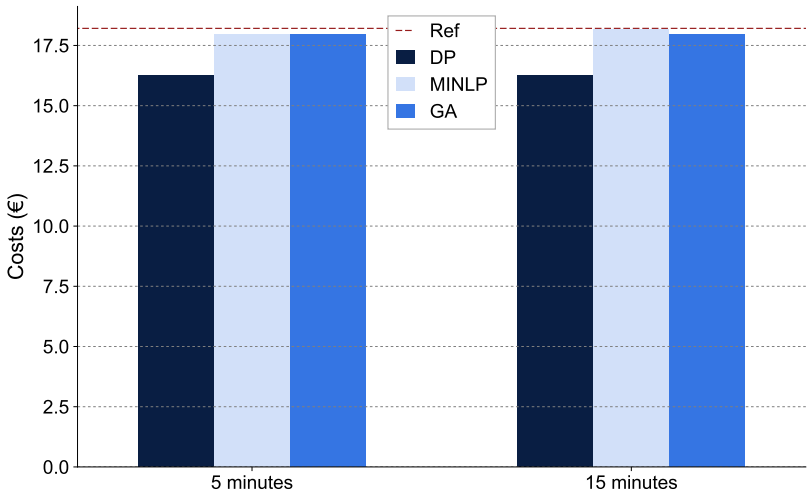

Figure 5.5: Cost comparison of the nonlinear optimization methods for scenario *perfect* forecast, air demand *working day* and *typical* el. price with 5 and 15 minutes timestep size

better solution than operating in *normal* mode for all calculated cases except the last one. The principle of the genetic algorithms is to evaluate a number of candidate solutions and create new candidates using different genetic operators. The number of possible solutions for this problem is 3^{96}, where only 10^{-40} % of these possibilities can be evaluated in the case with 4320 generations, which takes about 12 hours. This shows that the given problem is too big to reliably find a good solution using GA within the required time limit.

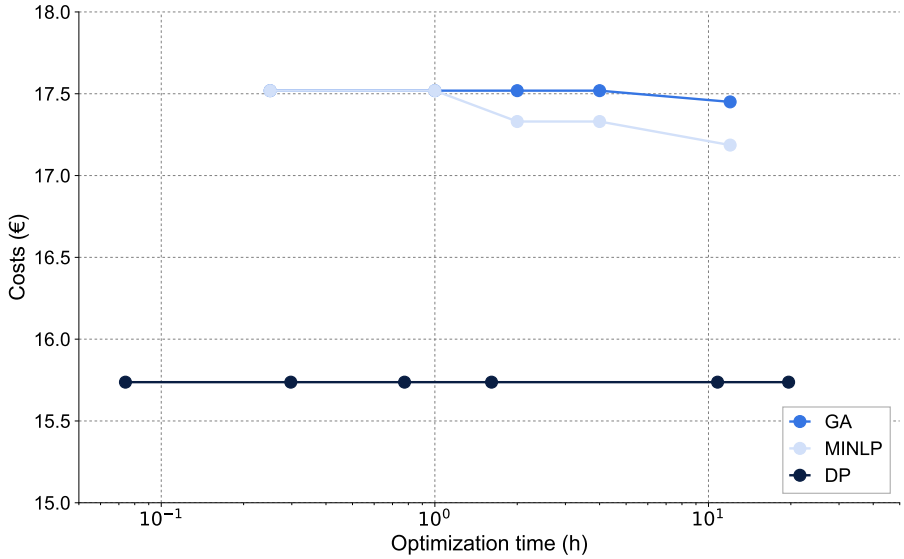

Figure 5.6: Simulated daily costs over solving time of the nonlinear optimization methods (air demand *working day*, *typical* el. price, 15 minutes timestep size)

The results show that DP is the most suitable method to solve the nonlinear optimization problems in this thesis. Therefore, in the following DP is compared with the LP and MILP method for MPC of the CAES system.

5.2.5 Differences of the models in completely charging/discharging the storage

How the pressure increases and decreases just before the storage is completely full or empty is implemented in the different models can have a distinct influence on the optimization results, especially for the MILP model. To illustrate the differences between the models, figure 5.7 shows the modeled time curves of the storage pressure used for the optimization methods LP, MILP and DP. The pressure curves are shown for a timestep size of 15 and 5 minutes.

For the 15 minute step size example, the storage pressure is at 36.5 bar at the beginning of timestep 1. When the CAES system is in operation mode *charge* during the first timestep, the maximum storage pressure of 38 bar is reached after half of the period. In this case, the superior mode controller changes the operation mode to *normal* (see chapter 3.3).

The nonlinear model used for DP is able to divide a time period in which the pressure limit is exceeded in two parts for internal calculations. As for the real system, the storage is in *charge* model until the pressure is full and switches to *normal* mode after. For the solution of the optimization problem, in which one period can only have one operation mode, here the mode is set to *charge*. As described before, the superior mode controller prevents the pressure from being raised above its maximum value when the result is applied to the CAES system.

Using the LP method, dividing one time period into two parts is not possible. But because the charging power, which represents the pressure increase, is only limited to an upper bound when charging (specifying an exact value is not possible without integer variables), it can be reduced so that the maximum pressure is reached exactly at the end of the period. This is not possible for the real system, since the booster can either be on or off and leads to an inaccurate calculation of the power consumption. But since any charging power greater than zero is treated as mode *charge* for the solution of the optimization problem, for this example it would lead to the same results as with the DP method.

In the MILP model, the pressure increase during one timestep is determined exactly. Also dividing the period into two parts is not possible. This is a more realistic representation than with the LP model, but it also means that the storage can not be completely charged in this case. For the internal calculations, running the system in *charge* mode during the first timestep would lead to a storage pressure that is greater than the maximum allowed value. Since this does not satisfy the constraint $p_{sto} \leq 38\,\text{bar}$, it is not a feasible solution of the MILP method. Further charging of the system using MPC with the MILP method is therefore not possible and it has to run in *normal* (or *discharge*) mode. The same problem can occur during discharging so that the storage can not be discharged completely. This limitation in using the whole storage capacity can lead to lower cost savings using the MILP method. As also shown in figure 5.7, a smaller timestep size of 5 minutes reduces this problem. The shorter periods allow the MILP model to use more of the storage capacity by getting closer to the pressure limits.

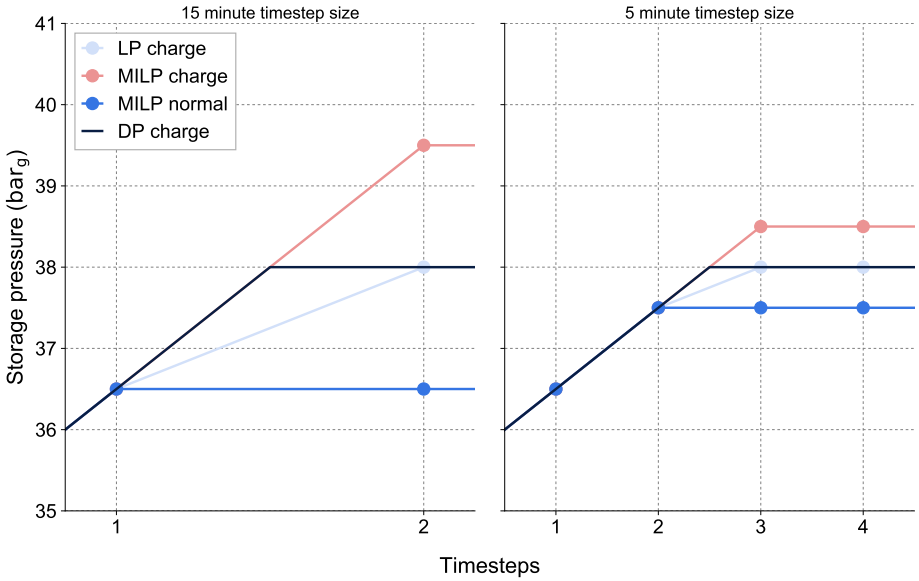

Figure 5.7: Pressure increase at the end of the charging process

In figure 5.8, the optimization results using MILP for the same scenario with slightly different initial storage pressures of 7.0 bar and 7.1 bar are shown. The small difference in the starting pressure results in very different solutions for the same optimization problem, which will lead to different costs when used for MPC. As explained in section 5.2.2, the initial storage pressure for the experiments is not always exactly the same. Therefore, the effects of this deviation on the results of the MILP model has to be taken into account when the results are discussed.

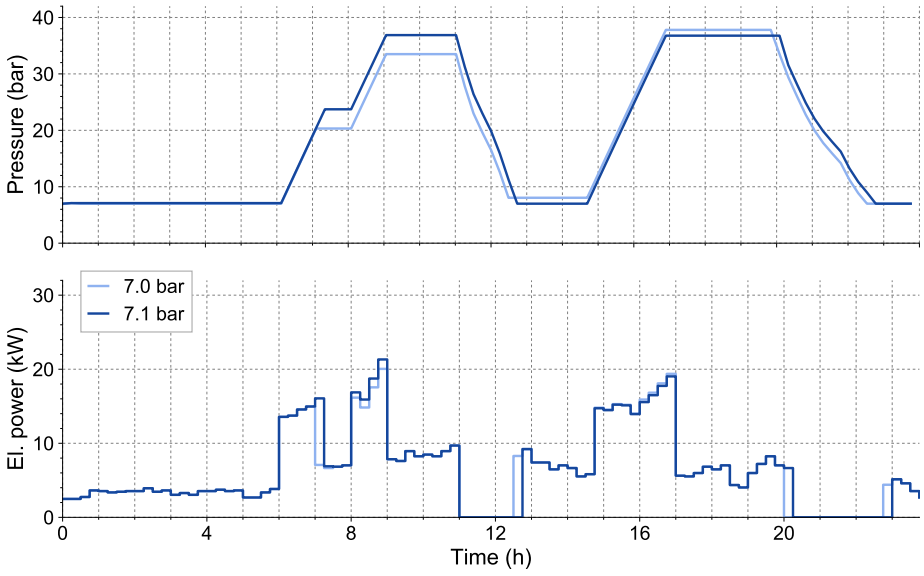

Figure 5.8: Comparison of the optimization results of the MILP model with different initial storage pressures

5.3 Results

To compare the optimization methods LP, MILP and DP for Model Predictive Control of the compressed air energy storage system, various experiments with different scenarios for the air demand, the electricity price and the forecast quality are performed. Primarily, the experiments are performed with a optimization timestep size of 15 minutes. The influence of the reduction of the timestep size to 5 minutes is then discussed in section 5.3.3. The results of the different methods and scenarios are evaluated based on the achieved cost savings compared to the respective reference costs (see chapter 5.2.1, table 5.4) over the 24 hour time horizon.

5.3.1 Perfect air demand forecast

At first, the optimization methods are compared using a *perfect* forecast of the air demand. As shown in table 5.1, two different air demand scenarios, *working day* and non-working day, each with two different electricity price scenarios, *typical* and *untypical*, are used for the comparison. Figure 5.9 shows the storage pressure and the electric power consumption over time for the three optimization methods for the *working day* air demand using the *typical* electricity price. For reasons of clarity, the electric power consumption is aggregated to 15 minute values, which is the case for all of the following figures in this section. The charging and discharging times of the MILP and the DP methods are different, but the general pattern is very similar, which results in almost the same costs for both approaches (see figure 5.14). With the LP method, the storage is not completely discharged in the first cycle, because the model does not take into account that the booster consumes more power when the storage pressure is higher during charging. Additionally, the charge and discharge processes are sometimes interrupted for some time. This happens, when the feedback of the MPC differs from the predicted system behavior of the model and the control schedule has to be adapted. Therefore, the resulting costs of the LP method are higher than for the other two methods.

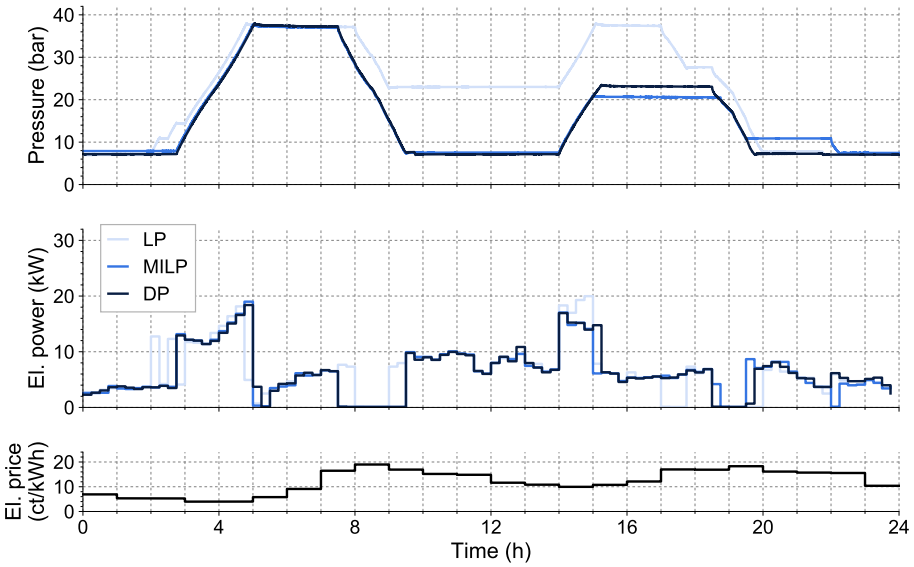

Figure 5.9: Results for *perfect* forecast, air demand *working day* and *typical* el. price

For the scenario using the *untypical* electricity price and the air demand *working day*, the charging and discharging times of all three methods have only little differences, as shown in figure 5.10. Using the DP method, the storage is charged completely and discharged without interruption during the first cycle. Using the LP and the MILP method, the storage is not fully charged, which leads to an interruption during discharging in a time with high electricity prices around hour 12. In the second charging process, it can be seen that the LP model overestimates the time for charging, as it starts charging a few minutes before the electricity price decreases at hour 15 but is already full a few minutes before the electricity price increases at hour 17. In contrast, the MILP model underestimates the charging time in such a way that the end of the charging process, where the most power is consumed, takes place after the price increase in hour 17. The DP model almost perfectly predicts the charging process, in such a way that it ends almost at the time of the price increase. This results in the lowest costs for the DP and the highest costs using the LP method, as shown in figure 5.14.

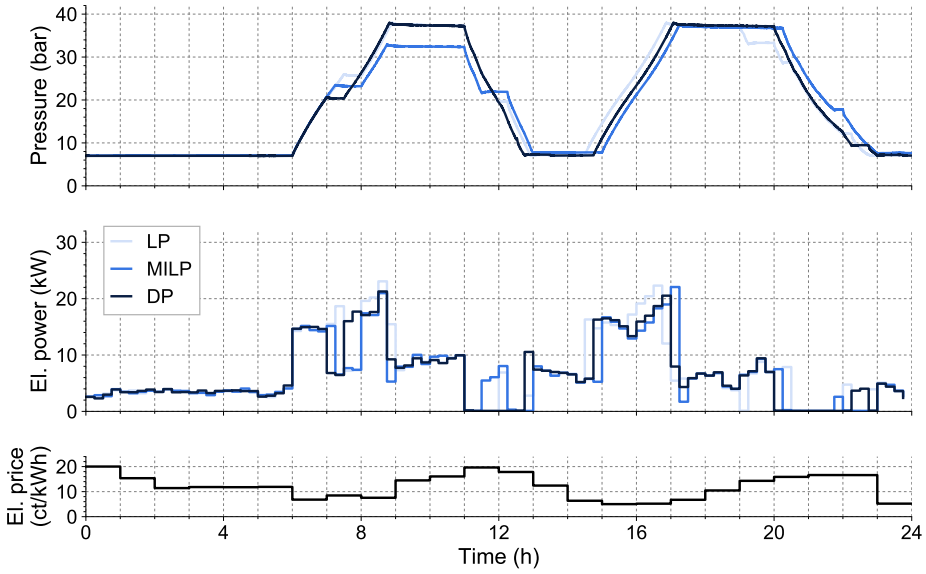

Figure 5.10: Results for *perfect* forecast, air demand *working day* and *untypical* el. price

The results of the scenario using the *untypical* electricity price and the air demand *non-working day* also show few differences between the optimization methods, as can be seen in figure 5.14. The resulting costs of the DP and the MILP method are almost the same, while the costs of the LP model are slightly higher caused by the corrections in the second cycle.

Figure 5.12 shows the storage pressure and power consumption for the scenario with air demand *non-working day* and the *typical* electricity price. Despite the repeated interruption during the first discharging process using the DP method and the correction using the LP method during the second cycle, the resulting costs for both methods are almost the same (see figure 5.14). One reason for the higher costs using the MILP model is that not the whole storage capacity can be used in the first cycle and that the storage is charged to a higher pressure level and cannot completely be discharged in the second cycle, because of the limitations of the MILP model described in section 5.2.5. Additionally, with the MILP method the charging of

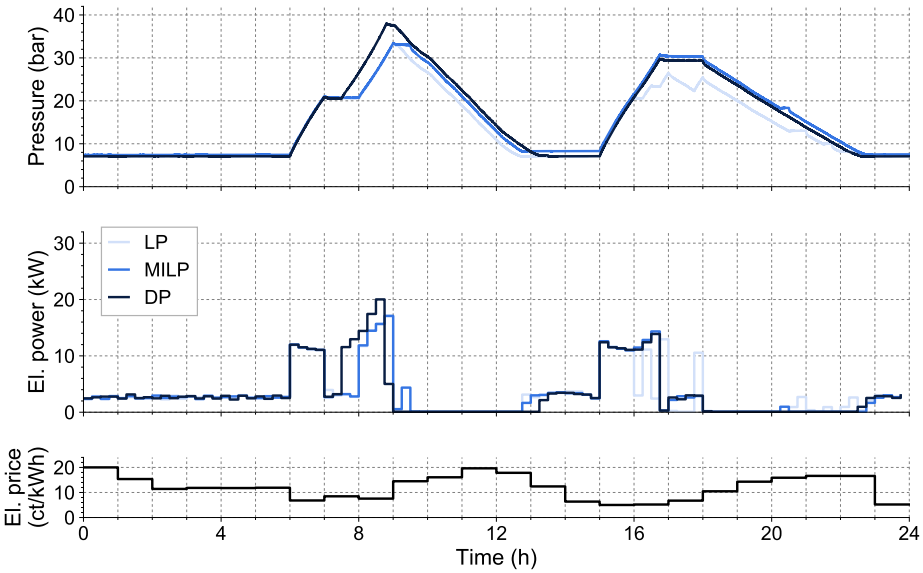

Figure 5.11: Results for *perfect* forecast, air demand *non-working day* and *untypical* el. price

the second cycle begins almost an hour before the charging with the LP and DP method. This happens because of the differences in modeling the power consumption during a charging process in combination with the electricity price, which has its minimum of the second half of the day in hour 15 (3.277 $\frac{\text{ct}}{\text{kWh}}$), while the prices of hour 14 (3.404 $\frac{\text{ct}}{\text{kWh}}$) and hour 16 (3.394 $\frac{\text{ct}}{\text{kWh}}$) are only slightly higher. Figure 5.13 shows an example of a measured power consumption during charging and the simulated power consumptions using the LP, MILP and nonlinear DP (NL) model. These are the first hours of the validation results for the scenario *2 cycles* for air demand *non-working day*, as described in chapter 4.5. All methods try to consume the most energy during hour 15. Since the charging power is constant for the LP model and the price in hour 16 is lower than in hour 14, it begins charging at the beginning of hour 15. For the DP model, the power consumption at the beginning of a charging process is higher than in the middle part. Therefore, here, the charging process starts at the beginning of hour 15 as well. As shown in figure 5.13, the MILP model underestimates the power consumption at the beginning and end of the charging process and overestimates it in the middle part. Therefore, the charging is started in hour 14 so the middle part of the charging process with the most energy consumption takes place during hour 15. This results in higher costs for the MILP model, because the real power consumption of the CAES system is more similar to the DP model.

Figure 5.14 shows the resulting cost savings of all scenarios with a *perfect* air demand forecast using an optimization timestep size of 15 minutes. Taking into account that the influence of measurement inaccuracy and the operation of the system can result in a cost difference of up to 0.20 € (see section 5.2.2), there is no significant variation in the results for the *non-working day* air demand. For the *working day* air demand, the resulting cost savings with the LP method are significantly lower than with the other methods. Except in the scenario with an *untypical* electricity price, the cost savings with the DP and the MILP method are very similar.

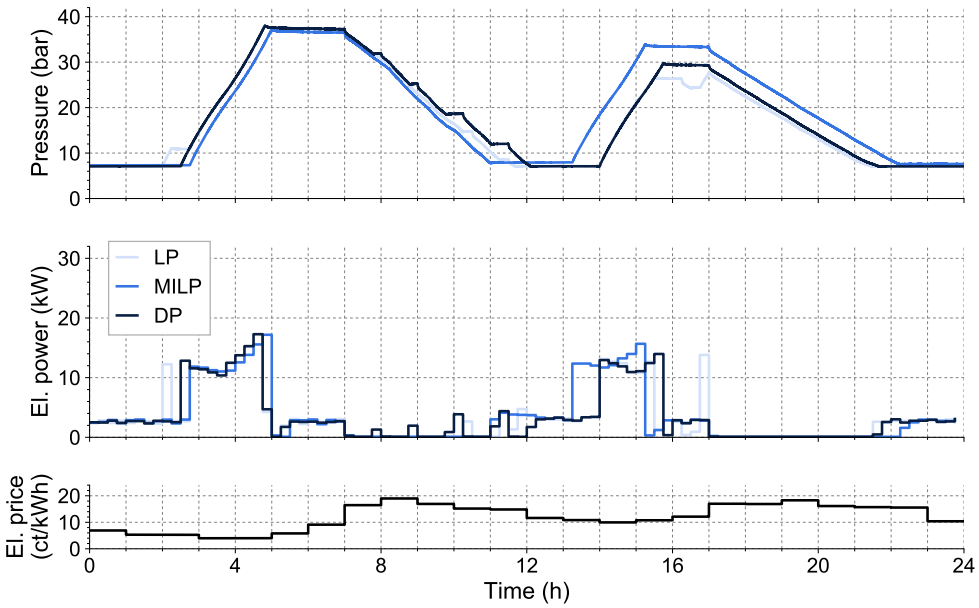

Figure 5.12: Results for *perfect* forecast, air demand *non-working day* and *typical* el. price

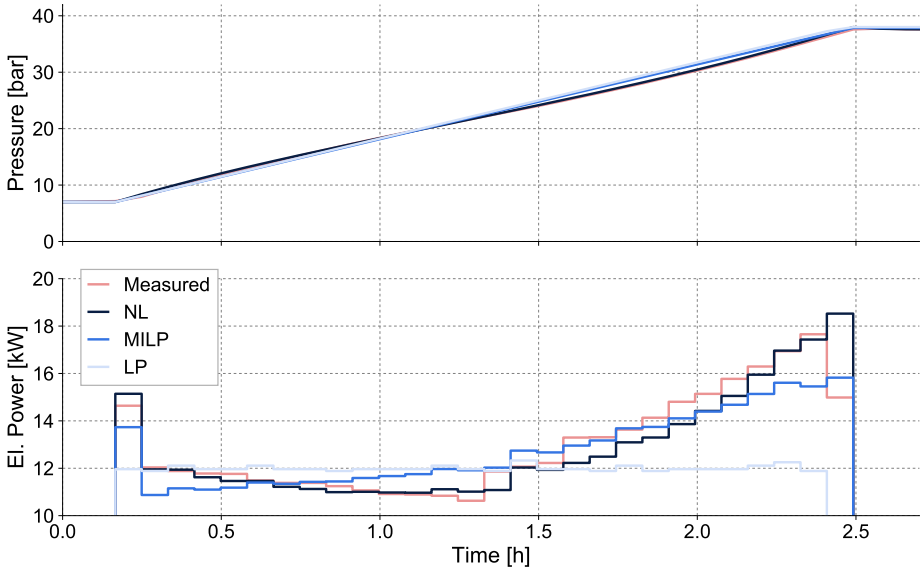

Figure 5.13: Simulated power consumption of a charging process using the linear programming (LP), the mixed-integer linear programming (MILP) and the nonlinear (NL) model compared to measured data

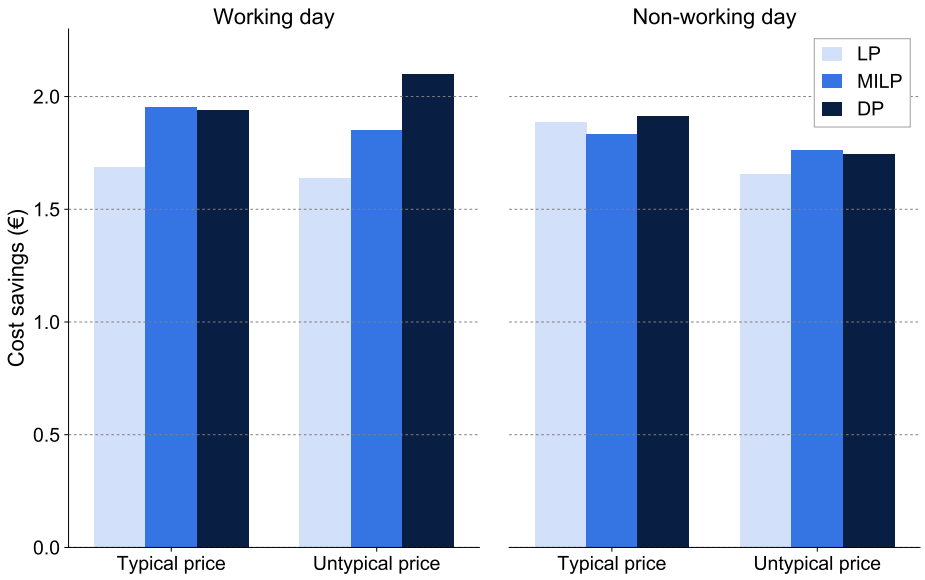

Figure 5.14: Cost savings for *perfect* air demand forecast with 15 minute optimization timestep size

5.3.2 Imperfect air demand forecast

To compare the influence of the quality of the air demand forecast on the performance of the different optimization methods, experiments with an *inaccurate* and a *worst-case* air demand forecast are performed, as described in section 5.1.1. For each forecast scenario, two different air demand scenarios, *working day* and *non-working day*, are used for the comparison.

Air demand *working day*

To investigate the influence of an imperfect air demand forecast, the air demand time series used for the optimization is different than the demand applied to the CAES system. The optimization always uses the typical air demand shown in figure 5.2, which is also applied for the *perfect* forecast scenarios (as described in section 5.1.1). For the scenarios with an *inaccurate* forecast, a demand time series that differs a little bit from the typical one is applied to the CAES system. For the scenarios with a *worst-case* forecast, the applied air demand is very different from the one used for the optimization.

Figure 5.15 shows the storage pressure and the electric power consumption over time for the three optimization methods using the *inaccurate* air demand forecast and an optimization timestep size of 15 minutes. With the LP method, the storage is not completely discharged in the first cycle because the model does not take into account that the booster consumes more power when the storage pressure is higher during charging. This results in higher costs than with the other two methods, as shown in figure 5.19. Because of the limitations of the MILP model described in section 5.2.5, in contrast to the DP method, the storage capacity is not used completely in the first cycle. Additionally, the more detailed DP model leads to a longer charging period in the second cycle. This results in higher costs savings using the DP method.

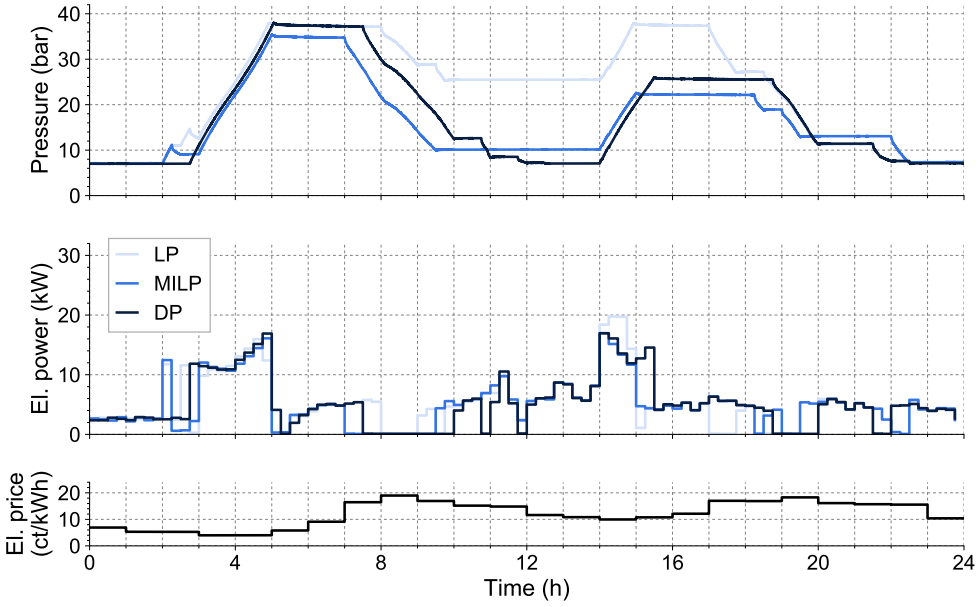

Figure 5.15: Results for *inaccurate* forecast, air demand *working day* and *typical* el. price

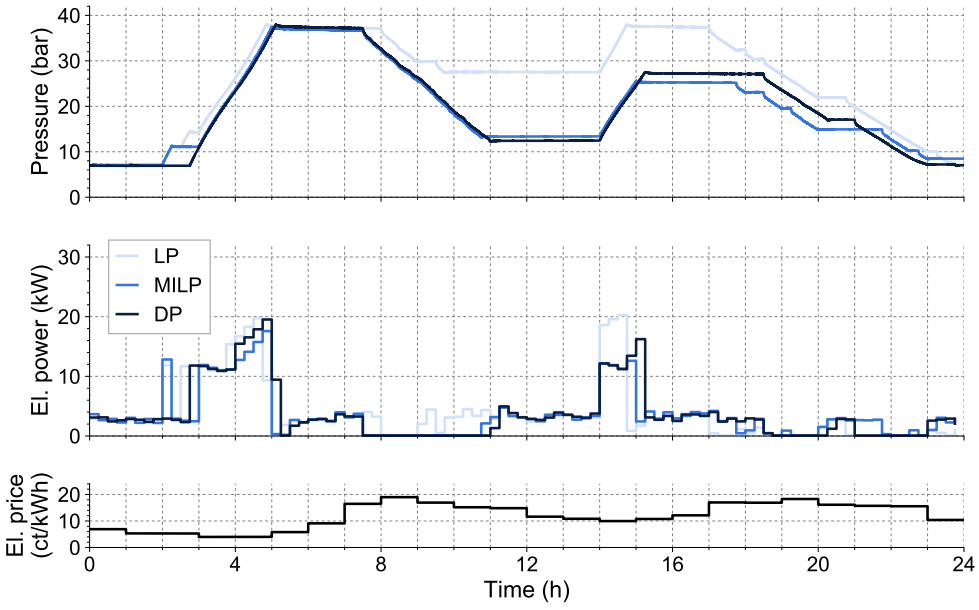

Figure 5.16: Results for *worst-case* forecast, air demand *working day* and *typical* el. price

For the *worst-case* forecast scenario with the *working day* air demand, the storage can be charged completely during the first cycle because of a slightly different starting pressure (as explained in section 5.2.5). Therefore, the behavior of the MILP and the DP method are very similar in this scenario, which leads to almost the same resulting cost savings. Because the applied air demand is much lower than the air demand used in the optimization (see figure 5.2), all three methods underestimate the discharging time. Because of the lower air demand, particularly at the end of the day, also less energy and money can be saved during discharging in the high price periods. This leads to lower cost savings especially for the LP method, in which the storage is completely discharged during this time.

Air demand *non-working day*

For the *non-working day* air demand also an *inaccurate* and a *worst-case* forecast scenario are investigated. The *non-working day* air demands used for the imperfect forecast scenarios are shown in Figure 5.3.

Figure 5.17 shows the storage pressure and power consumption for the *inaccurate* forecast scenario with air demand *non-working day*. The results for the *worst-case* forecast scenario with the same air demand are shown in figure 5.18. The charging times of both scenarios are very similar, whereby in the *worst-case* forecast scenario, the storage is discharged faster because of the higher air demand. The earlier charging process of the MILP method is caused by the difference in modeling the power consumption during charging, as explained in section 5.3.1 for the *non-working day* air demand with a *typical* electricity price and *perfect* forecast scenario (see figure 5.12).

In the *inaccurate* forecast scenario, the similar behavior of the LP and DP method lead to almost the same cost savings (see figure 5.19). Because of the low air demand, the short discharging and charging period in the middle of the second cycle using the LP method has only little influence on the costs. The earlier charging sequence of the MILP method together with the fact that the storage can not be completely discharged in this case (as explained in section 5.2.5) leads to lower savings.

In the *worst-case* forecast scenario, the short discharging and charging of the LP method has a bigger influence on the costs, as the higher air demand leads to a higher additional energy consumption. In this case, the storage can be discharged completely using the MILP method. Additionally, the higher storage pressure in the second cycle leads to higher cost savings. Therefore, the costs of the MILP and the DP are almost the same in this scenario.

Figure 5.19 shows the resulting cost savings of all scenarios with an imperfect air demand forecast using an optimization timestep size of 15 minutes. For both *inaccurate* forecast scenarios, the DP method leads to the highest cost savings, while the savings of the LP and the MILP model depend on the air demand. For the *worst-case* forecast scenarios, the results of the DP and the MILP model are very similar and significantly better than with the LP method.

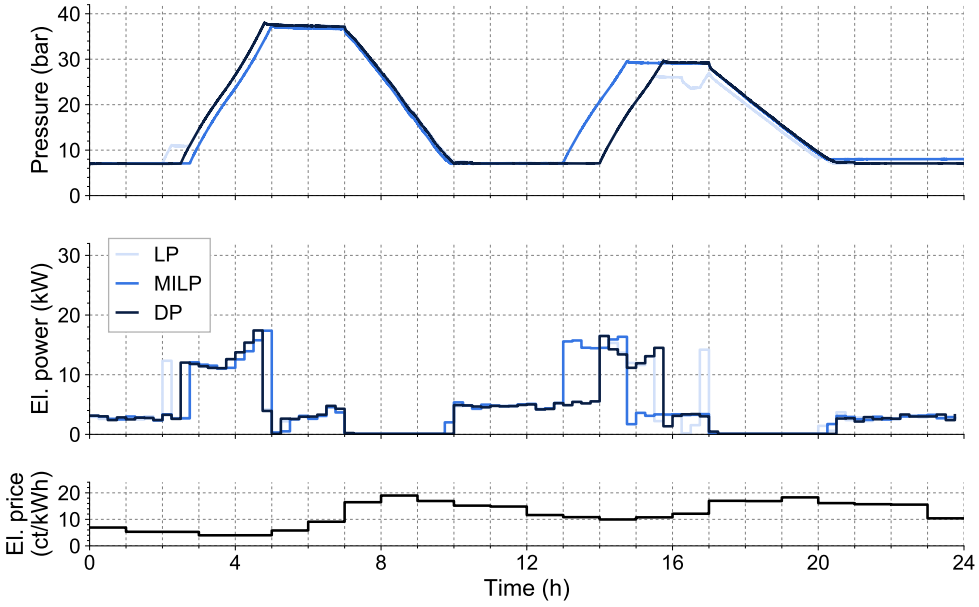

Figure 5.17: Results for *inaccurate* forecast, air demand *non-working day* and *typical* el. price

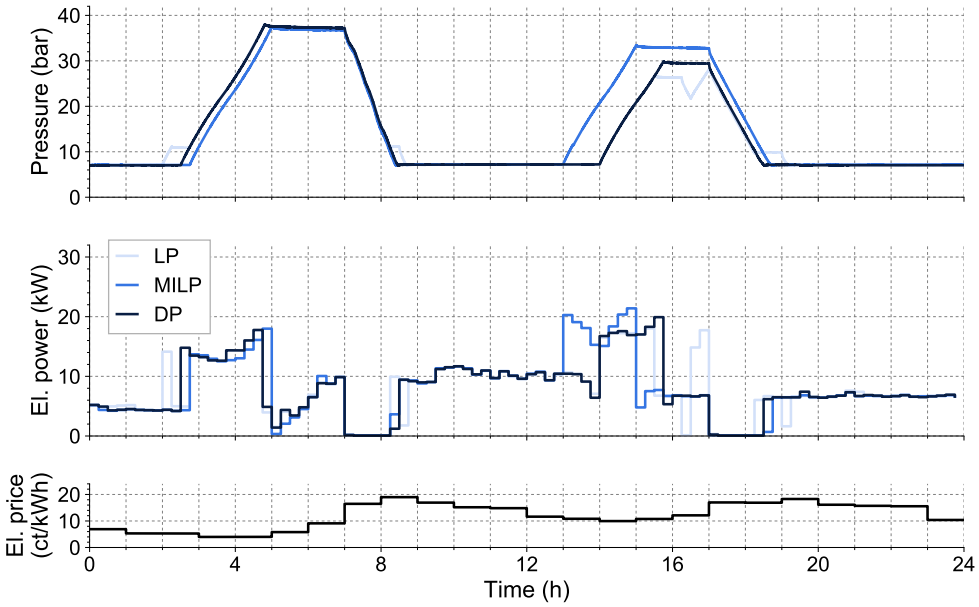

Figure 5.18: Results for *worst-case* forecast, air demand *non-working day* and *typical* el. price

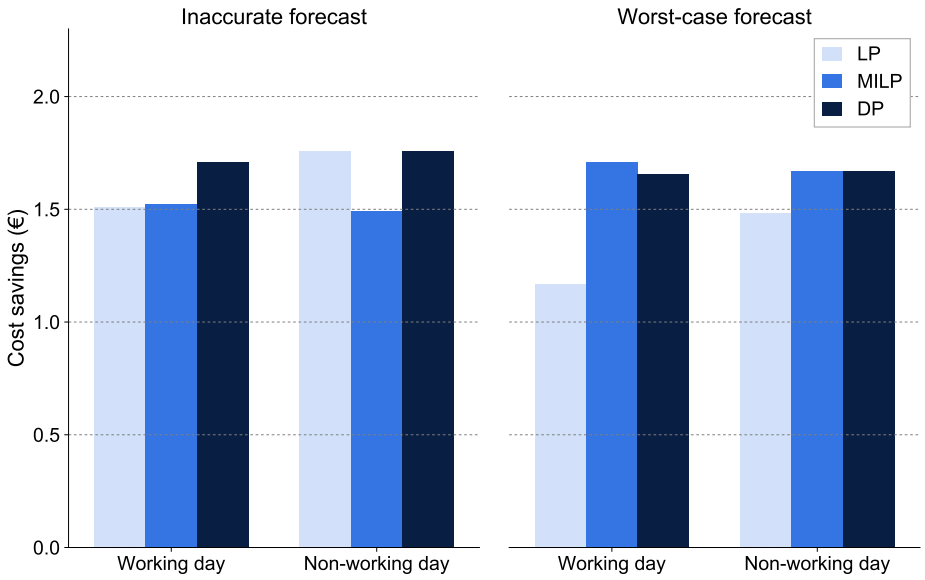

Figure 5.19: Cost savings for imperfect air demand forecast with 15 minute optimization timestep size

5.3.3 Influence of the optimization timestep size

To investigate the influence of the optimization timestep size, all experiments were performed with a timestep size of 5 and 15 minutes. A smaller timestep size allows a faster adjustment of the system operation, if the measured system behavior differs considerably from the one predicted by the model. Additionally, the system is modeled in more detail and it is possible to apply more operating state changes within a certain time period. But more timestep during the optimization horizon increases the complexity of the optimization problem. Instead of 96 operation state decisions with a 15 minute timestep size, 288 decisions with a 5 minute step size have to be calculated for a 24-hour optimization horizon. Additionally, the maximum solving time decreases with the timestep size, since the problem has to be solved within one time period. For the LP method, the optimization problem is always solved within the time limit for both variants. For the MILP model in some cases the solving process is stopped because the time limited is exceeded, before the absolute or relative MIP gap (see section 5.2.3) is reached, when a timestep size of 5 minutes is used. This may lead to a suboptimal solution and therefore higher costs. For the DP method, the discretization steps of the storage pressure have to be reduced when using a 5 minute step size, to ensure the problem is solved within the time limit (see section 5.2.3). This results in a less accurate model and therefore can also lead to worse optimization results than with a 15 minute step size.

Perfect forecast

Figure 5.20 shows the comparison of the cost savings between the two different optimization timestep sizes for all *perfect* forecast scenarios. For all three optimization methods, the difference in the resulting costs using a 5 minute or a 15 minute timestep size is very small. The most detailed nonlinear model used by the DP method leads to the least differences. The

less detailed LP model shows the highest deviations using the different timestep sizes, but as for the MILP model both variants can lead to lower costs, dependent on the given scenario.

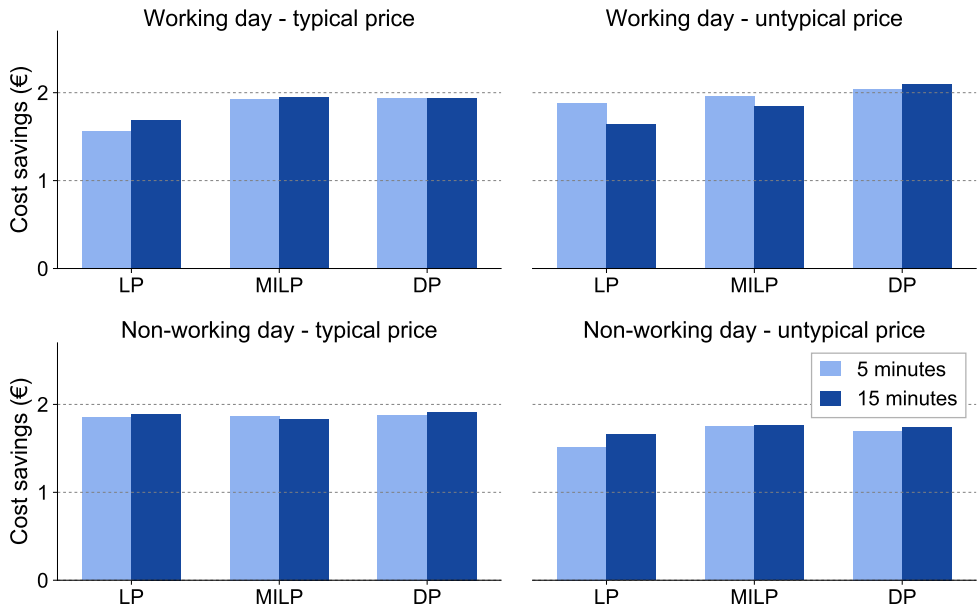

Figure 5.20: Cost savings compared by optimization timestep size for *perfect* forecast

With the MILP method, in two cases the 5 minute and in two cases the 15 minute timestep size lead to lower costs dependent on the air demand and electricity price. Figure 5.21 shows the results for both timestep variations for the scenario with the air demand *working day* and an *untypical* electricity price. The different charging and discharging times and pressure levels are mainly caused by the slightly different starting pressures, as explained in section 5.2.5. In this case, the costs for the 5 minute timestep size are lower. In contrast, for the scenario with *working day* air demand and *typical* electricity price, the costs using a 5 minute timestep size are higher. As shown in Figure 5.22, the storage cannot be completely discharged in the 5 minute case.

The LP method shows the widest cost difference between the two timestep size scenarios. Here in 3 of 4 cases the 15 minute step size results in higher cost savings, whereas in the scenario with the highest difference, the 5 minute step size results in higher savings. Figure 5.23 shows the storage pressure and the power consumption for both timestep variations for the scenario with the air demand *working day* and a *typical* electricity price. Here the short discharge period in hour 8, which is only performed in the 5 minute scenario, leads to a lower pressure level for the following hours and causes some interruptions during the discharging period in hour 20. The additional power consumption in this period with a high electricity price leads to higher costs than for the 15 minute step size. In the scenario with the air demand *working day* and a *untypical* electricity price, which is shown in figure 5.24, the discharging in hour 20 can be stopped after 5 minutes in the case with the lower step size. As a consequence the storage can be discharged longer in the following hours with higher electricity prices, which results in lower costs.

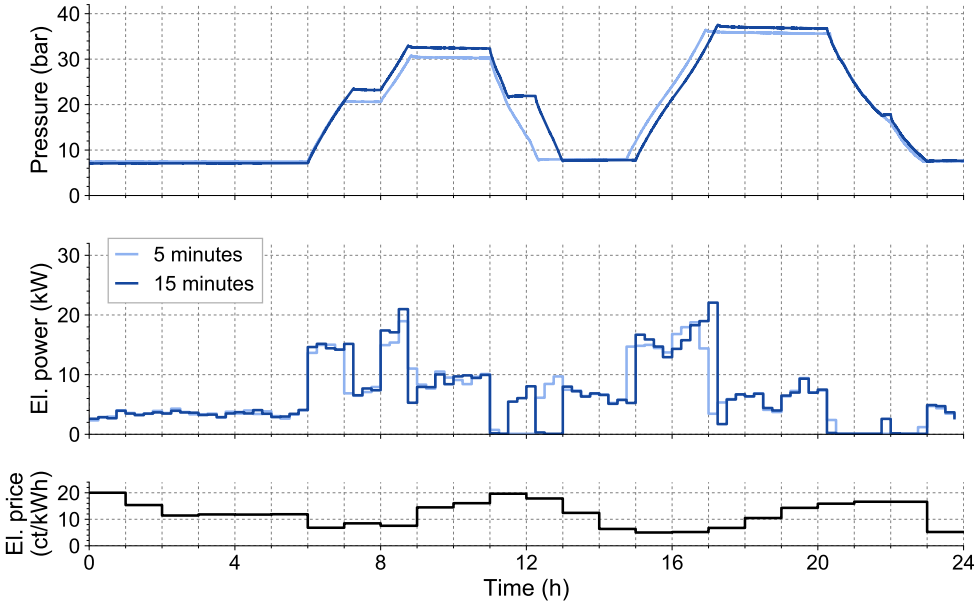

Figure 5.21: Results for *perfect* forecast, air demand *working day*, *untypical* el. price with optimization method MILP

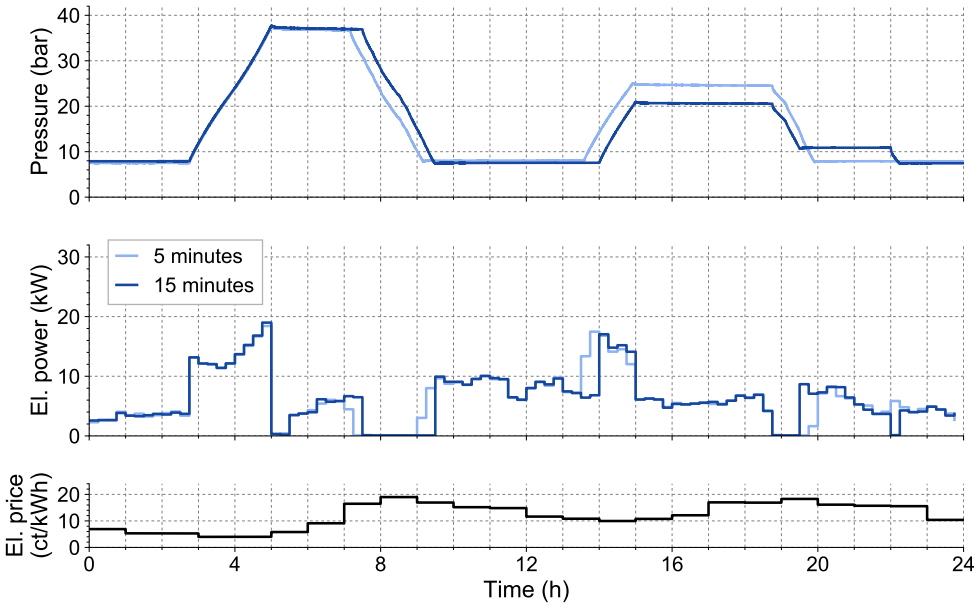

Figure 5.22: Results for *perfect* forecast, air demand *working day*, *typical* el. price with optimization method MILP

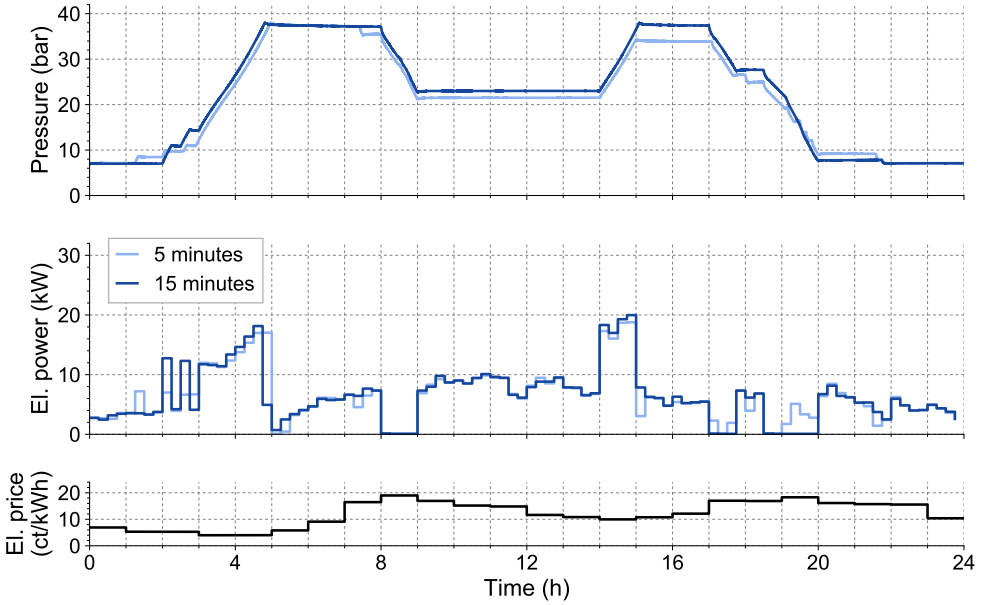

Figure 5.23: Results for *perfect* forecast, air demand *working day*, *typical* el. price with optimization method LP

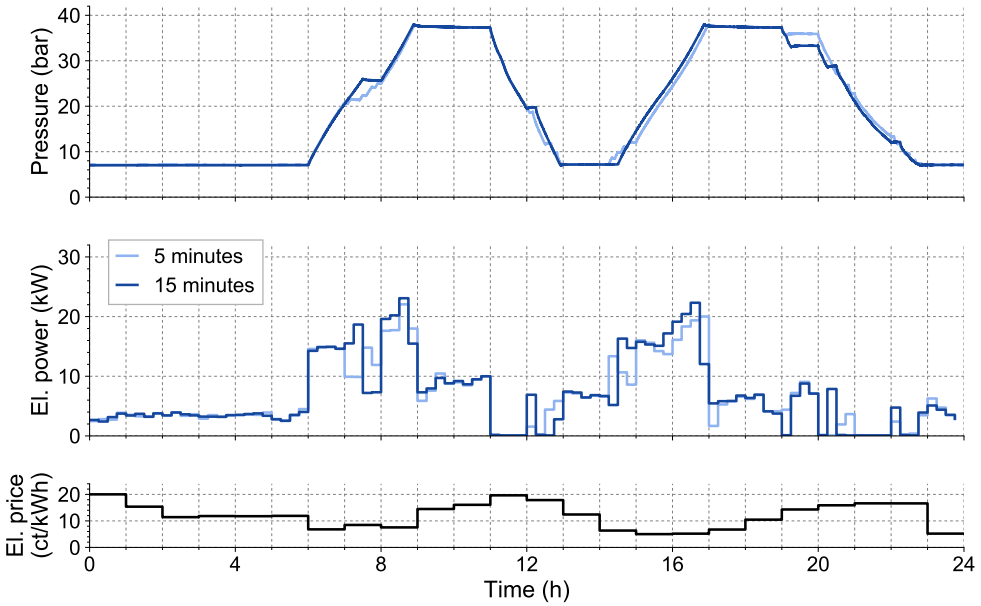

Figure 5.24: Results for *perfect* forecast, air demand *working day*, *untypical* el. price with optimization method LP

For the DP method, the cost savings using the 15 minute step size are slightly higher for all scenarios. Figure 5.25 shows the storage pressure and the power consumption for both timestep variations for the scenario with the air demand *working day* and an *untypical* electricity price. Although the curves are not exactly the same, there is no obvious explanation for the higher costs using the 5 minute step size. Therefore, the very small difference in the costs is probably caused by inaccuracy of the measurement and operation, as described in section 5.2.2.

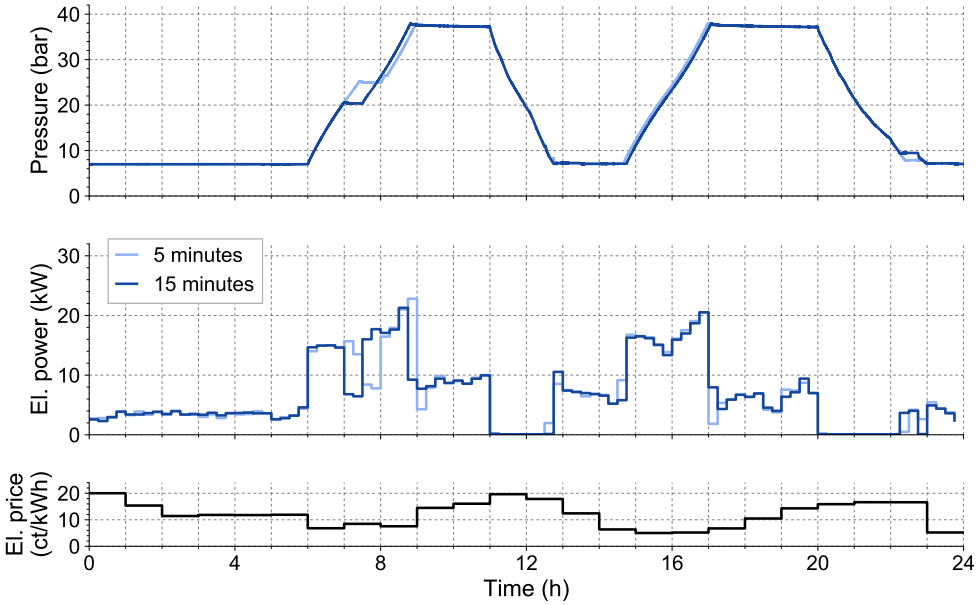

Figure 5.25: Results for *perfect* forecast, air demand *working day*, *untypical* el. price with optimization method DP

Imperfect forecast

Figure 5.26 compares the cost saving between the two optimization timestep sizes for all scenarios with an *inaccurate* and a *worst-case* forecast. In general, the differences in the resulting costs using a 5 minute or a 15 minute timestep size are higher than for the *perfect* forecast scenarios. For the LP method the 15 minute step size leads to better results, the 5 minute step size yields superior results for the MILP method. For the DP method both variants can lead to lower or higher costs.

For the MILP method, the cost savings using a 5 minute optimization timestep size are either higher or the same as for the 15 minute case. The reason being that for a larger timestep size, is that completely discharging the storage is not always possible, as explained in section 5.2.5. This is the case for scenario *inaccurate forecast - non-working day*, where the storage is completely discharged for only the 5 minute timestep size, which leads to lower costs (see figure 5.27). For scenario *inaccurate forecast - working day*, the storage is completely discharged using both variants, as shown in figure 5.28. Although the charging and discharging times and pressure levels are different for this scenario, the resulting cost savings are the same.

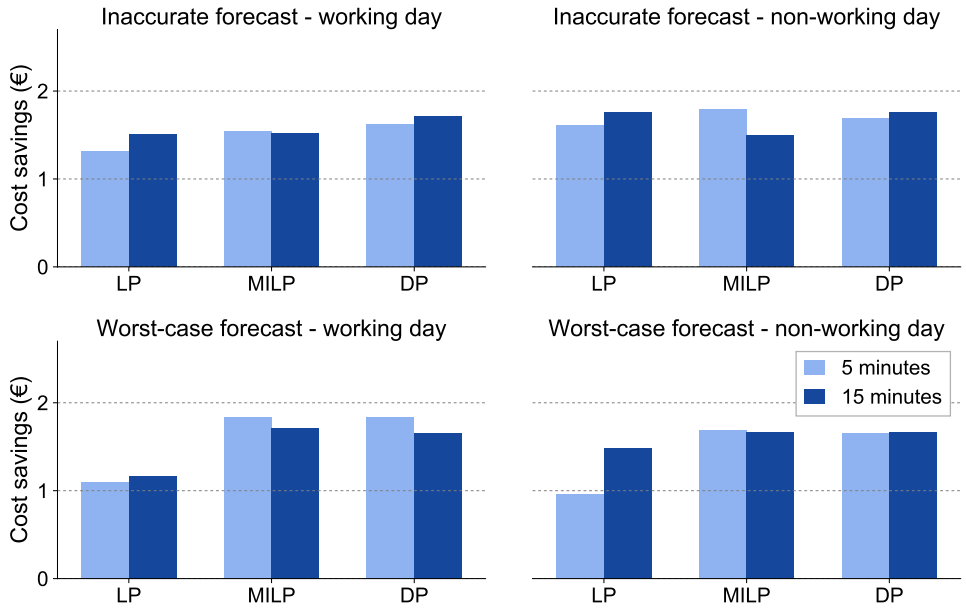

Figure 5.26: Cost savings compared by optimization timestep size for imperfect air demand forecast

The differences in cost savings between the 5 and 15 minute timestep size using the DP method are generally very small. Dependent on the scenario, the deviation of the real from the predicted system behavior because of the imperfect air demand forecast can lead to higher cost savings using both timestep sizes. For the *inaccurate forecast - working day* scenario, shown in figure 5.29, the fact that the air demand is slightly lower than predicted, leads to higher cost savings using the 15 minute timestep size. In contrast, for the *worst-case forecast - working day* scenario (see figure 5.30), where the air demand is much lower than the forecast used for the optimization, higher savings are achieved using the 5 minute step size.

For the LP method, the 15 minute timestep size results in higher cost savings for every scenario. Figure 5.31 shows the storage pressure and electric power consumption for the scenario with a *worst-case* forecast and *non-working day* air demand. The reason for the higher costs using the 5 minute step size are the frequent changes of the operation mode, especially during the second cycle. These changes are caused by the failure of the predicted system behavior of the inaccurate LP model and lead to additional start-up and shut-down losses of the system, which can not be modeled using linear programming.

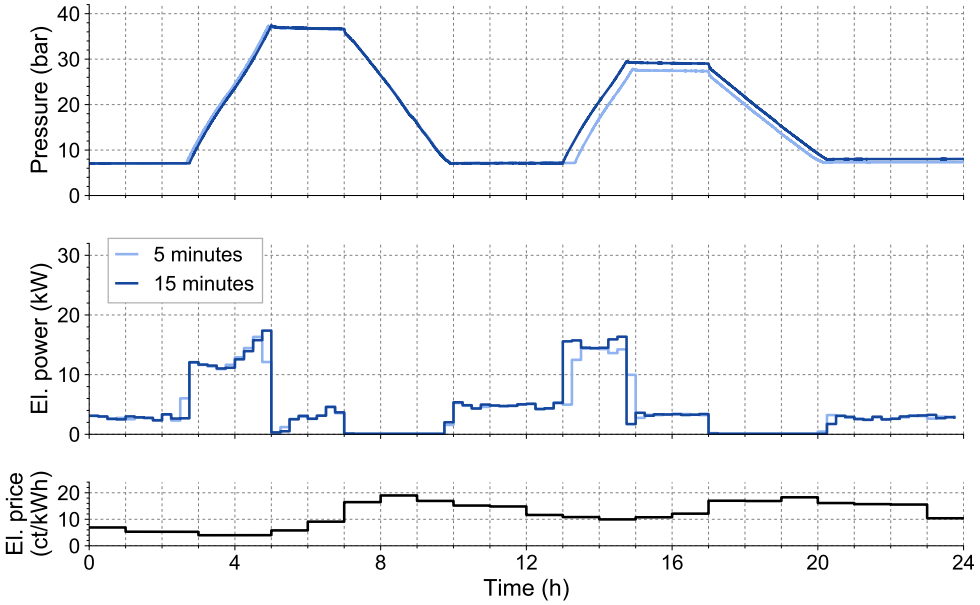

Figure 5.27: Results for *inaccurate* forecast, air demand *non-working day*, *typical* el. price with optimization method MILP

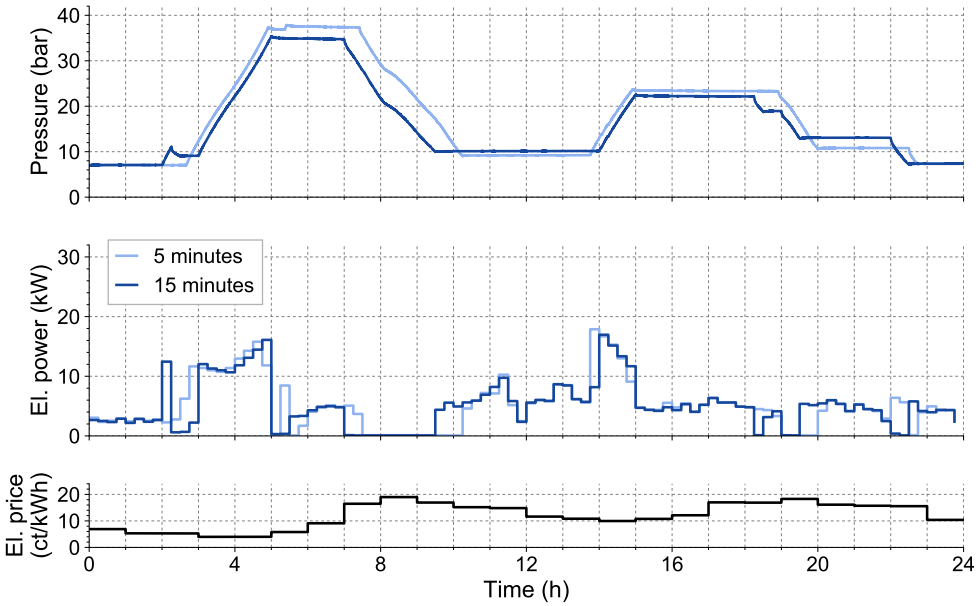

Figure 5.28: Results for *inaccurate* forecast, air demand *working day*, *typical* el. price with optimization method MILP

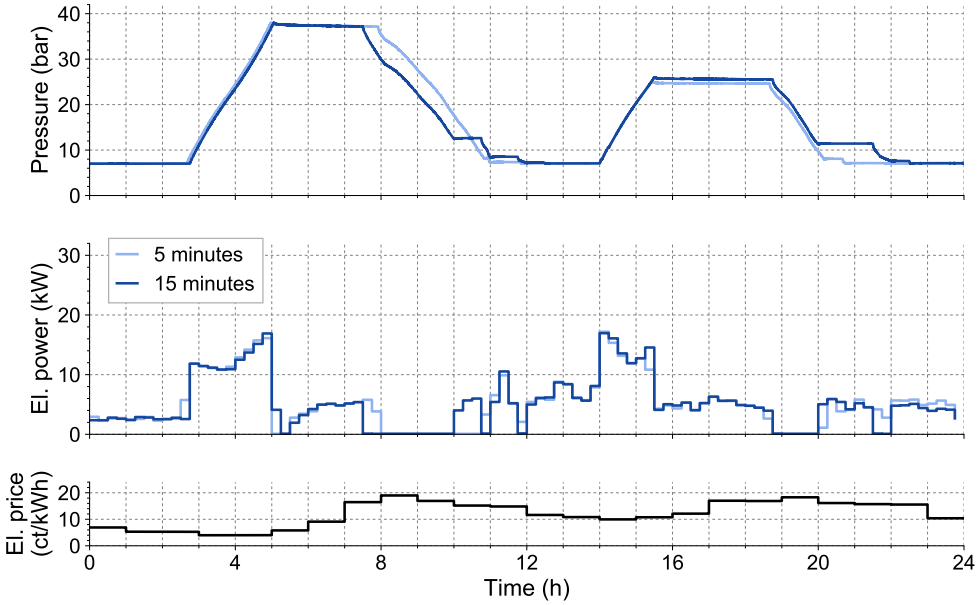

Figure 5.29: Results for *inaccurate* forecast, air demand *working day*, *typical* el. price with optimization method DP

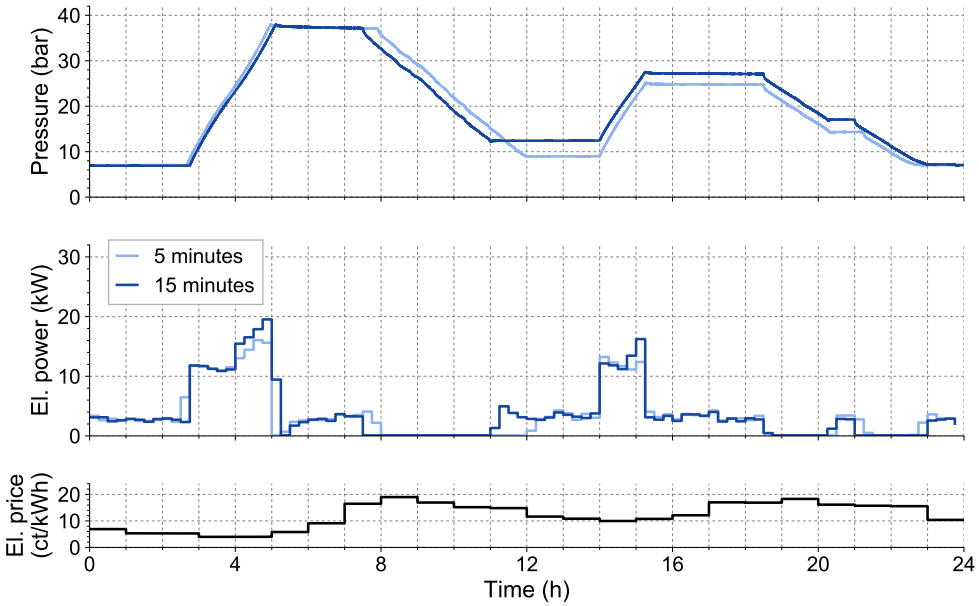

Figure 5.30: Results for *worst-case* forecast, air demand *working day*, *typical* el. price with optimization method DP

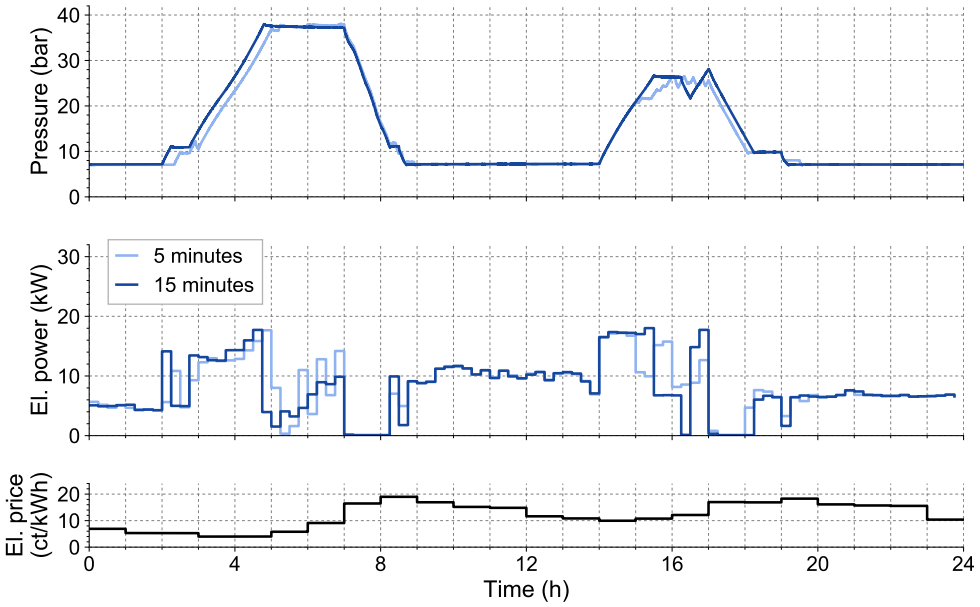

Figure 5.31: Results for *worst-case* forecast, air demand *non-working day*, *typical* el. price with optimization method LP

5.3.4 Result summary

Figure 5.32 shows the average cost savings for the scenarios with perfect and imperfect air demand forecast, as well as for all performed scenarios together (total), compared by the optimization timestep size and method. The results show that, in average, the highest cost savings can be achieved using the most detailed nonlinear model solved with the dynamic programming optimization method. However, the cost savings obtained by using the MILP method are only 0.9 % less for all scenarios taken together and even 0.8 % higher for the imperfect forecast scenarios. Although the LP method guarantees a fast and reliable solution of the optimization problem within the MPC, the limited accuracy of the model leads to obviously lower cost savings than the other methods (in average 11.7 % lower than DP fo all scenarios).

For the DP method, the influence of the two applied optimization timestep sizes is with 0.9 % difference for all scenarios very small. For the MILP method, a lower timestep size reduces the problem that the storage can not be completely charged and discharged in some cases, as explained in section 5.2.5. Therefore, using a 5 minute timestep size leads to higher costs saving for the MILP method. A lower step size causes an increased number of changes in operation mode because of the inaccuracies in the LP model. The resulting start-up and shut-down losses lead to increased costs at a lower step size and thus the higher cost savings are obtained for the 15 minute step size for the LP model.

Table 5.7 summarizes the cost savings of the different optimization methods for all performed experiments.

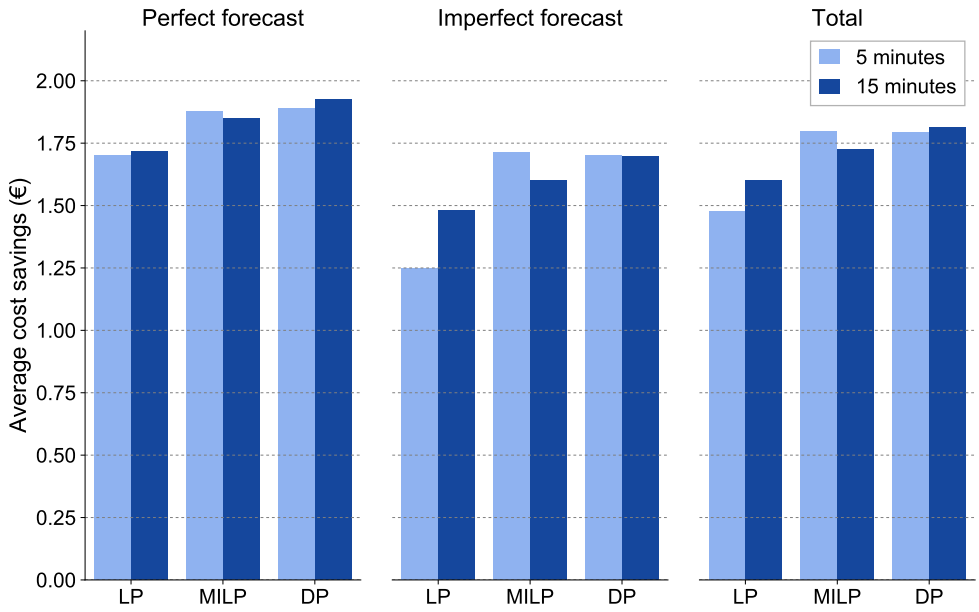

Figure 5.32: Mean cost savings compared by optimization timestep size and method for perfect and imperfect air demand forecast and all scenarios (total)

Table 5.7: Cost savings of the optimization methods for all scenarios

Forecast	**Air demand**	**Electricity price**	**Timestep size**	**LP** (€)	**MILP** (€)	**DP** (€)
Perfect	Working day	Typical	5 minutes	1.56	1.93	1.94
			15 minutes	1.69	1.95	1.94
		Untypical	5 minutes	1.88	1.97	2.04
			15 minutes	1.64	1.85	2.10
	Non-working day	Typical	5 minutes	1.85	1.87	1.88
			15 minutes	1.89	1.83	1.91
		Untypical	5 minutes	1.52	1.75	1.70
			15 minutes	1.66	1.76	1.74
Inaccurate	Working day	Typical	5 minutes	1.32	1.54	1.62
			15 minutes	1.51	1.52	1.71
	Non-working day	Typical	5 minutes	1.61	1.79	1.69
			15 minutes	1.76	1.49	1.76
Worst-case	Working day	Typical	5 minutes	1.10	1.83	1.84
			15 minutes	1.17	1.71	1.66
	Non-working day	Typical	5 minutes	0.96	1.69	1.65
			15 minutes	1.48	1.67	1.67

Chapter 6

Conclusion

In this thesis different optimization methods for Model Predictive Control (MPC) of a compressed air energy storage system were used and compared. In the first part of the thesis, the implemented optimization methods were introduced and theoretically analyzed by their advantages and disadvantages.

The compressed air energy storage (CAES) system, which was used to compare the optimization methods, was described in the second part of this thesis. The CAES system represents a typical compressed air system in the industry that is used to cover a given air demand. An additional booster is used to store compressed air in a high-pressure storage tank. The stored air can then be retrieved to cover the air demand. In this way, the electricity consumption of the system can be influenced and adapted to a given incentive.

A methodology, based on experimental measurements, to calculate the electrical round-trip efficiency of the storage system was introduced. It was shown that the round-trip efficiency of the system highly depends on the air demand during charging and discharging. The system has its best round-trip efficiency of 87 % when charging and discharging in times of low air demand, which can decrease down to 52 % in the worst-case when the air demand during charging and discharging is high. An economic evaluation showed that the specific costs of the CAES system are significantly higher compared to battery storages. Based on the performed measurements, a linear, a mixed-integer and a nonlinear model was developed and used for the different Model Predictive Control optimization methods.

The nonlinear model was used to compare the nonlinear optimization methods dynamic programming (DP), genetic algorithm (GA) and mixed-integer nonlinear programming (MINLP). Here the DP method showed the best results for MPC of the CAES system and was used for further investigations.

To compare the linear programming (LP), mixed-integer linear programming (MILP) and dynamic programming methods, several scenarios with different air demands, electricity prices, optimization timestep sizes and forecast quality were defined. The CAES system was controlled using MPC with each method for each scenario to cover the given 24-hour air demand with minimal operational costs. The methods were evaluated based on the cost savings compared to *normal* operation mode (covering the demand without using the storage).

The results showed, that over all performed experiments, using the DP method leads to the highest cost savings. With the LP method, in average 11.7 % less savings could be achieved.

Although LP is able to solve the given optimization problems very fast and with guaranteed optimality, this cannot compensate the limitations in the model representation. The difference in cost savings between the MILP model and the DP model was only 0.9 %. The MILP model is not able to represent the CAES system as exact as the nonlinear model used for DP but more in detail than the LP model. Here the inaccuracy compared to nonlinear model does not affect the results significantly. The identification of the model parameters and implementation of the optimization problem is much more complex for the DP than for the MILP method. The MILP method can also be used for larger energy systems with multiple storages, while the DP method is limited in the system complexity due to the "curse of dimensionality". Additionally, for the imperfect forecast scenarios, which are more realistic than a perfect forecast of all future parameters, the MILP model showed slightly better results in this thesis. Taking this into account, in general, a MILP programming model might be a better choice to use for MPC of an energy system with storages. For small systems with a good forecast, the results of this thesis showed that a nonlinear model using DP leads to the best results.

The general structure of the CAES system introduced in this thesis is very similar to other systems that can be used for load management in the electricity sector, such as CHP units or heat pumps in combination with a heat storage. While the main purpose of the system is to cover a given demand (air or heat), the storage is used to decouple electricity consumption or production and supply of air or heat. In this way, the storage systems provide flexibility to the electricity system. Battery storage in combination with a PV system, where the battery is also used to decouple demand and production, can be interpreted similarly.

Therefore, the most important question that has to be explored in further investigations is the way in which the results of this thesis can be transferred to other applications. The changes in performance of the different optimization methods when applied to more complex systems with additional storages or power conversion processes should also be further investigated. Additionally, the influence of the forecast quality and the optimization time horizon on the results should be explored further.

Appendix A

Compressed air energy storage system specifications

A.1 Technical data

Table A.1 summarizes the components of the compressed air energy storage systems.

Table A.1: Components of the compressed air energy storage system

Component	Manufacturer	Model	Type	
Dryer	KAESER	Secotec TB 19	Refrigeration dryer	[50]
Filter	KAESER	FE 18 D	Filter	[49]
High-pressure tank	Maschinen- und Behälterbau GmbH	2000 l, 50 bar_g, vertical	Air receiver	[44]
Air receiver tank	OKS Otto Klein GmbH	2000 l, 16 bar_g, vertical	air receiver	[44]
Valve	Gemü	751 40D 137 51AU08KC0	Ball valve	[33]
Control valve	Gemü	554 20D 1 9 51 1RS013	Control valve	[32]
Control valve	Gemü	1434000Z1A141A001030	Positioner	[32]
Pressure regulator	Aircom	R120 - 12 E01	Pressure regulator	[2]
T_1, T_2, T_3	tecsis	TEP11x222006	Resistance thermometer	[96]
p_1, p_2	HYDAC	HDA 4745-A-016-000	Pressure transmitter	[39]
p_3	HYDAC	HDA 4745-A-045-000	Pressure transmitter	[39]
P_1, P_2	Müller + Ziegler	Pdr-MU 50 Hz 400/230V 20/1A 10kW	Electric power meter	[74]
P_3, P_4	Müller + Ziegler	Pdr-MU 50 Hz 400/230V 10/1A 6kW	Electric power meter	[74]

A.2 Costs

Table A.2 shows the costs of the components for the CAES needed in addition to a typical compressed air system in the industry.

Table A.2: Component costs of the compressed air energy storage system

Component	**Costs**
Outlet valve	200 €
Pressure regulator	1.300 €
High-pressure storage tanks	45.000 €
Booster	8.700 €
Total	**55.200 €**

Appendix B

Mathematical description of the models

This chapter contains the detailed mathematical description of all optimization models used in this thesis.

The linear programming (LP), the mixed-integer linear programming (MILP) and the mixed-integer nonlinear programming (MINLP) models are implemented using Pyomo, a Python-based algebraic modeling language [83]. In Pyomo, as in other algebraic modeling languages, optimization problems are defined by sets, variables, parameters, an objective function and a number of equality and inequality constraints. The mathematical description of the models in this thesis is based on this formulation.

The simulation model used for the genetic algorithm (GA) and dynamic programming (DP) is implemented in Python.

B.1 Linear programming model

The LP model is described by a set of linear equality and inequality functions, shown in this section. The parameters and variables used to describe the problem are summarized in table B.2 and table B.1. The values of the constant parameters are shown in section C.1, table C.2. The optimization horizon is described by the set of timesteps $\mathcal{T} = \{t_1, ..., t_N\}$,where Δt is the duration of each timestep, and N is the number of timesteps $t \in \mathcal{T}$.

The objective of the LP model is to minimize the total costs over the optimization horizon, that depend on the electricity price C^t_{el} and the total power consumption of the system P^t_{tot} at each timestep. The total power consumption of the system P^t_{tot} is comprised of the power consumption of the compressors P^t_{co} and the charge power P^t_{ch} or discharge power P^t_{dch} of the electrical energy storage.

$$\min c_{tot} = \min \left(\sum_{t \in \mathcal{T}} C^t_{el} \cdot P^t_{tot} \cdot \frac{\Delta t}{3600 \, \frac{\mathrm{s}}{\mathrm{h}}} \right) \tag{B.1}$$

$$P^t_{tot} = P^t_{co} + P^t_{ch} - P^t_{dch} \qquad \forall t \in \mathcal{T} \tag{B.2}$$

Table B.1: Variables of the LP model

Name	$\in$	Unit	Description
$\dot{V}_{co}^{t}$	$\mathbb{R}_0^+$	$\frac{m_n^3}{min}$	Compressed air produced by the compressors at timestep t
P_{co}^{t}	$\mathbb{R}_0^+$	kW	Electrical power consumed by the compressors at timestep t
P_{tot}^{t}	$\mathbb{R}_0^+$	kW	Total electrical power consumed by the CAES system at timestep t
P_{ch}^{t}	$\mathbb{R}_0^+$	kW	Electrical charge power of the storage at timestep t
P_{dch}^{t}	$\mathbb{R}_0^+$	kW	Electrical discharge power of the storage at timestep t
E_{sto}^{t}	$\mathbb{R}_0^+$	kWh	Electrical energy content of the storage at timestep t
c_{tot}	$\mathbb{R}_0^+$	€	Total costs to be minimized

Table B.2: Parameters of the LP model

Name	Unit	Description
$\overline{E}_{sto}$	kWh	Maximum electrical energy capacity of storage
ς_1	$\frac{kW}{m_n^3/min}$	Slope of the linear function used to model the electrical power consumption of the compressors
η_{ch}^{t}	1	Storage electrical charge efficiency at timestep t
η_{dch}^{t}	1	Storage electrical discharge efficiency at timestep t
$\dot{V}_{d}^{t}$	$\frac{m_n^3}{min}$	Air demand at timestep t
$\overline{P}_{ch}^{t}$	kW	Upper limit of the electrical charge power at timestep t dependent on $\dot{V}_{d}^{t}$
C_{el}^{t}	$\frac{€}{kWh}$	Electricity price at timestep t
ΔT	h	Duration of the optimization horizon
Δt	s	Timebase of the optimization (duration of one time period)
N	1	Number of timesteps $N = \frac{\Delta T}{\Delta t/3600}$

The power consumption of the compressors P_{co}^{t} is modeled as a linear function of the air demand $\dot{V}_{d}^{t}$ with the slope ς_1.

$$P_{co}^{t} = \varsigma_1 \cdot \dot{V}_{d}^{t} \qquad \forall t \in \mathcal{T} \tag{B.3}$$

The energy content E_{sto}^{t+1} of the electrical energy storage for the timestep $t + 1$ is calculated based on the energy content E_{sto}^{t}, the charge power P_{ch}^{t}, and the discharge power P_{dch}^{t} at timestep t. The losses during charging and discharging are represented by the charge efficiency η_{ch}^{t} and the discharge efficiency η_{dch}^{t}, that are dependent on the corresponding air demand at each timestep.

$$E_{sto}^{t+1} = E_{sto}^{t} + \eta_{ch}^{t} \cdot P_{ch}^{t} - \frac{1}{\eta_{dch}^{t}} \cdot P_{dch}^{t} \qquad \forall t \in \mathcal{T} \tag{B.4}$$

The energy storage content E_{sto}^{t} is limited by the maximum energy capacity of the storage $\overline{E}_{sto}$.

$$E_{sto}^{t} \leq \overline{E}_{sto} \qquad \forall t \in \mathcal{T} \tag{B.5}$$

The power consumption of the compressors is used as an upper limit of discharge power P^t_{dch} in every timestep.

$$P^t_{dch} \leq P^t_{co} \qquad \forall t \in \mathcal{T} \tag{B.6}$$

The mean charge power $\overline{P}^t_{ch}$ is used as an upper limit of the charge power P^t_{ch} in every timestep.

$$P^t_{ch} \leq \overline{P}^t_{ch} \qquad \forall t \in \mathcal{T} \tag{B.7}$$

The compressed air energy storage (CAES) system expects a target operation mode, *normal*, *charge*, or *discharge* as an input. Therefore the results of the solved LP problem has to be converted to an adequate operation mode. Therefore, in every timestep where the storage is charged ($P^t_{ch} > 0$) the target operation mode is set to *charge*, and in every state where the storage is discharged ($P^t_{dch} > 0$) it is set to *discharge*. If both, charge and discharge power are zero, the target operation mode is set to *normal*.

B.2 Mixed-integer linear programming model

This section describes the set of linear equality and inequality functions used to model the mixed-integer linear programming (MILP) optimization problem. The parameters and variables used to describe the problem are summarized in table B.3 and table B.4. The values of the constant parameters are shown in section C.2, table C.3. The optimization horizon is described by the set of timesteps $\mathcal{T} = \{t_1, ..., t_N\}$,where Δt is the duration of each timestep, and N is the number of timesteps $t \in \mathcal{T}$.

Table B.3: Parameters of the MILP model

Name	Unit	Description
$\hat{p}_{sys}^{norm}$	$\mathrm{bar_g}$	Setpoint pressure in normal mode (normal system pressure)
$\bar{p}_{sto}$	$\mathrm{bar_g}$	Maximum storage pressure
$\underline{p}_{sto}$	$\mathrm{bar_g}$	Minimum storage pressure
$\bar{\dot{V}}_{co}$	$\frac{\mathrm{m_n^3}}{\mathrm{min}}$	Maximum free air delivery of the compressors
$E_{co,su}$	kWh	Start-up losses of the compressors
$E_{co,sd}$	kWh	Shut-down losses of the compressors
$E_{bo,su}$	kWh	Start-up losses of the booster
$E_{bo,sd}$	kWh	Shut-down losses of the booster
ς_i		Parameters used to model the electrical power consumption of the compressors
β_i		Parameters used to model the electrical power consumption of the booster
$\delta_{ch,i}$, $\delta_{dch,i}$		Parameters used to model the storage pressure state equation
r_{bo}	1	Maximum compression ratio of the booster
$\dot{V}_d^t$	$\frac{\mathrm{m_n^3}}{\mathrm{min}}$	Air demand at timestep t
C_{el}^t	$\frac{€}{\mathrm{kWh}}$	Electricity price at timestep t
ΔT	h	Duration of the optimization horizon
Δt	s	Timebase of the optimization (duration of one time period)
N	1	Number of timesteps $N = \frac{\Delta T}{\Delta t/3600}$

In the MILP formulation of the optimization problem binary variables representing the operation mode of the CAES system can be used. Here the three modes *normal*, *charge* and *discharge* are represented by two binary variables b_{ch}^t and b_{dch}^t that can be either 0 or 1. At timestep t, the CAES system is in *charge* mode, when $b_{ch}^t = 1$, and in *discharge* mode, when $b_{dch}^t = 1$. When both variables are zero, the system is in *normal* operation mode. The constraint in eq. B.8 avoids that both variables become 1 at the same timestep.

$$b_{ch}^t + b_{dch}^t \leq 1 \tag{B.8}$$

The objective of the MILP model is to minimize the total costs over the optimization horizon, that depend on the electricity price C_{el}^t and the total power consumption of the system P_{tot}^t at each timestep. The total power consumption of the system P_{tot}^t is comprised of the power consumptions of the compressors P_{co}^t and of the booster P_{bo}^t.

Table B.4: Variables of the MILP model

Name	$\in$	Unit	Description
p^t_{sys}	$\mathbb{R}^+_0$	bar_g	System pressure at timestep t
$\tilde{p}^t_{sys,ch}$	$\mathbb{R}^+_0$	bar_g	Auxiliary variable representing the product of the system pressure and the binary variable b^t_{ch}
$\tilde{p}^t_{sys,dch}$	$\mathbb{R}^+_0$	bar_g	Auxiliary variable representing the product of the system pressure and the binary variable b^t_{dch}
p^t_{sto}	$\mathbb{R}^+_0$	bar_g	Storage pressure at timestep t
$\Delta p^t_{sto,ch}$	$\mathbb{R}^+_0$	bar_g	Pressure difference at timestep t when charging
$\Delta \tilde{p}^t_{sto,ch}$	$\mathbb{R}^+_0$	bar_g	Auxiliary variable for calculating $\Delta p^t_{sto,ch}$
$\Delta p^t_{sto,dch}$	$\mathbb{R}^+_0$	bar_g	Pressure difference at timestep t when discharging
$\Delta \tilde{p}^t_{sto,dch}$	$\mathbb{R}^+_0$	bar_g	Auxiliary variable for calculating $\Delta p^t_{sto,dch}$
p^t_{bo}	$\mathbb{R}^+_0$	bar_g	Pressure for calculating the power consumption of the booster
$\dot{V}^t_{co}$	$\mathbb{R}^+_0$	$\frac{\text{m}^3_\text{n}}{\text{min}}$	Compressed air produced by the compressors at timestep t
P^t_{co}	$\mathbb{R}^+_0$	kW	Electrical power consumed by the compressors at timestep t
P^t_{bo}	$\mathbb{R}^+_0$	kW	Electrical power consumed by the booster at timestep t
P^t_{tot}	$\mathbb{R}^+_0$	kW	Total electrical power consumed by the CAES system at timestep t
b^t_{ch}	$[0, 1]$	1	Binary variable related to the operation mode *charge* at timestep t
b^t_{dch}	$[0, 1]$	1	Binary variable related to the operation mode *discharge* at timestep t
$b^t_{co,su}$	$[0, 1]$	1	Binary variable related to the compressors startup at timestep t
$b^t_{co,sd}$	$[0, 1]$	1	Binary variable related to the compressors shut-down at timestep t
$b^t_{bo,su}$	$[0, 1]$	1	Binary variable related to the booster startup at timestep t
$b^t_{bo,sd}$	$[0, 1]$	1	Binary variable related to the booster shut-down at timestep t
c_{tot}	$\mathbb{R}^+_0$	€	Total costs to be minimized

$$\min c_{tot} = \min \left(\sum_{t \in \mathcal{T}} C^t_{el} \cdot P^t_{tot} \cdot \frac{\Delta t}{3600 \, \frac{\text{s}}{\text{h}}} \right) \tag{B.9}$$

$$P^t_{tot} = P^t_{co} + P^t_{bo} \qquad \forall t \in \mathcal{T} \tag{B.10}$$

Booster

The power consumption of the booster P^t_{bo} is modeled as a linear function dependent on the pressure p^t_{bo} at its output. The offset β_2 is added if the system is in *charge* mode (b^t_{ch}=1). Additionally, energy losses $E_{bo,su}$ during startup ($b^t_{bo,su} = 1$, when the system changes from *charge* or *normal* to *discharge* mode) and energy losses $E_{bo,sd}$ during shut-down ($b^t_{bo,sd} = 1$, when the system switches from *discharge* to another mode) are considered.

$$\begin{aligned} P^t_{bo} = \quad & \beta_1 \cdot p^t_{bo} + \beta_2 \cdot b^t_{ch} \\ & + b^t_{bo,su} \cdot E_{bo,su} \cdot \frac{3600 \, \frac{\text{s}}{\text{h}}}{\Delta t} \\ & + b^t_{bo,sd} \cdot E_{bo,sd} \cdot \frac{3600 \, \frac{\text{s}}{\text{h}}}{\Delta t} \qquad \forall t \in \mathcal{T} \end{aligned} \tag{B.11}$$

$$b^t_{bo,su} \geq b^t_{ch} - b^{t-1}_{ch} \qquad \forall t \in \mathcal{T} \tag{B.12}$$

$$b^t_{bo,sd} \geq b^{t-1}_{ch} - b^t_{ch} \qquad \forall t \in \mathcal{T} \tag{B.13}$$

When the booster is running (b^t_{dch}=1), its output pressure p^t_{bo} corresponds to the pressure in the high pressure storage p^t_{sto}. To make sure, that the power consumption of the booster is zero when it is not running, p^t_{bo} has to be zero in this case.

$$p^t_{bo} - p^t_{sto} \geq -\bar{p}_{sto} \cdot (1 - b^t_{dch}) \qquad \forall t \in \mathcal{T} \tag{B.14}$$

Compressors

The power consumption of the compressors is modeled as a linear function dependent on the air covered by the compressors $\dot{V}^t_{co}$, the difference of the system pressure and the normal system pressure (p^t_{sys}-$\hat{p}^{norm}_{sys}$) and the product of both. To implement the multiplication $\dot{V}^t_{co} \cdot (p^t_{sys} - \hat{p}^{norm}_{sys})$ as a linear expression, the auxiliary variables $\tilde{p}^t_{sys,ch}$and $\tilde{p}^t_{sys,dch}$, representing the multiplication of (p^t_{sys}-$\hat{p}^{norm}_{sys}$) with the binary variables b^t_{ch} and b^t_{dch} (as definde in eqs. B.22 - B.27), and the definition of the air covered by the compressors $\dot{V}^t_{co}$ in eq. B.18 are used. The offset ς_4 is added if the system is in *charge* or *normal* mode ($b^t_{dch} = 0$). Additionally, energy losses $E_{co,su}$ during startup ($b^t_{co,su} = 1$, when the system changes from *discharge* to another mode) and energy losses $E_{co,sd}$ during shut-down ($b^t_{co,sd} = 1$, when the system switches from *normal* or *charge* to *discharge* mode) are considered.

$$\begin{aligned} P^t_{co} = \quad & \varsigma_1 \cdot \dot{V}^t_{co} + \varsigma_2 \cdot (p^t_{sys} - \hat{p}^{norm}_{sys}) \\ & + \varsigma_3 \cdot \left(\dot{V}^t_{d} \cdot (p^t_{sys} - \hat{p}^{norm}_{sys}) - \dot{V}^t_{d} \cdot \tilde{p}^t_{sys,dch} + \dot{V}_{bo} \cdot \tilde{p}^t_{sys,ch}\right) \\ & + \varsigma_4 \cdot (1 - b^t_{dch}) \\ & + b^t_{co,su} \cdot E_{co,su} \cdot \frac{3600\ \frac{\mathrm{s}}{\mathrm{h}}}{\Delta t} \\ & + b^t_{co,sd} \cdot E_{co,sd} \cdot \frac{3600\ \frac{\mathrm{s}}{\mathrm{h}}}{\Delta t} \qquad \forall t \in \mathcal{T} \end{aligned} \tag{B.15}$$

$$b^t_{co,su} \geq b^{t-1}_{dch} - b^t_{dch} \qquad \forall t \in \mathcal{T} \tag{B.16}$$

$$b^t_{co,sd} \geq b^t_{dch} - b^{t-1}_{dch} \qquad \forall t \in \mathcal{T} \tag{B.17}$$

When the system is in *normal* mode ($b^t_{ch} = b^t_{dch} = 0$), the compressors have to cover the complete air demand $\dot{V}^t_{d}$. In the operation mode *charge* ($b^t_{ch} = 1$), additionally the air demand of the booster $\dot{V}_{bo}$ has to be covered. In *discharge* mode, the air demand is covered by the high-pressure storage and the air delivered by the compressors is zero. The air that can be delivered by the compressors is limited to $\bar{\dot{V}}_{co}$.

$$\dot{V}^t_{co} = (1 - b^t_{dch}) \cdot \dot{V}^t_{d} + b^t_{ch} \cdot \dot{V}_{bo} \qquad \forall t \in \mathcal{T} \tag{B.18}$$

$$\dot{V}_{co}^{t} \leq \bar{\dot{V}}_{co} \qquad \forall t \in \mathcal{T} \tag{B.19}$$

As described in chapter 4.3 (see eq. 4.11 and figure 4.5), the system pressure p_{sys}^{t} during charging depends on the storage pressure p_{sto}^{t}. In *normal* or *discharge* operation mode, the system pressure p_{sys}^{t} corresponds to the normal system pressure $\hat{p}_{sys}^{norm}$. Using the output pressure of the booster p_{bo}^{t}, which is equal to the storage pressure in charge mode and zero else (see eq. B.14), this can be formulated as follows.

$$p_{sys}^{t} \geq \hat{p}_{sys}^{norm} \qquad \forall t \in \mathcal{T} \tag{B.20}$$

$$p_{sys}^{t} \geq \frac{p_{bo}^{t} + 2}{r_{bo}} \qquad \forall t \in \mathcal{T} \tag{B.21}$$

The definition of the power consumption of the compressors (eq. B.15) includes the product of the the air covered by the compressors and difference of the system pressure and the normal system pressure $\dot{V}_{co}^{t} \cdot (p_{sys}^{t} - \hat{p}_{sys}^{norm})$. Using the expression of the air covered by the compressors $\dot{V}_{co}^{t}$ in eq. B.18 this can be stated as:
$\dot{V}_{d}^{t} \cdot (p_{sys}^{t} - \hat{p}_{sys}^{norm}) - \dot{V}_{d}^{t} \cdot b_{dch}^{t} \cdot (p_{sys}^{t} - \hat{p}_{sys}^{norm}) + \dot{V}_{bo} \cdot b_{ch}^{t} \cdot (p_{sys}^{t} - \hat{p}_{sys}^{norm})$.
Since multiplication of the two variables b_{ch}^{t} and p_{sys}^{t} would lead to a discontinuous problem, the expression $b_{ch}^{t} \cdot (p_{sys}^{t} - \hat{p}_{sys}^{norm})$ is substituted with the auxiliary variable $\tilde{p}_{sys,ch}^{t}$, which is defined as follows:

$$\tilde{p}_{sys,ch}^{t} - (p_{sys}^{t} - \hat{p}_{sys}^{norm}) \leq \bar{p}_{sto} \cdot (1 - b_{ch}^{t}) \qquad \forall t \in \mathcal{T} \tag{B.22}$$

$$\tilde{p}_{sys,ch}^{t} - (p_{sys}^{t} - \hat{p}_{sys}^{norm}) \geq -\bar{p}_{sto} \cdot (1 - b_{ch}^{t}) \qquad \forall t \in \mathcal{T} \tag{B.23}$$

$$\tilde{p}_{sys,ch}^{t} \leq \bar{p}_{sto} \cdot b_{ch}^{t} \qquad \forall t \in \mathcal{T} \tag{B.24}$$

The same applies to the expression $b_{dch}^{t} \cdot (p_{sys}^{t} - \hat{p}_{sys}^{norm})$, which is substituted with the auxiliary variable $\tilde{p}_{sys,dch}^{t}$.

$$\tilde{p}_{sys,dch}^{t} - (p_{sys}^{t} - \hat{p}_{sys}^{norm}) \leq \bar{p}_{sto} \cdot (1 - b_{dch}^{t}) \qquad \forall t \in \mathcal{T} \tag{B.25}$$

$$\tilde{p}_{sys,dch}^{t} - (p_{sys}^{t} - \hat{p}_{sys}^{norm}) \geq -\bar{p}_{sto} \cdot (1 - b_{dch}^{t}) \qquad \forall t \in \mathcal{T} \tag{B.26}$$

$$\tilde{p}_{sys,dch}^{t} \leq \bar{p}_{sto} \cdot b_{dch}^{t} \qquad \forall t \in \mathcal{T} \tag{B.27}$$

Storage

The pressure in the high pressure storage tank at the beginning of the next timestep p_{sto}^{t+1} depends on the storage pressure p_{sto}^{t} at timestep t and the operation mode of the system. In *charge* mode, the pressure difference $\Delta p_{sto,ch}^{t}$ is added. In *discharge* mode the pressure is

reduced by $\Delta p^t_{sto,dch}$. The storage pressure is limited by the lower bound $\underline{p}_{sto}$ and the upper bound $\bar{p}_{sto}$.

$$p^{t+1}_{sto} = p^t_{sto} + \Delta p^t_{sto,ch} - \Delta p^t_{sto,dch} \qquad \forall t \in \mathcal{T} \tag{B.28}$$

$$\underline{p}_{sto} \leq p^t_{sto} \leq \bar{p}_{sto} \qquad \forall t \in \mathcal{T} \tag{B.29}$$

The pressure increase during charging is modeled as a linear function dependent on the previous storage pressure p^t_{sto}.

$$\Delta \tilde{p}^t_{sto,ch} = \Delta t \cdot \left(\delta_{ch,1} \cdot p^t_{sto} + \delta_{ch,2}\right) \qquad \forall t \in \mathcal{T} \tag{B.30}$$

The pressure difference $\Delta p^t_{sto,ch}$ corresponds to the pressure increase $\Delta \tilde{p}^t_{sto,ch}$ only during charging (b^t_{ch}=1), and has to be zero else. This can be stated using the following equations:

$$\Delta p^t_{sto,ch} \leq b^t_{ch} \cdot \bar{p}_{sto} \qquad \forall t \in \mathcal{T} \tag{B.31}$$

$$\Delta p^t_{sto,ch} - \Delta \tilde{p}^t_{sto,ch} \leq \bar{p}_{sto} \cdot (1 - b^t_{ch}) \qquad \forall t \in \mathcal{T} \tag{B.32}$$

$$\Delta p^t_{sto,ch} - \Delta \tilde{p}^t_{sto,ch} \geq -\bar{p}_{sto} \cdot (1 - b^t_{ch}) \qquad \forall t \in \mathcal{T} \tag{B.33}$$

The pressure decrease during discharging is modeled as a linear function dependent on the air demand of the system $\dot{V}^t_d$ and the previous storage pressure p^t_{sto}. The additional pressure decrease at the beginning of a discharge period ($b^t_{co,sd}$=1) is modeled with the parameter $\delta_{dch,4}$.

$$\Delta \tilde{p}^t_{sto,dch} = \Delta t \cdot \left(\delta_{dch,1} \cdot \dot{V}^t_d + \delta_{dch,2} \cdot p^t_{sto} + \delta_{dch,3}\right) + \delta_{dch,4} \cdot b^t_{co,sd} \qquad \forall t \in \mathcal{T} \tag{B.34}$$

As for charging, the pressure difference $\Delta p^t_{sto,dch}$ corresponds to the pressure increase $\Delta \tilde{p}^t_{sto,dch}$ only during discharging (b^t_{dch}=1), and has to be zero else. This can be stated using the following equations:

$$\Delta p^t_{sto,dch} \leq b^t_{dch} \cdot \bar{p}_{sto} \qquad \forall t \in \mathcal{T} \tag{B.35}$$

$$\Delta p^t_{sto,dch} - \Delta \tilde{p}^t_{sto,dch} \leq \bar{p}_{sto} \cdot (1 - b^t_{dch}) \qquad \forall t \in \mathcal{T} \tag{B.36}$$

$$\Delta p^t_{sto,dch} - \Delta \tilde{p}^t_{sto,dch} \geq -\bar{p}_{sto} \cdot (1 - b^t_{dch}) \qquad \forall t \in \mathcal{T} \tag{B.37}$$

B.3 Nonlinear simulation model for dynamic programming and the genetic algorithm

This section describes the simulation model, which is used for dynamic programming (DP) and the genetic algorithm (GA) optimization methods. For the GA algorithm the model is simulated for every individual that is evaluated, returning costs for the whole optimization horizon. For the DP algorithm the model is used to calculate the cost and follow up state (storage pressure) for every timestep and state independently. The parameters and variables to describe the model are summarized in table B.5 and table B.6. The parameter values are shown in appendix C.2, table 4.4. The simulation model is split into three parts, one part for each operation mode (*normal*, *charge*, *discharge*).

Table B.5: Parameters of the nonlinear model

Name	Unit	Description
$\hat{p}_{sys}^{norm}$	$\mathrm{bar_g}$	Setpoint pressure in normal mode (normal system pressure)
$\overline{p}_{sto}$	$\mathrm{bar_g}$	Maximum storage pressure
$\underline{p}_{sto}$	$\mathrm{bar_g}$	Minimum storage pressure
p_n	$\mathrm{bar_a}$	Normal pressure
$\overline{\dot{V}}_{co}$	$\frac{\mathrm{m_n^3}}{\mathrm{min}}$	Maximum free air delivery of the compressors
V_{rec}	$\mathrm{m^3}$	Volume of air receiver tank
$E_{co,su}$	kWh	Start-up losses of the compressors
$E_{co,sd}$	kWh	Shut-down losses of the compressors
$E_{bo,su}$	kWh	Start-up losses of the booster
$E_{bo,sd}$	kWh	Shut-down losses of the booster
ς_i		Parameters used to model the electrical power consumption of the compressors
β_i		Parameters used to model the electrical power and air consumption of the booster
δ_i		Parameters used to model the storage pressure state equation
r_{bo}	1	Maximum compression ratio of the booster
C_{pen}	€	Penalty charge t
$\dot{V}_d^t$	$\frac{\mathrm{m_n^3}}{\mathrm{min}}$	Air demand at timestep t
C_{el}^t	$\frac{€}{\mathrm{kWh}}$	Electricity price at timestep t
ΔT	h	Duration of the optimization horizon
Δt	s	Timebase of the optimization (duration of one time period)
N	1	Number of timesteps $N = \frac{\Delta T}{\Delta t/3600}$

Table B.6: Variables of the nonlinear model

Name	$\in$	Unit	Description
p_{sys}^t	$\mathbb{R}_0^+$	bar_g	System pressure at timestep t
$\tilde{p}_{sys}^t$	$\mathbb{R}_0^+$	bar_g	Theoretical system pressure (auxiliary variable)
p_{sto}^t	$\mathbb{R}_0^+$	bar_g	Storage pressure at timestep t
$\Delta p_{sto,ch}^t$	$\mathbb{R}_0^+$	bar_g	Pressure difference at timestep t when charging
$\Delta \tilde{p}_{sto,ch}^t$	$\mathbb{R}_0^+$	bar_g	Auxiliary variable for calculating $\Delta p_{sto,ch}^t$
$\Delta p_{sto,dch}^t$	$\mathbb{R}_0^+$	bar_g	Pressure difference at timestep t when discharging
$\Delta \tilde{p}_{sto,dch}^t$	$\mathbb{R}_0^+$	bar_g	Auxiliary variable for calculating $\Delta p_{sto,dch}^t$
$\Delta p_{ch,last}^t$	$\mathbb{R}_0^+$	bar	Pressure growth of last charge process
$\Delta p_{dch,last}^t$	$\mathbb{R}_0^+$	bar	Pressure reduction of last discharge process
$\Delta p_{th,de}^t$	$\mathbb{R}_0^+$	bar	Pressure decrease caused by temperature decrease after charging
$\Delta p_{th,in}^t$	$\mathbb{R}_0^+$	bar	Pressure increase caused by temperature increase after discharging
$\Delta p_{dch,first}^t$	$\mathbb{R}_0^+$	bar	Additional pressure decrease when starting discharge process
$t_{ch,last}^t$	$\mathbb{R}_0^+$	1	Timestep of last charge process
$t_{dch,last}^t$	$\mathbb{R}_0^+$	1	Timestep of last discharge process
τ_{ch}	$\mathbb{R}_0^+$	1	Relative charging time during one timestep
τ_{dch}	$\mathbb{R}_0^+$	1	Relative discharging time during one timestep
$\dot{V}_{co}^t$	$\mathbb{R}_0^+$	$\frac{\text{m}_\text{n}^3}{\text{min}}$	Compressed air produced by the compressors at timestep t
$\dot{V}_{rec}^t$	$\mathbb{R}$	$\frac{\text{m}_\text{n}^3}{\text{min}}$	Compressed air into (positive) or out of (negative) the air receiver tank
$\dot{V}_{bo}^t$	$\mathbb{R}_0^+$	$\frac{\text{m}_\text{n}^3}{\text{min}}$	Compressed air consumption of the booster at timestep t
P_{co}^t	$\mathbb{R}_0^+$	kW	Electrical power consumed by the compressors at timestep t
$P_{co,su}^t$	$\mathbb{R}_0^+$	kW	Electrical power consumed when compressors start up at timestep t
$P_{co,sd}^t$	$\mathbb{R}_0^+$	kW	Electrical power consumed when compressors shut down at timestep t
P_{bo}^t	$\mathbb{R}_0^+$	kW	Electrical power consumed by the booster at timestep t
$P_{bo,su}^t$	$\mathbb{R}_0^+$	kW	Electrical power consumed when booster starts up at timestep t
$P_{bo,sd}^t$	$\mathbb{R}_0^+$	kW	Electrical power consumed when booster shuts down at timestep t
$P_{tot,ch}^t$	$\mathbb{R}_0^+$	kW	Total electrical power consumed by the CAES system in charge mode during timestep t
$P_{tot,dch}^t$	$\mathbb{R}_0^+$	kW	Total electrical power consumed by the CAES system in discharge mode during timestep t
$P_{tot,n}^t$	$\mathbb{R}_0^+$	kW	Total electrical power consumed by the CAES system in normal operation during timestep t
P_{tot}^t	$\mathbb{R}_0^+$	kW	Total electrical power consumed by the CAES system at timestep t
Θ^t	$[-1, 0, 1]$	1	Operation mode of the CAES system at timestep t (-1=*discharge*, 0=*normal*, 1=*charge*)
$b_{co,run}^t$	$[0, 1]$	1	Binary variable related to the compressors running status at timestep t
$b_{bo,run}^t$	$[0, 1]$	1	Binary variable related to the booster running status at timestep t
s_{sto}^t	$[-1, 0, 1]$	1	State of the storage at timestep t (-1=*empty*,1=*full*)
c_{en}^t	$\mathbb{R}_0^+$	€	Energy costs at timestep t
c_{pen}^t	$\mathbb{R}_0^+$	€	Penalty costs at timestep t
c_{tot}^t	$\mathbb{R}_0^+$	€	Total costs at timestep t
c_{tot}	$\mathbb{R}_0^+$	€	Total costs to be minimized

B.3.1 Normal mode

In *normal* mode the compressors have to cover the air demand. If the system pressure is greater than the normal system pressure (because the storage was charge previously), a part or all of the air demand is covered by the air from the air receiver tank. At first the theoretical system pressure $\tilde{p}_{sys}^{t}$ if the complete air demand would be covered by the air receiver tank is calculated using the ideal gas equation of state[1] (eq. 3.1).

$$\tilde{p}_{sys}^{t} = p_{sys}^{t-1} - \dot{V}_{d}^{t} \cdot \frac{\Delta t}{60\ \frac{\mathrm{s}}{\mathrm{min}}} \cdot \frac{p_n}{V_{rec}} \tag{B.38}$$

The concrete system pressure p_{sys}^{t} has to be al least $\hat{p}_{sys}^{norm}$.

$$p_{sys}^{t} = \begin{cases} \tilde{p}_{sys}^{t} & \text{if} \quad \tilde{p}_{sys}^{t} > \hat{p}_{sys}^{norm} \\ \hat{p}_{sys}^{norm} & \text{else.} \end{cases} \tag{B.39}$$

The air, that is covered by the air receiver tank, then can be calculated dependent on the system pressure change, using again the ideal gas equation of state[1] (eq. 3.1).

$$\dot{V}_{rec}^{t} = \frac{60\ \frac{\mathrm{s}}{\mathrm{min}}}{\Delta t} \cdot (p_{sys}^{t} - p_{sys}^{t-1}) \cdot \frac{V_{rec}}{p_n} \tag{B.40}$$

The air, that has to be covered by the compressors, is composed of the air demand and the air from the receiver tank[2] $\dot{V}_{rec}^{t}$.

$$\dot{V}_{co}^{t} = \dot{V}_{d}^{t} + \dot{V}_{rec}^{t} \tag{B.41}$$

If the compressor have to deliver air, they need to run. In this case the power consumption of the compressors is calculated

$$b_{co,run}^{t} = \begin{cases} 1 & \text{if} \quad \dot{V}_{co}^{t} > 0 \\ 0 & \text{else.} \end{cases} \tag{B.42}$$

The power consumption of the compressors is modeled dependent on the air covered by the compressors $\dot{V}_{co}^{t}$. It is zero, when all the air is covered by the receiver tank and.

$$P_{co}^{t} = \begin{cases} \varsigma_1 \cdot \dot{V}_{co}^{t} + \varsigma_2 & \text{if} \quad \dot{V}_{co}^{t} > 0 \\ 0 & \text{else.} \end{cases} \tag{B.43}$$

Additionally, energy losses $E_{co,su}$ during startup are considered, if the compressors are running at the end of timestep t and were were not running at the beginning.

$$P_{co,su}^{t} = \begin{cases} E_{co,su} \cdot \frac{3600\ \frac{\mathrm{s}}{\mathrm{h}}}{\Delta t} & \text{if} \quad (b_{co,run}^{t} = 1) \wedge (b_{co,run}^{t-1} = 0 \quad \vee \quad \dot{V}_{rec}^{t} < 0), \\ 0 & \text{else.} \end{cases} \tag{B.44}$$

[1] It is assumed, that the air temperature is constant. The parameters of this equation have to be converted to SI units. The absolute pressure value has to be used.

[2] $\dot{V}_{rec}^{t}$ is negative for air out of the storage

The booster is not running in normal mode. But shut-down losses have to be considered if the booster was running in the previous timestep.

$$P^t_{bo,sd} = \begin{cases} E_{bo,sd} \cdot \dfrac{3600\ \frac{\mathrm{s}}{\mathrm{h}}}{\Delta t} & \text{if} \quad b^{t-1}_{bo,run} = 1, \\ 0 & \text{else.} \end{cases} \tag{B.45}$$

The total power consumption of the system is comprised of the power consumption of the compressors with their start-up losses and the shut-down losses of the booster.

$$P^t_{tot} = P^t_{co} + P^t_{co,su} + P^t_{bo,sd} \tag{B.46}$$

In normal mode the pressure storage is neither charged nor discharged. Nevertheless, changes of the storage pressure caused by temperature variation have to be taken into account. During charging, the air in the storage is heated up. After switching from charge to normal mode, the air in the storage slowly cools down, which leads to a pressure decrease $\Delta p^t_{th,de}$. This is modeled by an exponential decrease of the storage pressure of the form $\Delta p = \Delta p_0 \cdot e^{-kt}$. The pressure decrease between two timesteps can be stated as follows.

$$\Delta p^t_{th,de} = \begin{cases} \left(\delta_{ch,5} \cdot \Delta p^{t-1}_{ch,last} + \delta_{ch,6} \cdot p^t_{sto} + \delta_{ch,7}\right) \\ \cdot \left(e^{-\delta_{ch,8} \cdot \Delta t \cdot (t-1-t^{t-1}_{ch,last})} - e^{-\delta_{ch,8} \cdot \Delta t \cdot (t-t^{t-1}_{ch,last})}\right) & \text{if} \quad \Delta p^t_{ch,last} > 0, \\ 0 & \text{else.} \end{cases} \tag{B.47}$$

Analog to the up-heating during charging, the air in the storage cools down when the CAES system is discharged. After switching from discharge to normal mode, the air in the storage slowly heats up, which leads to a pressure increase $\Delta p^t_{th,in}$. This is modeled in the same way as the pressure decrease after charging. This effect does not occur if the pressure decrease of the last discharging process $\Delta p^t_{ch,last}$ is small. Therefore, it is only taken into account after pressure decreases greater than 5 bar.

$$\Delta p^t_{th,in} = \begin{cases} \left(\delta_{dch,6} \cdot \Delta p^{t-1}_{dch,last} + \delta_{dch,7} \cdot p^t_{sto} + \delta_{dch,8}\right) \\ \cdot \left(e^{-\delta_{dch,9} \cdot \Delta t \cdot (t-1-t^{t-1}_{dch,last})} - e^{-\delta_{dch,9} \cdot \Delta t \cdot (t-t^{t-1}_{dch,last})}\right) & \text{if} \quad \Delta p^t_{dch,last} > 5, \\ 0 & \text{else.} \end{cases} \tag{B.48}$$

The storage pressure p^{t+1}_{sto} at the beginning of the next timestep t+1, is calculated based on the storage pressure the beginning of timestep t, taking this thermal pressure in- and decrease into account.

$$p^{t+1}_{sto} = p^t_{sto} + \Delta p^t_{th,in} - \Delta p^t_{th,de} \tag{B.49}$$

The total costs of the CAES system at timestep t can be calculated using the electricity price C^t_{el} and the total power consumption P^t_{tot}.

$$c_{tot}^{t} = C_{el}^{t} \cdot P_{tot}^{t} \cdot \frac{\Delta t}{3600\ \frac{\mathrm{s}}{\mathrm{h}}} \tag{B.50}$$

At the end some variables needed for the following timesteps have to be specified. The booster is never running in *normal* mode. The pressure growth of the last charging process $\Delta p_{ch,last}^{t}$ and the corresponding timestep $t_{ch,last}^{t}$ as well as the pressure reduction of the last discharging process $\Delta p_{dch,last}^{t}$ and its last timestep $t_{dch,last}^{t}$ are unchanged. Also the state of the storage does not change in normal mode.

$$b_{bo,run}^{t} = 0 \tag{B.51}$$

$$\Delta p_{ch,last}^{t} = \Delta p_{ch,last}^{t-1} \tag{B.52}$$

$$t_{ch,last}^{t} = t_{ch,last}^{t-1} \tag{B.53}$$

$$\Delta p_{dch,last}^{t} = \Delta p_{dch,last}^{t-1} \tag{B.54}$$

$$t_{dch,last}^{t} = t_{dch,last}^{t-1} \tag{B.55}$$

$$s_{sto}^{t} = s_{sto}^{t-1} \tag{B.56}$$

B.3.2 Charge mode

As described in section 3.3 (eq. 3.3), the system pressure p_{sys}^{t} during charging depends on the storage pressure p_{sto}^{t}. Its minimum value is given by the normal system pressure $\hat{p}_{sys}^{norm}$.

$$p_{sys}^{t} = \begin{cases} (p_{sto}^{t} + 2\,\mathrm{bar})/r_{bo} & \text{if} \quad p_{sto}^{t} > \hat{p}_{sys} \cdot r_{bo} - 1\,\mathrm{bar} \\ \hat{p}_{sys}^{norm} & \text{else.} \end{cases} \tag{B.57}$$

With the system pressure, the pressure in the air receiver storage is increased as well. The air flow needed for this can be calculated using the ideal gas equation of state[3] (eq. 3.1).

$$\dot{V}_{rec}^{t} = \frac{60\ \frac{\mathrm{s}}{\mathrm{min}}}{\Delta t} \cdot (p_{sys}^{t} - p_{sys}^{t-1}) \cdot \frac{V_{rec}}{p_n} \tag{B.58}$$

In *charge* mode, the compressors have to cover the air demand $\dot{V}_{d}^{t}$, the air consumed by the booster $\dot{V}_{bo}^{t}$ and the air needed to raise the pressure in the air receiver tank $\dot{V}_{rec}^{t}$. The air consumed by the booster $\dot{V}_{bo}^{t}$ depends on the storgae pressure and is modeled as a quadratic function.

[3] It is assumed, that the air temperature is constant. The parameters of this equation have to be converted to SI units. The absolute pressure value has to be used.

$$\dot{V}_{bo}^{t} = \beta_7 \cdot {p_{sto}^{t}}^2 + \beta_8 \cdot p_{sto}^{t} + \beta_9 \tag{B.59}$$

$$\dot{V}_{co}^{t} = \dot{V}_{d}^{t} + \dot{V}_{bo}^{t} + \dot{V}_{rec}^{t} \tag{B.60}$$

The power consumption of the compressors is modeled as a polynomial function of degree 3 dependent on the air covered by the compressors $\dot{V}_{co}^{t}$ and the difference of the system pressure p_{sys}^{t} and the normal system pressure $\hat{p}_{sys}^{norm}$.

$$\begin{aligned} P_{co}^{t} = \quad & \varsigma_1 \cdot \dot{V}_{co}^{t} + \varsigma_2 \\ & + (p_{sys}^{t} - \hat{p}_{sys}^{norm}) \cdot \left(\varsigma_3 \cdot (\dot{V}_{co}^{t})^3 + \varsigma_4 \cdot (\dot{V}_{co}^{t})^2 + \varsigma_5 \cdot \dot{V}_{co}^{t} + \varsigma_6 \right) \end{aligned} \tag{B.61}$$

Additionally, energy losses $E_{co,su}$ during startup are considered, if the compressors were not running in the previous timestep ($b_{co,run}^{t-1} = 0$).

$$P_{co,su}^{t} = \begin{cases} E_{co,su} \cdot \dfrac{3600\ \frac{\mathrm{s}}{\mathrm{h}}}{\Delta t} & \text{if} \quad b_{co,run}^{t-1} = 0, \\ 0 & \text{else.} \end{cases} \tag{B.62}$$

The power consumption of the booster P_{bo}^{t} is modeled as a polynomial function of degree 5 dependent on the storage pressure p_{sto}^{t} at its output.

$$\begin{aligned} P_{bo}^{t} = \quad & \beta_1 \cdot (p_{sto}^{t})^5 + \beta_2 \cdot (p_{sto}^{t})^4 + \beta_3 \cdot (p_{sto}^{t})^3 \\ & + \beta_4 \cdot (p_{sto}^{t})^2 + \beta_5 \cdot (p_{sto}^{t}) + \beta_6 \end{aligned} \tag{B.63}$$

Additionally, energy losses $E_{bo,su}$ during startup are considered, if the booster was not running in the previous timestep ($b_{bo,run}^{t-1} = 0$).

$$P_{bo,su}^{t} = \begin{cases} E_{bo,su} \cdot \dfrac{3600\ \frac{\mathrm{s}}{\mathrm{h}}}{\Delta t} & \text{if} \quad b_{bo,run}^{t-1} = 0, \\ 0 & \text{else.} \end{cases} \tag{B.64}$$

The total power consumption of the system is comprised of the power consumption of the compressors and the booster with their respective start-up losses.

$$P_{tot,ch}^{t} = P_{co}^{t} + P_{co,su}^{t} + P_{bo}^{t} + P_{bo,su}^{t} \tag{B.65}$$

The theoretical pressure increase $\Delta\tilde{p}_{sto,ch}^{t}$ of the storage tank during charging is calculated based on the storage pressure p_{sto}^{t} at the beginning of timestep t using a polynomial function of degree 3.

$$\Delta\tilde{p}_{sto,ch}^{t} = \Delta t \cdot \left(\delta_{ch,1} \cdot (p_{sto}^{t})^3 + \delta_{ch,2} \cdot (p_{sto}^{t})^2 + \delta_{ch,3} \cdot p_{sto}^{t} + \delta_{ch,4} \right) \tag{B.66}$$

To avoid that the storage pressure exceeds its maximum $\bar{p}_{sto}$, the concrete pressure increase $\Delta p_{sto,ch}^{t}$ is calculated.

$$\Delta p_{sto,ch}^{t} = \begin{cases} \bar{p}_{sto} - p_{sto}^{t} & \text{if} \quad p_{sto}^{t} + \Delta\tilde{p}_{sto,ch}^{t} > \bar{p}_{sto}, \\ \Delta\tilde{p}_{sto,ch}^{t} & \text{else.} \end{cases} \tag{B.67}$$

To calculate the storage pressure p_{sto}^{t+1} at the beginning of the next timestep t+1, the concrete pressure increase $\Delta p_{sto,ch}^{t}$ is added to the storage pressure the beginning of timestep t.

$$p_{sto}^{t+1} = p_{sto}^{t} + \Delta p_{sto,ch}^{t} \tag{B.68}$$

If the concrete pressure increase $\Delta p_{sto,ch}^{t}$ is lower than the theoretical $\Delta\tilde{p}_{sto,ch}^{t}$, this means that the the CAES system is not in *charge* mode during the whole time Δt in this timestep. As soon as the maximum storage pressure is reached, the system switches to *normal* mode (see 3.3). The relative time where the system is in charge mode can be calculated as follows:

$$\tau_{ch} = \frac{\Delta p_{sto,ch}^{t}}{\Delta\tilde{p}_{sto,ch}^{t}} \tag{B.69}$$

If τ_{ch} is equal to 1, the system is charged the whole time Δt. If τ_{ch} is e.g. 0.7, the system is 70 % of the time Δt in charge mode and 30 % in normal mode. To determine the total power of the CAES system for this case, the power consumption in *normal* mode $P_{tot,n}^{t}$ has to be calculated. In *normal* mode, the booster is not running and the compressors only have the cover the air demand $\dot{V}_{d}^{t}$.

$$P_{tot,n}^{t} = \varsigma_1 \cdot \dot{V}_{d}^{t} + \varsigma_2 \tag{B.70}$$

Changing from *charge* to *normal* mode, the shut-down losses of the booster $P_{bo,sd}^{t}$ have to be considered as well.

$$P_{bo,sd}^{t} = E_{bo,sd} \cdot \frac{3600\ \frac{\mathrm{s}}{\mathrm{h}}}{\Delta t} \tag{B.71}$$

The total power consumption P_{tot}^{t} of the CAES system during timestep t can then be calculated as follows:

$$P_{tot}^{t} = \begin{cases} P_{tot,ch}^{t} & \text{if} \quad \tau_{ch} = 1, \\ \tau_{ch} \cdot P_{tot,ch}^{t} + (1 - \tau_{ch}) \cdot P_{tot,n}^{t} + P_{bo,sd}^{t} & \text{else.} \end{cases} \tag{B.72}$$

The energy costs of the CAES system at timestep t can be calculated using the electricity price C_{el}^{t} and the total power consumption P_{tot}^{t}.

$$c_{en}^{t} = C_{el}^{t} \cdot P_{tot}^{t} \cdot \frac{\Delta t}{3600\ \frac{\mathrm{s}}{\mathrm{h}}} \tag{B.73}$$

In some cases charging the CAES system is not possible. To avoid that the optimization algorithm chooses *charge* mode as cost optimal in these cases, penalty costs are applied. For *charging* penalty costs are used if the air demand $\dot{V}_{d}^{t}$ is greater 1.26 $\frac{\mathrm{m_n^3}}{\mathrm{min}}$ (maximum air demand where the system can be charged), the storage pressure p_{sto}^{t} or the air delivered by the compressors $\dot{V}_{co}^{t}$ exceed their maximum or the state of the storage is already *full* (s_{sto}^{t-1}=1).

$$c_{pen}^{t} = \begin{cases} C_{pen} & \text{if} \quad \dot{V}_{d}^{t} > 1.26\,\frac{\mathrm{m_n^3}}{\mathrm{min}} \quad \vee \quad p_{sto}^{t} \geq \bar{p}_{sto} \quad \vee \quad \dot{V}_{co}^{t} > \bar{\dot{V}}_{co} \quad \vee \quad s_{sto}^{t-1} = 1, \\ 0 & \text{else.} \end{cases} \tag{B.74}$$

The total cost in timestep t are composed of the energy costs c_{en}^{t} and the penalty costs c_{pen}^{t}.

$$c_{tot}^{t} = c_{en}^{t} + c_{pen}^{t} \tag{B.75}$$

At the end some variables needed for the following timestep have to be specified. In *charge* mode the compressors are always running. The booster is only running at the end of timestep t if the system is in *charge* mode during the whole timestep (τ_{ch} = 1). The pressure growth of this charging process $\Delta p_{ch,last}^{t}$ is either initialized with (if the system was not in charge mode in the previous timestep) or raised by the pressure increase of this timestep. The timestep representing the end of the last charging process $t_{ch,last}^{t}$ is set to t. The pressure reduction of the last discharging process $\Delta p_{dch,last}^{t}$ is reseted to zero. The state of the storage is set to *full* (s_{sto}^{t}=1) if the storage pressure equals its maximum $\bar{p}_{sto}$.

$$b_{co,run}^{t} = 1 \tag{B.76}$$

$$b_{bo,run}^{t} = \begin{cases} 1 & \text{if} \quad \tau_{ch} = 1, \\ 0 & \text{else.} \end{cases} \tag{B.77}$$

$$\Delta p_{ch,last}^{t} = \begin{cases} \Delta p_{ch,last}^{t-1} + \Delta p_{sto,ch}^{t} & \text{if} \quad \Theta^{t-1} = 1, \\ \Delta p_{sto,ch}^{t} & \text{else.} \end{cases} \tag{B.78}$$

$$t_{ch,last}^{t} = t \tag{B.79}$$

$$\Delta p_{dch,last}^{t} = 0 \tag{B.80}$$

$$s_{sto}^{t} = \begin{cases} 1 & \text{if} \quad p_{sto}^{t+1} = \bar{p}_{sto}, \\ 0 & \text{else.} \end{cases} \tag{B.81}$$

B.3.3 Discharge mode

In discharge mode the compressors and the booster are shut down and the air demand is covered by the storage tank. If the system pressure is greater than the normal system pressure (because the storage was charged previously), a part or all of the air demand is covered by the air from the air receiver tank. At first the theoretical system pressure $\tilde{p}_{sys}^{t}$ if the complete air demand would be covered by the air of the air receiver tank is calculated using the ideal gas equation of state[4] (eq. 3.1).

[4] It is assumed, that the air temperature is constant. The parameters of this equation have to be converted to SI units. The absolute pressure value has to be used.

$$\tilde{p}_{sys}^{t} = p_{sys}^{t-1} - \dot{V}_{d}^{t} \cdot \frac{\Delta t}{60\ \frac{\mathrm{s}}{\mathrm{min}}} \cdot \frac{p_n}{V_{rec}} \tag{B.82}$$

The concrete system pressure has to be al least $\hat{p}_{sys}^{norm}$.

$$p_{sys}^{t} = \begin{cases} \tilde{p}_{sys}^{t} & \text{if} \quad \tilde{p}_{sys}^{t} > \hat{p}_{sys}^{norm} \\ \hat{p}_{sys}^{norm} & \text{else.} \end{cases} \tag{B.83}$$

The air, that is covered by the air receiver tank, then can be calculated dependent on the system pressure change, using again the ideal gas equation of state[1] (eq. 3.1).

$$\dot{V}_{rec}^{t} = \frac{60\ \frac{\mathrm{s}}{\mathrm{min}}}{\Delta t} \cdot (p_{sys}^{t} - p_{sys}^{t-1}) \cdot \frac{V_{rec}}{p_n} \tag{B.84}$$

In discharge mode, the compressors and the booster are not running and therefore not consuming electrical power. Only shut-down losses of both systems are considered, if they were running in the previous timestep.

$$P_{co,sd}^{t} = \begin{cases} E_{co,sd} \cdot \frac{3600\ \frac{\mathrm{s}}{\mathrm{h}}}{\Delta t} & \text{if} \quad b_{co,run}^{t-1} = 1, \\ 0 & \text{else.} \end{cases} \tag{B.85}$$

$$P_{bo,sd}^{t} = \begin{cases} E_{bo,sd} \cdot \frac{3600\ \frac{\mathrm{s}}{\mathrm{h}}}{\Delta t} & \text{if} \quad b_{bo,run}^{t-1} = 1, \\ 0 & \text{else.} \end{cases} \tag{B.86}$$

$$P_{tot,dch}^{t} = P_{co,sd}^{t} + P_{bo,sd}^{t} \tag{B.87}$$

The theoretical pressure decrease $\Delta\tilde{p}_{sto,dch}^{t}$ of the storage tank during discharging is calculated based on the air demand $\dot{V}_{d}^{t}$, taking into account the air covered by the receiver tank $\dot{V}_{rec}^{t}$, and the storage pressure p_{sto}^{t} at the beginning of timestep t.

$$\Delta\tilde{p}_{sto,dch}^{t} = \Delta t \cdot \left(\frac{\delta_{dch,1} \cdot (\dot{V}_{d}^{t} + \dot{V}_{rec}^{t})}{\delta_{dch,2} + (\dot{V}_{d}^{t} + \dot{V}_{rec}^{t})} + \delta_{dch,3} \cdot p_{sto}^{t} + \delta_{dch,4} \right) \tag{B.88}$$

To avoid that the storage pressure deceeds its minimum $\underline{p}_{sto}$, the concrete pressure decrease $\Delta p_{sto,dch}^{t}$ is calculated.

$$\Delta p_{sto,dch}^{t} = \begin{cases} p_{sto}^{t} - \underline{p}_{sto} & \text{if} \quad p_{sto}^{t} - \Delta\tilde{p}_{sto,dch}^{t} > \underline{p}_{sto}, \\ \Delta\tilde{p}_{sto,dch}^{t} & \text{else.} \end{cases} \tag{B.89}$$

To calculate the storage pressure p_{sto}^{t+1} at the beginning of the next timestep t+1, the concrete pressure decrease $\Delta p_{sto,dch}^{t}$ is subtracted from the storage pressure the beginning of timestep t.

$$p_{sto}^{t+1} = p_{sto}^{t} - \Delta p_{sto,dch}^{t} \tag{B.90}$$

If the concrete pressure increase $\Delta p^t_{sto,dch}$ is higher than the theoretical $\Delta \tilde{p}^t_{sto,dch}$, this means that the the CAES system is not in *discharge* mode during the whole time Δt in this timestep. As soon as the minimum storage pressure is reached, the system switches to *normal* mode (as described in chapter 3.3). The relative time, during which the system is in discharge mode can be calculated as follows:

$$\tau_{dch} = \frac{\Delta p^t_{sto,dch}}{\Delta \tilde{p}^t_{sto,dch}} \tag{B.91}$$

If τ_{dch} is equal to 1, the system is discharged the whole time Δt. If τ_{dch} is e.g. 0.7, the system is 70 % of the time Δt in *discharge* mode and 30 % in *normal* mode. To determine the total power of the CAES system for this case, the power consumption in *normal* mode $P^t_{tot,n}$ has to be calculated. In *normal* mode, compressors are running and have the cover the air demand $\dot{V}^t_d$.

$$P^t_{tot,n} = \varsigma_1 \cdot \dot{V}^t_d + \varsigma_2 \tag{B.92}$$

Changing from *discharge* to *normal* mode, the start-up losses of the compressors $P^t_{co,su}$ have to be considered as well.

$$P^t_{co,su} = E_{co,su} \cdot \frac{3600\,\frac{\mathrm{s}}{\mathrm{h}}}{\Delta t} \tag{B.93}$$

The total power consumption P^t_{tot} of the CAES system during timestep t can then be calculated. While the power consumption in *normal* mode $P^t_{tot,n}$ is only taken into account partly (with the relative time 1-τ_{dch} the system is in normal mode in this timestep), the start-up and shut-down losses always are fully considered.

$$P^t_{tot} = \begin{cases} P^t_{tot,dch} & \text{if} \quad \tau_{dch} = 1, \\ \tau_{dch} \cdot P^t_{tot,dch} + (1 - \tau_{dch}) \cdot P^t_{tot,n} + P^t_{co,su} & \text{else.} \end{cases} \tag{B.94}$$

The energy costs of the CAES system at timestep t can be calculated using the electricity price C^t_{el} and the total power consumption P^t_{tot}.

$$c^t_{en} = C^t_{el} \cdot P^t_{tot} \cdot \frac{\Delta t}{3600\,\frac{\mathrm{s}}{\mathrm{h}}} \tag{B.95}$$

In some cases discharging the CAES system is not possible. To avoid that the optimization algorithm chooses *discharge* mode as cost optimal in these cases, penalty costs are applied. For *discharging* penalty costs are used the state of the storage has already been *empty* ($s^{t-1}_{sto} = -1$).

$$c^t_{pen} = \begin{cases} C_{pen} & \text{if} \quad s^{t-1}_{sto} = -1, \\ 0 & \text{else.} \end{cases} \tag{B.96}$$

The total cost in timestep t are composed of the energy costs c^t_{en} and the penalty costs c^t_{pen}.

$$c_{tot}^{t} = c_{en}^{t} + c_{pen}^{t} \tag{B.97}$$

At the beginning of each discharge process, an additional pressure reductions was observed, which is modeled using the constant parameter $\delta_{dch,4}$.

$$\Delta p_{dch,first}^{t} = \begin{cases} \delta_{dch,5} & \text{if} \quad \Theta^{t-1} > -1, \\ 0 & \text{else.} \end{cases} \tag{B.98}$$

Additionally, changes of the storage pressure caused by temperature variation have to be taken into account. During charging, the air in the storage is heated up. After switching from *charge* to *discharge* mode, the air cools down, which leads to a pressure decrease $\Delta p_{th,de}^{t}$. This is modeled by an exponential decrease of the storage pressure of the form $\Delta p = \Delta p_0 \cdot e^{-kt}$ (see eq. B.47).

$$\Delta p_{th,de}^{t} = \begin{cases} \left(\delta_{ch,5} \cdot \Delta p_{ch,last}^{t-1} + \delta_{ch,6} \cdot p_{sto}^{t} + \delta_{ch,7}\right) \\ \cdot \left(e^{-\delta_{ch,8} \cdot \Delta t \cdot (t - 1 - t_{ch,last}^{t-1})} - e^{-\delta_{ch,8} \cdot \Delta t \cdot (t - t_{ch,last}^{t-1})}\right) & \text{if} \quad \Delta p_{ch,last}^{t} > 0, \\ 0 & \text{else.} \end{cases} \tag{B.99}$$

To calculate the pressure at the beginning of the next timestep, these pressure reductions have to be taken into account.

$$p_{sto}^{t+1} = p_{sto}^{t+1} - \Delta p_{dch,first}^{t} - \Delta p_{th,de}^{t} \tag{B.100}$$

At the end some variables needed for the following timesteps have to be specified. In *discharge* mode the compressors are running at the end of timestep t if the system is not in *discharge* mode during the whole timestep ($\tau_{dch} < 1$). The booster is never running. The pressure reduction of this discharging process $\Delta p_{dch,last}^{t}$ is either initialized with (if the system was not in discharge mode in the previous timestep) or declined by the pressure decrease of this timestep $\Delta p_{sto,dch}^{t}$. The timestep of the end of the last discharging process $t_{dch,last}^{t}$ is set to t. The pressure growth of the last charging process $\Delta p_{ch,last}^{t}$ is reseted to zero. The state of the storage is set to *empty* ($s_{sto}^{t} = -1$) if the storage pressure equals its minimum $\underline{p}_{sto}$.

$$b_{co,run}^{t} = \begin{cases} 1 & \text{if} \quad \tau_{dch} < 1, \\ 0 & \text{else.} \end{cases} \tag{B.101}$$

$$b_{bo,run}^{t} = 0 \tag{B.102}$$

$$\Delta p_{ch,last}^{t} = 0 \tag{B.103}$$

$$\Delta p_{dch,last}^{t} = \begin{cases} \Delta p_{dch,last}^{t-1} + \Delta p_{sto,dch}^{t} & \text{if} \quad \Theta^{t-1} = -1, \\ \Delta p_{sto,dch}^{t} & \text{else.} \end{cases} \tag{B.104}$$

$$t^t_{dch,last} = t \tag{B.105}$$

$$s^t_{sto} = \begin{cases} -1 & \text{if} \quad p^{t+1}_{sto} = \underline{p}_{sto}, \\ 0 & \text{else.} \end{cases} \tag{B.106}$$

B.4 Mixed-integer nonlinear programming model

The mixed-integer nonlinear programming (MINLP) model is formulated as a set of equality and inequality functions, that are described in this chapter. The variables used for the definition of the optimization problem are summarized in table B.7. The parameters are the same as for the nonlinear simulation model described in section B.3, table B.5, with the values shown in section C.3, table C.4. The optimization horizon is described by the set of timesteps $\mathcal{T} = \{t_1, ..., t_N\}$,where Δt is the duration of each timestep, and N is the number of timesteps $t \in \mathcal{T}$.

The CAES system is represented in the same way as for the simulation model, except the pressure decrease and increase after charging and discharging as well as the air receiver tank are not considered in the MINLP model to reduce the solving time.

Table B.7: Variables of the MINLP model

Name	$\in$	Unit	Description
p_{sys}^t	$\mathbb{R}_0^+$	bar_g	System pressure at timestep t
p_{sto}^t	$\mathbb{R}_0^+$	bar_g	Storage pressure at timestep t
$\Delta p_{sto,ch}^t$	$\mathbb{R}_0^+$	bar_g	Pressure difference at timestep t when charging
$\Delta p_{sto,dch}^t$	$\mathbb{R}_0^+$	bar_g	Pressure difference at timestep t when discharging
$\dot{V}_{co}^t$	$\mathbb{R}_0^+$	$\frac{\text{m}_\text{n}^3}{\text{min}}$	Compressed air produced by the compressors at timestep t
P_{co}^t	$\mathbb{R}_0^+$	kW	Electrical power consumed by the compressors at timestep t
P_{bo}^t	$\mathbb{R}_0^+$	kW	Electrical power consumed by the booster at timestep t
P_{tot}^t	$\mathbb{R}_0^+$	kW	Total electrical power consumed by the CAES system at timestep t
b_{ch}^t	$[0, 1]$	1	Binary variable related to the operation mode *charge* at timestep t
b_{dch}^t	$[0, 1]$	1	Binary variable related to the operation mode *discharge* at timestep t
$b_{co,su}^t$	$[0, 1]$	1	Binary variable related to the compressors startup at timestep t
$b_{co,sd}^t$	$[0, 1]$	1	Binary variable related to the compressors shut-down at timestep t
$b_{bo,su}^t$	$[0, 1]$	1	Binary variable related to the booster startup at timestep t
$b_{bo,sd}^t$	$[0, 1]$	1	Binary variable related to the booster shut-down at timestep t
$b_{p,raise}^t$	$[0, 1]$	1	Binary variable related to the necessity of raising the system pressure during charging at timestep t
c_{tot}	$\mathbb{R}_0^+$	€	Total costs to be minimized

As for the MILP model, in the MINLP formulation of the optimization problem binary variables representing the operation mode of the CAES system can be used. The three modes *normal*, *charge* and *discharge* are represented by two binary variables b_{ch}^t and b_{dch}^t that can be either 0 or 1. At timestep t, the CAES system is in *charge* mode, when $b_{ch}^t = 1$, and in *discharge* mode, when $b_{dch}^t = 1$. When both variables are zero, the system is in *normal* operation mode. The constraint in eq. B.107 avoids that both variables become 1 at the same timestep.

$$b_{ch}^t + b_{dch}^t \leq 1 \tag{B.107}$$

The objective of the MINLP model is to minimize the total costs over the optimization horizon, that depend on the electricity price C_{el}^t and the total power consumption of the system P_{tot}^t

at each timestep. The total power consumption of the system P^t_{tot} is comprised of the power consumptions of the compressors P^t_{co} and of the booster P^t_{bo}.

$$\min c_{tot} = \min \left(\sum_{t \in \mathcal{T}} C^t_{el} \cdot P^t_{tot} \cdot \frac{\Delta t}{3600 \, \frac{\mathrm{s}}{\mathrm{h}}} \right) \tag{B.108}$$

$$P^t_{tot} = P^t_{co} + P^t_{bo} \qquad \forall t \in \mathcal{T} \tag{B.109}$$

Booster

The power consumption of the booster P^t_{bo} is modeled as a polynomial function of degree 5 dependent on the pressure p^t_{bo} at its output. The booster is only running when the system is in *charge* mode ($b^t_{ch} = 1$). Additionally, energy losses $E_{bo,su}$ during startup ($b^t_{bo,su} = 1$, when the system changes from *charge* or *normal* to *discharge* mode) and energy losses $E_{bo,sd}$ during shut-down ($b^t_{bo,sd} = 1$, when the system switches from *discharge* to another mode) are considered.

$$\begin{aligned} P^t_{bo} = \quad & b^t_{ch} \cdot (\beta_1 \cdot (p^t_{sto})^5 + \beta_2 \cdot (p^t_{sto})^4 + \beta_3 \cdot (p^t_{sto})^3 \\ & \quad + \beta_4 \cdot (p^t_{sto})^2 + \beta_5 \cdot (p^t_{sto}) + \beta_6) \\ & + b^t_{bo,su} \cdot E_{bo,su} \cdot \frac{3600 \, \frac{\mathrm{s}}{\mathrm{h}}}{\Delta t} \\ & + b^t_{bo,sd} \cdot E_{bo,sd} \cdot \frac{3600 \, \frac{\mathrm{s}}{\mathrm{h}}}{\Delta t} \qquad \forall t \in \mathcal{T} \end{aligned} \tag{B.110}$$

$$b^t_{bo,su} \geq b^t_{ch} - b^{t-1}_{ch} \qquad \forall t \in \mathcal{T} \tag{B.111}$$

$$b^t_{bo,sd} \geq b^{t-1}_{ch} - b^t_{ch} \qquad \forall t \in \mathcal{T} \tag{B.112}$$

Compressors

The power consumption of the compressors is modeled as a polynomial function of degree 3 depending on the air covered by the compressors $\dot{V}^t_{co}$, the difference of the system pressure and the normal system pressure ($p^t_{sys} - \hat{p}^{norm}_{sys}$) and the product of both. The offset ς_2 is added if the system is in *charge* or *normal* mode ($b^t_{dch} = 0$). Additionally, energy losses $E_{co,su}$ during startup ($b^t_{co,su} = 1$, when the system changes from *discharge* to another mode) and energy losses $E_{co,sd}$ during shut-down ($b^t_{co,sd} = 1$, when the system switches from *normal* or *charge* to *discharge* mode) are considered.

$$\begin{aligned} P^t_{co} = \quad & \varsigma_1 \cdot \dot{V}^t_{co} + \varsigma_2 \cdot (1 - b^t_{dch}) \\ & + (p^t_{sys} - \hat{p}^{norm}_{sys}) \cdot \left(\varsigma_3 \cdot (\dot{V}^t_{co})^3 + \varsigma_4 \cdot (\dot{V}^t_{co})^2 + \varsigma_5 \cdot \dot{V}^t_{co} + \varsigma_6 \right) \\ & + b^t_{co,su} \cdot E_{co,su} \cdot \frac{3600 \, \frac{\mathrm{s}}{\mathrm{h}}}{\Delta t} \\ & + b^t_{co,sd} \cdot E_{co,sd} \cdot \frac{3600 \, \frac{\mathrm{s}}{\mathrm{h}}}{\Delta t} \qquad \forall t \in \mathcal{T} \end{aligned} \tag{B.113}$$

$$b^t_{co,su} \geq b^{t-1}_{dch} - b^t_{dch} \qquad \forall t \in \mathcal{T} \tag{B.114}$$

$$b^t_{co,sd} \geq b^t_{dch} - b^{t-1}_{dch} \qquad \forall t \in \mathcal{T} \tag{B.115}$$

When the system is in *normal* mode ($b^t_{ch} = b^t_{dch} = 0$), the compressors have to cover the complete air demand $\dot{V}^t_d$. In the operation mode *charge* ($b^t_{ch} = 1$), additionally the air demand of the booster $\dot{V}_{bo}$ has to be covered. In *discharge* model, the air demand is covered by the high pressure storage and the air delivered by the compressors is zero. The air that can be delivered by the compressors is limited to $\bar{\dot{V}}_{co}$.

$$\dot{V}^t_{co} = (1 - b^t_{dch}) \cdot \dot{V}^t_d + b^t_{ch} \cdot \dot{V}_{bo} \qquad \forall t \in \mathcal{T} \tag{B.116}$$

$$\dot{V}^t_{co} \leq \bar{\dot{V}}_{co} \qquad \forall t \in \mathcal{T} \tag{B.117}$$

As described in chapter 4.3 (see eq. 4.11 and figure 4.5), the system pressure p^t_{sys} during charging depends on the storage pressure p^t_{sto}. In *normal* or *discharge* operation mode, the system pressure p^t_{sys} corresponds to the normal system pressure $\hat{p}^{norm}_{sys}$. In *charge* mode the system pressure has to be raised, if the storage pressure is higher than $\hat{p}^{norm}_{sys} \cdot r_{bo} - 1$. In the MINLP model therefore the binary variable $b^t_{p,raise}$ is introduced, which is 1 if the system pressure has to be raised (the system is in charge mode and the storage pressure is greater than $\hat{p}^{norm}_{sys} \cdot r_{bo} - 1$) and 0, else.

$$p^t_{sto} \cdot (1 - b^t_{p,raise}) \cdot b^t_{ch} \leq \hat{p}^{norm}_{sys} \cdot r_{bo} - 1 \qquad \forall t \in \mathcal{T} \tag{B.118}$$

$$p^t_{sto} \cdot \cdot b^t_{ch} \geq (\hat{p}^{norm}_{sys} \cdot r_{bo} - 1) \cdot b^t_{p,raise} \qquad \forall t \in \mathcal{T} \tag{B.119}$$

$$b^t_{p,raise} \leq b^t_{ch} \qquad \forall t \in \mathcal{T} \tag{B.120}$$

$$p^t_{sys} \geq \hat{p}^{norm}_{sys} \cdot (1 - b^t_{p,raise}) + b^t_{p,raise} \cdot \frac{p^t_{sto} + 2}{r_{bo}} \qquad \forall t \in \mathcal{T} \tag{B.121}$$

Storage

The pressure in the high pressure storage tank at the beginning of the next timestep p^{t+1}_{sto} depends on the storage pressure p^t_{sto} at timestep t and the operation mode of the system. In *charge* mode, the pressure difference $\Delta p^t_{sto,ch}$ is added. In *discharge* mode the pressure is reduced by $\Delta p^t_{sto,dch}$. The storage pressure is limited by the lower bound $\underline{p}_{sto}$ and the upper bound $\bar{p}_{sto}$.

$$p^{t+1}_{sto} = p^t_{sto} + \Delta p^t_{sto,ch} - \Delta p^t_{sto,dch} \qquad \forall t \in \mathcal{T} \tag{B.122}$$

$$\underline{p}_{sto} \leq p^t_{sto} \leq \bar{p}_{sto} \qquad \forall t \in \mathcal{T} \tag{B.123}$$

The pressure increase during charging ($b^t_{ch} = 1$) is modeled as a polynomial function of degree 3 depending on the previous storage pressure p^t_{sto}.

$$\Delta p^t_{sto,ch} = b^t_{ch} \cdot \Delta t \cdot \left(\delta_{ch,1} \cdot (p^t_{sto})^3 + \delta_{ch,2} \cdot (p^t_{sto})^2 + \delta_{ch,3} \cdot p^t_{sto} + \delta_{ch,4}\right) \qquad \forall t \in \mathcal{T} \tag{B.124}$$

The pressure decrease during discharging ($b^t_{dch} = 1$) is modeled as a function depending on the air demand of the system $\dot{V}^t_d$ and the previous storage pressure p^t_{sto}. The additional pressure decrease at the beginning of a discharge period ($b^t_{co,sd}$=1) is modeled with the parameter $\delta_{dch,5}$.

$$\begin{aligned} \Delta p^t_{sto,dch} = \quad & b^t_{dch} \cdot \Delta t \cdot \left(\frac{\delta_{dch,1} \cdot (\dot{V}^t_d + \dot{V}^t_{rec})}{\delta_{dch,2} + (\dot{V}^t_d + \dot{V}^t_{rec})} + \delta_{dch,3} \cdot p^t_{sto} + \delta_{dch,4}\right) \\ & + \delta_{dch,5} \cdot b^t_{co,sd} \qquad \forall t \in \mathcal{T} \end{aligned} \tag{B.125}$$

Appendix C

Values of the constant model parameters

In this chapter, the values of the constant parameters used to describe the different models of the CAES system are summarized. If not specified otherwise, the parameters are calculated using linear regression to find the optimal values for the given functions so that they match the measured data. In this thesis the "curve_fit" method within the python package SciPy [91] is used for calculating the values. Table C.1 shows the values for parameters that are used for more than one optimization model. The model specific values are summarized in the following sections.

Table C.1: General parameters of the CAES system

Symbol	Value	Unit	Description
$\hat{p}_{sys}^{norm}$	6	$\mathrm{bar_g}$	Normal setpoint pressure
$\bar{p}_{sto}$	38	$\mathrm{bar_g}$	Maximum storage pressure
$\underline{p}_{sto}$	7	$\mathrm{bar_g}$	Minimum storage pressure
$\bar{\dot{V}}_{co}$	2.5	$\frac{\mathrm{m_n^3}}{\mathrm{min}}$	Maximum free air delivery of the compressors
r_{bo}	4	1	Maximum compression ratio of the booster
$E_{co,su}$	0.01	kWh	Start-up losses of the compressors
$E_{co,sd}$	0.02	kWh	Shut-down losses of the compressors
$E_{bo,su}$	0.24	kWh	Start-up losses of the booster
$E_{bo,sd}$	0.06	kWh	Shut-down losses of the booster

C.1 Linear programming model

Table C.2 summarizes the values used to describe the linear programming (LP) model. The following subsections describe how the time-dependent parameters η_{ch}^{t}, η_{dch}^{t} and $\overline{P}_{ch}^{t}$ are calculated.

Table C.2: Parameter values of the LP model

Name	Value	Unit	Description
$\overline{E}_{sto}$	20.12	kWh	Maximum electrical energy capacity of storage
ς_1	7.684	$\frac{\text{kW}}{\text{m}_\text{n}^3/\text{min}}$	Slope of the linear function used to model the electrical power consumption of the compressors
$\overline{P}_{ch}^{t}$		kW	Upper limit of the electrical charge power at timestep t depending on $\dot{V}_d^t$ (see section C.1.1)
η_{ch}^{t} η_{dch}^{t}		%	Storage electrical charge/discharge efficiency at timestep t (see section C.1.2)

C.1.1 Charge power

As explained in chapter 3.4.3, the electrical charge energy of the CAES system is depending on the air demand during charging (see figure 3.10). The charge energy E_{ch} can be calculated by integrating the difference of P_{tot} and P_{ref} over the charging time (t_0^{ch} to t_1^{ch}) (see eq. 3.5). Thus, the mean charge power $\overline{P}_{ch}$ for each measured charge energy of figure 3.9 can be calculated as follows.

$$\overline{P}_{ch} = \frac{E_{ch}}{t_1^{ch} - t_0^{ch}} \tag{C.1}$$

To calculate the mean charge power $\overline{P}_{ch}^{t}$ for a specific air demand $\dot{V}_d^t$ at timestep t, a linear interpolation between the measured points is used. For each air demand $\dot{V}_d^t$ the corresponding $\overline{P}_{ch}^{t}$ is calculated and can be used as an upper limit for the LP optimization model. Because the CAES system can not be charged for air demands greater than 1.26 $\frac{\text{m}_\text{n}^3}{\text{min}}$, in these cases $\overline{P}_{ch}^{t}$ is set to zero. Figure C.2 shows the mean charge power $\overline{P}_{ch}^{t}$ used in the LP model as a function of the air demand .

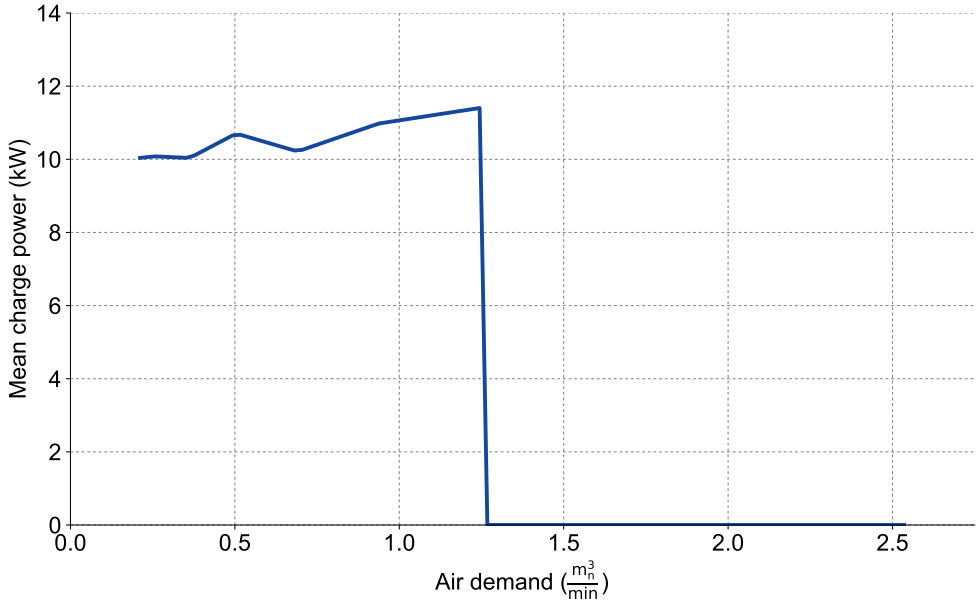

Figure C.1: Mean charge power as a function of the air demand

C.1.2 Charge and discharge efficiencies

As shown in chapter 3.4.3 (figure 3.10), the electrical round-trip efficiency of the CAES system is depending on the air demand during charging and discharging. Therefore, also the charge efficiency and the discharge efficiency for each timestep are depending on the corresponding air demand. To calculate the charge and discharge efficiencies, first the best round-trip efficiency η_{best} and its corresponding charge energy $E_{ch,best}$ and discharge energy $E_{dch,best}$ are identified from the measured values of figure 3.9.

$$\eta_{best} = \frac{E_{dch,best}}{E_{ch,best}} \tag{C.2}$$

Then the charge energy E^t_{ch} and the discharge energy E^t_{dch} for the respective air demand $\dot{V}^t_d$ is calculated by linearly interpolating the measured values shown in figure 3.9.

The discharge efficiency η^t_{dch} is defined to be $\eta_{dch,best} = 1$, when the discharge energy E^t_{dch} equals the best discharge energy $E_{dch,best}$. For lower values of E^t_{dch}, the efficiency decreases.

$$\eta^t_{dch} = \frac{E^t_{dch}}{E_{dch,best}} \tag{C.3}$$

The round-trip efficiency is defined as product of the charge and the discharge efficiency.

$$\eta = \eta^t_{ch} \cdot \eta^t_{dch} \tag{C.4}$$

With $\eta_{dch,best} = 1$, this means that the best charge efficiency $\eta_{ch,best}$ (when $E^t_{ch} = E_{ch,best}$) is defined as the best round-trip efficiency η_{best}

$$\eta_{best} = \eta_{ch,best} \cdot \eta_{dch,best} = \eta_{ch,best} \cdot 1 = \eta_{ch,best} \tag{C.5}$$

The charge efficiency η_{ch}^{t} of a specific air demand $\dot{V}_{d}^{t}$ and its corresponding charge energy E_{ch}^{t} can therefore be calculated as follows.

$$\eta_{ch}^{t} = \frac{E_{ch,best}}{E_{ch}^{t}} \cdot \eta_{best} \tag{C.6}$$

Because the CAES system can not be charged for air demands greater than 1.26 $\frac{m_n^3}{min}$, in these cases the charge efficiency is set to zero. Figure C.2 shows the charge and discharge efficiencies used in the LP model as a function of the air demand. They have the same behavior as the charge and discharge energy shown in figure 3.9.

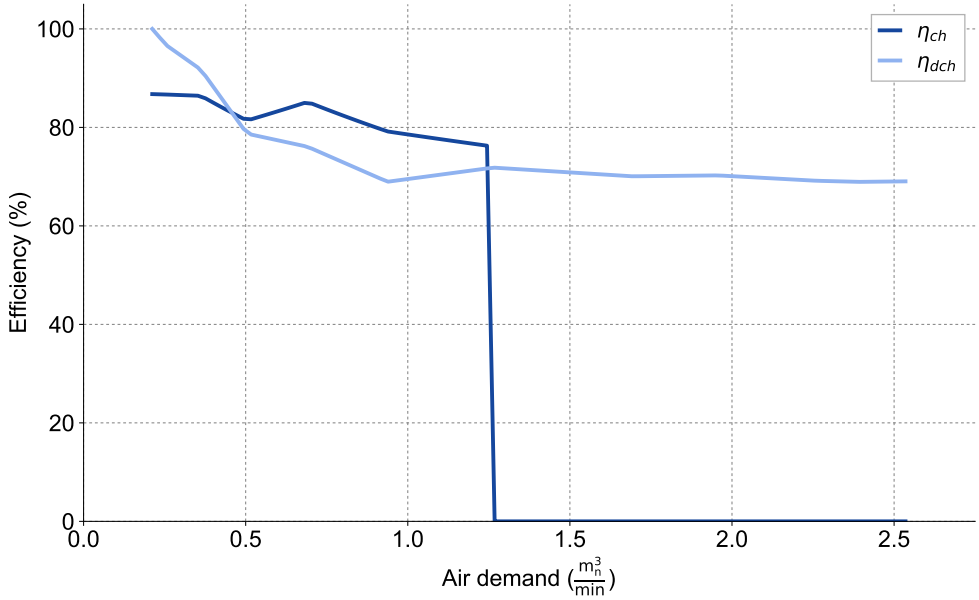

Figure C.2: Charge and discharge effciencies as a function of the air demand

C.2 Mixed-integer linear programming model

Table C.3 shows the values of the parameters for the mixed-integer linear programming (MILP) model.

Table C.3: Parameter values of the MILP model

Name	Value	Unit	Description
ς_1	7.225 01	$\frac{\mathrm{kW}}{\mathrm{m_n^3/min}}$	Parameters used to model the electrical power consumption of the compressors
ς_2	$-8.845 \cdot 10^{-3}$	$\frac{\mathrm{kW}}{\mathrm{bar_g}}$	
ς_3	0.662 25	1	
ς_4	0.835 88	kW	
β_1	0.073 54	$\frac{\mathrm{kW}}{\mathrm{bar_g}}$	Parameters used to model the electrical power consumption of the booster
β_2	1.180 55	kW	
$\delta_{ch,1}$	$2.877 \cdot 10^{-6}$	$\frac{1}{\mathrm{s}}$	Parameters used to model the storage pressure state equation
$\delta_{ch,2}$	$3.737 \cdot 10^{-3}$	$\frac{\mathrm{bar}}{\mathrm{s}}$	
$\delta_{dch,1}$	$4.670 \cdot 10^{-3}$	$\frac{\mathrm{bar}}{\mathrm{m_n^3/60}}$	
$\delta_{dch,2}$	$9.423 \cdot 10^{-6}$	$\frac{1}{\mathrm{s}}$	
$\delta_{dch,3}$	$1.524 \cdot 10^{-4}$	$\frac{\mathrm{bar}}{\mathrm{s}}$	
$\delta_{dch,4}$	0.739 84	kW	

C.3 Nonlinear model

The parameters used for the nonlinear models are summarized in table C.4.

Table C.4: Parameter values of the nonlinear models

Name	Value	Unit	Description
ς_1	7.225 01	$\frac{\mathrm{kW}}{\mathrm{m_n^3/min}}$	Parameters used to model the electrical power consumption of the compressors
ς_2	0.835 88	kW	
ς_3	–0.177 06	$\frac{1}{(\mathrm{m_n^3/min})^2}$	
ς_4	0.803 36	$\frac{1}{\mathrm{m_n^3/min}}$	
ς_5	–0.359 59	1	
ς_6	0.282 38	$\frac{\mathrm{kW}}{\mathrm{bar_g}}$	
β_1	$-1.916 \cdot 10^{-7}$	$\frac{\mathrm{kW}}{(\mathrm{bar_g})^5}$	Parameters used to model the electrical power consumption of the booster
β_2	$1.504 \cdot 10^{-6}$	$\frac{\mathrm{kW}}{(\mathrm{bar_g})^4}$	
β_3	$2.595 \cdot 10^{-5}$	$\frac{\mathrm{kW}}{(\mathrm{bar_g})^3}$	
β_4	$5.005 \cdot 10^{-3}$	$\frac{\mathrm{kW}}{(\mathrm{bar_g})^2}$	
β_5	0.240 19	$\frac{\mathrm{kW}}{\mathrm{bar_g}}$	
β_6	0.138 50	kW	
β_7	0.240 19	$\frac{\mathrm{m_n^3}}{\mathrm{bar^2}}$	Parameters used to model the air consumption of the booster
β_8	0.240 19	$\frac{\mathrm{m_n^3}}{\mathrm{bar}}$	
β_9	0.138 50	$\frac{\mathrm{m_n^3}}{\mathrm{min}}$	
$\delta_{ch,1}$	$-6.292 \cdot 10^{-8}$	$\frac{1}{(\mathrm{bar_g})^2 \cdot \mathrm{s}}$	Parameters used to model pressure increase during charging
$\delta_{ch,2}$	$1.082 \cdot 10^{-5}$	$\frac{1}{(\mathrm{bar_g})^1 \cdot \mathrm{s}}$	
$\delta_{ch,3}$	$3.620 \cdot 10^{-4}$	$\frac{1}{\mathrm{s}}$	
$\delta_{ch,4}$	$6.623 \cdot 10^{-3}$	$\frac{\mathrm{bar}}{\mathrm{s}}$	
$\delta_{ch,5}$	$2.688 \cdot 10^{-3}$	1	Parameters used to model the pressure reduction due to temperature decrease after charging
$\delta_{ch,6}$	$5.153 \cdot 10^{-3}$	1	
$\delta_{ch,7}$	0.150 70	bar	
$\delta_{ch,8}$	$3.741 \cdot 10^{-3}$	1	
$\delta_{dch,1}$	0.102 63	$\frac{\mathrm{bar}}{\mathrm{s}}$	Parameters used to model pressure decrease during discharging
$\delta_{dch,2}$	20.1408	$\frac{\mathrm{m_n^3}}{\mathrm{min}}$	
$\delta_{dch,3}$	$9.103 \cdot 10^{-6}$	$\frac{1}{\mathrm{s}}$	
$\delta_{dch,4}$	$2.725 \cdot 10^{-4}$	$\frac{\mathrm{bar}}{\mathrm{s}}$	
$\delta_{dch,5}$	0.745 82	bar	
$\delta_{dch,6}$	$3.216 \cdot 10^{-3}$	1	Parameters used to model the pressure raise due to temperature increase after discharging
$\delta_{dch,7}$	$7.091 \cdot 10^{-3}$	1	
$\delta_{dch,8}$	0.066 36	bar	
$\delta_{dch,9}$	$4.836 \cdot 10^{-3}$	1	

List of Figures

List of Tables

Acronyms

CAES compressed air energy storage
CHP combined heat and power

DP dynamic programming

FAD free air delivery

GA genetic algorithm

HVAC heating, ventilation, and air conditioning

LP linear programming

MILP mixed-integer linear programming
MINLP mixed-integer nonlinear programming
MPC Model Predictive Control

SAM Sigma Air Manager
SMC superior mode controller

Bibliography

[1] A. Afram and F. Janabi-Sharifi. Theory and applications of hvac control systems – a review of model predictive control (mpc). *Building and Environment*, 72:343–355, 2014. doi:10.1016/j.buildenv.2013.11.016. 3

[2] Aircom. Brass pressure regulator up to 50 bar - r120. URL: https://www.aircom.net/en/high-pressure/r120,157.html. 77

[3] F. Allerding, I. Mauser, and H. Schmeck. Customizable energy management in smart buildings using evolutionary algorithms. In A. I. Esparcia-Alcázar and A. M. Mora, editors, *Applications of Evolutionary Computation*, volume 8602 of *Lecture Notes in Computer Science*, pages 153–164. Springer Berlin Heidelberg, Berlin, Heidelberg, 2014. doi:10.1007/978-3-662-45523-4{\textunderscore}13. 7

[4] R. Baños, F. Manzano-Agugliaro, F. G. Montoya, C. Gil, A. Alcayde, and J. Gómez. Optimization methods applied to renewable and sustainable energy: A review. *Renewable and Sustainable Energy Reviews*, 15(4):1753–1766, 2011. doi:10.1016/j.rser.2010.12.008. 3

[5] R. C. Bansal. Optimization methods for electric power systems: An overview. *International Journal of Emerging Electric Power Systems*, 2(1), 2005. doi:10.2202/1553-779X.1021. 3

[6] R. Bellman. *Dynamic programming*. Princeton University Press, New Jersey, 1957. 8

[7] D. P. Bertsekas. *Dynamic programming and optimal control*. Athena Scientific optimization and computation series. Athena Scientific, Belmont, Mass., 3rd ed. edition, 2005. 8

[8] S. P. Boyd and L. Vandenberghe. *Convex optimization*. Cambridge University Press, Cambridge, UK and New York, 2004. 5

[9] W. Boyes. *Instrumentation reference book*. Butterworth-Heinemann/Elsevier, Amsterdam and Boston, 4th ed. edition, 2010. 11

[10] M. C. Bozchalui, S. A. Hashmi, H. Hassen, C. A. Canizares, and K. Bhattacharya. Optimal operation of residential energy hubs in smart grids. *IEEE Transactions on Smart Grid*, 3(4):1755–1766, 2012. doi:10.1109/TSG.2012.2212032. 6

[11] S. Bracco, F. Delfino, F. Pampararo, M. Robba, and M. Rossi. A mathematical model for the optimal operation of the university of genoa smart polygeneration microgrid: Evaluation of technical, economic and environmental performance indicators. *Energy*, 64:912–922, 2014. doi:10.1016/j.energy.2013.10.039. 6

[12] Bundesministerium für Justiz. Erneuerbare-energien-gesetz vom 21. juli 2014 (bgbl. i s. 1066), das durch artikel 2 des gesetzes vom 22. dezember 2016 (bgbl. i s. 3106) geändert worden ist. 1

[13] Bundesministerium für Justiz. Kraft-wärme-kopplungsgesetz vom 21. dezember 2015 (bgbl. i s. 2498), das durch artikel 1 des gesetzes vom 22. dezember 2016 (bgbl. i s. 3106) geändert worden ist. 1

[14] Bundesministerium für Umwelt, Naturschutz, Bau und Reaktorsicherheit. Klimaschutzplan 2050 - klimaschutzpolitische grundsätze und ziele der bundesregierung, 14. November 2016. URL: www.bmub.bund.de/N53483/. 1

[15] Bundesministerium für Wirtschaft und Energie. Gesamtausgabe der energiedaten - datensammlung des bmwi, 01.11.2016. URL: http://www.bmwi.de/Redaktion/DE/Downloads/Energiedaten/energie-daten-gesamt.xls?__blob=publicationFile&v=13. 1

[16] Bundesministerium für Wirtschaft und Energie. Richtlinien zur förderung von maßnahmen zur nutzung erneuerbarer energien im wärmemarkt, 11. März 2015. 1

[17] Bundesministerium für Wirtschaft und Energie. Förderung von stationären und dezentralen batteriespeichersystemen zur nutzung in verbindung mit photovoltaikanlagen, Bekanntmachung vom 17. Februar 2016, BAnz AT 29.02.2016 B1. 1

[18] S. Burer and A. N. Letchford. Non-convex mixed-integer nonlinear programming: A survey. *Surveys in Operations Research and Management Science*, 17(2):97–106, 2012. doi:10.1016/j.sorms.2012.08.001. 7

[19] E. F. Camacho and C. Bordons. *Model predictive control*. Advanced textbooks in control and signal processing. Springer, London and New York, 2nd ed. edition, 2007. 2, 3

[20] E. Cardona, P. Sannino, A. Piacentino, and F. Cardona. Energy saving in airports by trigeneration. part ii: Short and long term planning for the malpensa 2000 chcp plant. *Applied Thermal Engineering*, 26(14-15):1437–1447, 2006. doi:10.1016/j.applthermaleng.2006.01.020. 5

[21] Christoph Passenberg, Dominik Meyer, Johannes Feldmaier, Hao Shen. Optimal water heater control in smart home environments. In *IEEE Energycon 2016*, Leuven, Belgien, 2016. 8

[22] M. Conforti, G. Cornuejols, and G. Zambelli. *Integer programming*, volume 271 of *Graduate Texts in Mathematics*. Springer International Publishing and Imprint and Springer, Cham, 2014. 6

[23] DEAP. Distributed evolutionary algorithms in python, version 1.0.2. URL: https://github.com/DEAP/deap. 52

[24] Dennis Atabay. prodyn: Generic implementation of the dynamic programming algorithm for optimal system control. URL: https://github.com/yabata/prodyn. 52

[25] J. Dorfner. *Open Source Modelling and Optimisation of Energy Infrastructure at Urban Scale*. Doctoral thesis, Technische Universität München, 2016. 9

[26] M. Ellis, H. Durand, and P. D. Christofides. A tutorial review of economic model predictive control methods. *Journal of Process Control*, 24(8):1156–1178, 2014. doi:10.1016/j.jprocont.2014.03.010. 2

[27] T. Erseghe, A. Zanella, and C. G. Codemo. Optimal and compact control policies for energy storage units with single and multiple batteries. *IEEE Transactions on Smart Grid*, 5(3):1308–1317, 2014. doi:10.1109/TSG.2014.2303824. 8

[28] M. Fiorentini, P. Cooper, Z. Ma, and D. A. Robinson. Hybrid model predictive control of a residential hvac system with pvt energy generation and pcm thermal storage. *Energy Procedia*, 83:21–30, 2015. doi:10.1016/j.egypro.2015.12.192. 6

[29] M. Fiorentini, J. Wall, Z. Ma, J. H. Braslavsky, and P. Cooper. Hybrid model predictive control of a residential hvac system with on-site thermal energy generation and storage. *Applied Energy*, 187:465–479, 2017. doi:10.1016/j.apenergy.2016.11.041. 6

[30] V. Francois-Lavet, R. Fonteneau, and D. Ernst. Using approximate dynamic programming for estimating the revenues of a hydrogen-based high-capacity storage device. In *2014 IEEE Symposium on Adaptive Dynamic Programming and Reinforcement Learning (ADPRL)*, pages 1–8. doi:10.1109/ADPRL.2014.7010624. 8

[31] C. Gamarra and J. M. Guerrero. Computational optimization techniques applied to microgrids planning: A review. *Renewable and Sustainable Energy Reviews*, 48:413–424, 2015. doi:10.1016/j.rser.2015.04.025. 3

[32] Gemü. Angle seat globe control valve, metal, 554. URL: https://www.gemu-group.com/gemu-cdn/dokumente/2/db_554regel_gb.pdf. 77

[33] Gemü. Ball valve, ball valve, stainless steel multi-port, 711, 728, 751. URL: https://www.gemu-group.com/gemu-cdn/dokumente/2/db_711_728_751_3-piece_3-2-way_gb.pdf. 77

[34] P. S. Georgilakis and N. D. Hatziargyriou. A review of power distribution planning in the modern power systems era: Models, methods and future research. *Electric Power Systems Research*, 121:89–100, 2015. doi:10.1016/j.epsr.2014.12.010. 3

[35] Gregor P. Henze, Doreen E. Kalz, Simeng Liu, and Clemens Felsmann. Experimental analysis of model-based predictive optimal control for active and passive building thermal storage inventory. *HVAC&R Research*, 11(2):189–213, 2005. doi:10.1080/10789669.2005.10391134. 8

[36] L. Grüne and J. Pannek. *Nonlinear model predictive control: Theory and agorithms*. Communications and control engineering. Springer, London [u.a.], 2011. 2

[37] W. Gu, Z. Wu, R. Bo, W. Liu, G. Zhou, W. Chen, and Z. Wu. Modeling, planning and optimal energy management of combined cooling, heating and power microgrid: A review. *International Journal of Electrical Power & Energy Systems*, 54:26–37, 2014. doi:10.1016/j.ijepes.2013.06.028. 3

[38] G. P. Henze, C. Felsmann, and G. Knabe. Evaluation of optimal control for active and passive building thermal storage. *International Journal of Thermal Sciences*, 43(2):173–183, 2004. doi:10.1016/j.ijthermalsci.2003.06.001. 8

[39] HYDAC. Electronic pressure transmitter hda 4400. URL: http://www.hydac.com/fileadmin/pdb/pdf/PRO000000000000000000000018305050011.pdf. 77

[40] IBM ILOG CPLEX Interactive Optimizer. version 12.6.3.0. URL: http://www-01.ibm.com/software/commerce/optimization/cplex-optimizer/index.html. 51

[41] M. Iqbal, M. Azam, M. Naeem, A. S. Khwaja, and A. Anpalagan. Optimization classification, algorithms and tools for renewable energy: A review. *Renewable and Sustainable Energy Reviews*, 39:640–654, 2014. doi:10.1016/j.rser.2014.07.120. 3

[42] Johannes Jungwirth. *Lastmanagement in Gebäuden: Entwicklung einer modellprädiktiven Regelung mit einem adaptiven Gebäudemodell zur Flexibilisierung der Wärme- und Kälteversorgung von Gebäuden*. Dissertation, Technische Universität München, 2014. 7, 52

[43] Josef Lipp. *Flexible Stromerzeugung mit Mikro-KWK-Anlagen: Experimentelle Untersuchung der Möglichkeiten einer flexiblen Stromerzeugung von Mikro-KWK-Anlagen mit Hilfe einer Wärmebedarfsprognose und einem intelligenten Speichermanagementsystem*. Dissertation, Technische Universität München, 2015. 7

[44] KAESER KOMPRESSOREN SE. Air receivers. URL: http://www.kaeser.com/Images/P-775-ED-tcm8-7411.pdf. 77

[45] KAESER KOMPRESSOREN SE. Betriebsanleitung schraubenkompressor sm sfc sigma control 2 (9__5873 24 d). 17

[46] KAESER KOMPRESSOREN SE. Betriebsanleitung schraubenkompressor sm sigma control 2 (9__5871 24 d). 17

[47] KAESER KOMPRESSOREN SE. Betriebsanleitung schraubenkompressor sx sigma control 2 (9_6925 21 d). 17

[48] KAESER KOMPRESSOREN SE. Boosters - n series. URL: http://www.kaeser.com/Images/P-480-ED-tcm8-13912.pdf. 13

[49] KAESER KOMPRESSOREN SE. Filters & centrifugal separators. URL: http://www.kaeser.com/Images/P-725-ED-tcm8-6771.pdf. 77

[50] KAESER KOMPRESSOREN SE. Refrigeration dryers secotec. URL: http://www.kaeser.com/Images/P-013-ED-tcm8-6741.pdf. 77

[51] KAESER KOMPRESSOREN SE. Rotary screw compressors - sm series. URL: http://www.kaeser.com/Images/P-651-24-ED-tcm8-52847.pdf. 13

[52] KAESER KOMPRESSOREN SE. Rotary screw compressors - sx series. URL: http://www.kaeser.com/Images/P-651-0-ED-tcm8-6759.pdf. 13

[53] KAESER KOMPRESSOREN SE. Technische daten sm12 sfc sigma 026 (t10085). 18, 19

[54] S. Kochanneck, I. Mauser, B. Bohnet, S. Hubschneider, H. Schmeck, M. Braun, and T. Leibfried. Establishing a hardware-in-the-loop research environment with a hybrid energy storage system. In *2016 IEEE Innovative Smart Grid Technologies - Asia (ISGT-Asia)*, pages 497–503. doi:10.1109/ISGT-Asia.2016.7796435. 7

[55] B. Kouvaritakis and M. Cannon. *Model predictive control: Classical, robust and stochastic*. Advanced textbooks in control and signal processing. Springer, Cham and Heidelberg and New York and Dordrecht and London, 2015. 2

[56] P. O. Kriett and M. Salani. Optimal control of a residential microgrid. *Energy*, 42(1):321–330, 2012. doi:10.1016/j.energy.2012.03.049. 6

[57] P. Kuhn. *Iteratives Modell zur Optimierung von Speicherausbau und -betrieb in einem Stromsystem mit zunehmend fluktuierender Erzeugung*. Doctoral thesis, Technische Universität München, 2012. URL: https://mediatum.ub.tum.de/?id=1271192. 9

[58] K. S. Kwan and D. K. Maly. Optimal battery energy storage system (bess) charge scheduling with dynamic programming. *IEE Proceedings - Science, Measurement and Technology*, 142(6):453–458, 1995. doi:10.1049/ip-smt:19951929. 8

[59] Lei Zhang and Yaoyu Li. Optimal energy management of wind-battery hybrid power system with two-scale dynamic programming. *IEEE Transactions on Sustainable Energy*, 4(3):765–773, 2013. doi:10.1109/TSTE.2013.2246875. 8

[60] M. A. Lozano, M. Carvalho, and L. M. Serra. Operational strategy and marginal costs in simple trigeneration systems. *Energy*, 34(11):2001–2008, 2009. doi:10.1016/j.energy.2009.08.015. 5

[61] J. Ma, J. Qin, T. Salsbury, and P. Xu. Demand reduction in building energy systems based on economic model predictive control. *Chemical Engineering Science*, 67(1):92–100, 2012. doi:10.1016/j.ces.2011.07.052. 5

[62] Y. Ma, F. Borrelli, B. Hencey, A. Packard, and S. Bortoff. Model predictive control of thermal energy storage in building cooling systems. In *2009 Joint 48th IEEE Conference on Decision and Control (CDC) and 28th Chinese Control Conference (CCC)*, pages 392–397. doi:10.1109/CDC.2009.5400677. 7

[63] L. Majic and Krzelj, I. Delimar, M. Optimal scheduling of a chp system with energy storage. In *36th International Convention on Information & Communication Technology, Electronics & Microelectronics (MIPRO), 2013*, pages 1253–1257, Piscataway, NJ, 2013. IEEE. 5

[64] I. Mauser, J. Müller, F. Allerding, and H. Schmeck. Adaptive building energy management with multiple commodities and flexible evolutionary optimization. *Renewable Energy*, 87:911–921, 2016. doi:10.1016/j.renene.2015.09.003. 7, 50

[65] B. Mayer, M. Killian, and M. Kozek. Management of hybrid energy supply systems in buildings using mixed-integer model predictive control. *Energy Conversion and Management*, 98:470–483, 2015. doi:10.1016/j.enconman.2015.02.076. 6

[66] B. Mayer, M. Killian, and M. Kozek. A branch and bound approach for building cooling supply control with hybrid model predictive control. *Energy and Buildings*, 128:553–566, 2016. doi:10.1016/j.enbuild.2016.07.027. 6

[67] D. Q. Mayne. Model predictive control: Recent developments and future promise. *Automatica*, 50(12):2967–2986, 2014. doi:10.1016/j.automatica.2014.10.128. 2

[68] E. D. Mehleri, H. Sarimveis, L. G. Papageorgiou, and N. C. Markatos. Model predictive control of distributed energy resources. In *2012 20th Mediterranean Conference on Control & Automation (MED 2012)*, pages 672–678. doi:10.1109/MED.2012.6265715. 6

[69] L. Meng, E. R. Sanseverino, A. Luna, T. Dragicevic, J. C. Vasquez, and J. M. Guerrero. Microgrid supervisory controllers and energy management systems: A literature review. *Renewable and Sustainable Energy Reviews*, 60:1263–1273, 2016. doi:10.1016/j.rser.2016.03.003. 3

[70] H. Morais, P. Kádár, P. Faria, Z. A. Vale, and H. M. Khodr. Optimal scheduling of a renewable micro-grid in an isolated load area using mixed-integer linear programming. *Renewable Energy*, 35(1):151–156, 2010. doi:10.1016/j.renene.2009.02.031. 6

[71] M. J. Moran. *Fundamentals of engineering thermodynamics*. Wiley, [Hoboken, N.J.?], 7th ed. edition, 2011. 12

[72] M. Morari and J. H. Lee. Model predictive control: Past, present and future. *Computers & Chemical Engineering*, 23(4-5):667–682, 1999. doi:10.1016/S0098-1354(98)00301-9. 2, 3

[73] J. Müller, M. März, I. Mauser, and H. Schmeck. Optimization of operation and control strategies for battery energy storage systems by evolutionary algorithms. In G. Squillero and P. Burelli, editors, *Applications of Evolutionary Computation*, volume 9597 of *Lecture Notes in Computer Science*, pages 507–522. Springer International Publishing, Cham, 2016. doi:10.1007/978-3-319-31204-0{\textunderscore}33. 7, 50

[74] MÜLLER + ZIEGLER GmbH & Co. KG. Messumformer für wirkleistung, wechselstrom und drehstrom. URL: http://www.mueller-ziegler.de/fileadmin/user_upload/Messumformer_Netzgroessen/MZ_Messumformer_Pw-MU.pdf. 77

[75] M. Nguyen, D. Nguyen, and Y. Yoon. A new battery energy storage charging/discharging scheme for wind power producers in real-time markets. *Energies*, 5(12):5439–5452, 2012. doi:10.3390/en5125439. 8

[76] S. Nojavan, K. Zare, and B. Mohammadi-Ivatloo. Optimal stochastic energy management of retailer based on selling price determination under smart grid environment in the presence of demand response program. *Applied Energy*, 187:449–464, 2017. doi:10.1016/j.apenergy.2016.11.024. 7

[77] S. M. Nosratabadi, R.-A. Hooshmand, and E. Gholipour. A comprehensive review on microgrid and virtual power plant concepts employed for distributed energy resources scheduling in power systems. *Renewable and Sustainable Energy Reviews*, 67:341–363, 2017. doi:10.1016/j.rser.2016.09.025. 3

[78] A. Núñez-Reyes, D. Marcos Rodríguez, C. Bordons Alba, and M. Á. Ridao Carlini. Optimal scheduling of grid-connected pv plants with energy storage for integration in the electricity market. *Solar Energy*, 144:502–516, 2017. doi:10.1016/j.solener.2016.12.034. 5

[79] R. Ooka and S. Ikeda. A review on optimization techniques for active thermal energy storage control. *Energy and Buildings*, 106:225–233, 2015. doi:10.1016/j.enbuild.2015.07.031. 3

[80] R. Palma-Behnke, C. Benavides, F. Lanas, B. Severino, L. Reyes, J. Llanos, and D. Saez. A microgrid energy management system based on the rolling horizon strategy. *IEEE Transactions on Smart Grid*, 4(2):996–1006, 2013. doi:10.1109/TSG.2012.2231440. 6

[81] A. Parisio, E. Rikos, and L. Glielmo. A model predictive control approach to microgrid operation optimization. *IEEE Transactions on Control Systems Technology*, 22(5):1813–1827, 2014. doi:10.1109/TCST.2013.2295737. 6

[82] A. Parisio, E. Rikos, G. Tzamalis, and L. Glielmo. Use of model predictive control for experimental microgrid optimization. *Applied Energy*, 115:37–46, 2014. doi:10.1016/j.apenergy.2013.10.027. 6

[83] Pyomo. version 4.2.10487. URL: http://www.pyomo.org/. 51, 79

[84] S. Qin and T. A. Badgwell. A survey of industrial model predictive control technology. *Control Engineering Practice*, 11(7):733–764, 2003. doi:10.1016/S0967-0661(02)00186-7. 2

[85] D. Quiggin, S. Cornell, M. Tierney, and R. Buswell. A simulation and optimisation study: Towards a decentralised microgrid, using real world fluctuation data. *Energy*, 41(1):549–559, 2012. doi:10.1016/j.energy.2012.02.007. 5

[86] S. S. Rao. *Engineering optimization: theory and praxis.* Wiley, New York, N.Y, 4th ed. edition, 2009. 5, 9

[87] J. B. Rawlings and D. Q. Mayne. *Model predictive control: Theory and design*. Nob Hill Pub, Madison, Wis., 2009. 2

[88] Y. Riffonneau, S. Bacha, F. Barruel, and S. Ploix. Optimal power flow management for grid connected pv systems with batteries. *IEEE Transactions on Sustainable Energy*, 2(3):309–320, 2011. doi:10.1109/TSTE.2011.2114901. 8

[89] J. A. Rossiter. *Model-based predictive control: A practical approach*. Control series. CRC Press, Boca Raton, 2003. 2

[90] J. Sachs, A. Gienger, and O. Sawodny. Combined probabilistic and set-based uncertainties for a stochastic model predictive control of island energy systems. In *2016 American Control Conference (ACC)*, pages 6767–6772. doi:10.1109/ACC.2016.7526737. 7

[91] SciPy. version 0.18.1. URL: https://www.scipy.org/. 103

[92] E. Shirazi and S. Jadid. Optimal residential appliance scheduling under dynamic pricing scheme via hemdas. *Energy and Buildings*, 93:40–49, 2015. doi:10.1016/j.enbuild.2015.01.061. 7

[93] S. N. Sivanandam and S. N. Deepa. *Introduction to genetic algorithms*. Springer, Berlin and New York, 2007. 7

[94] sonnen GmbH. Die sonnenbatterie. URL: https://www.sonnenbatterie.de/. 24

[95] P. Stadler, A. Ashouri, and F. Maréchal. Model-based optimization of distributed and renewable energy systems in buildings. *Energy and Buildings*, 120:103–113, 2016. doi:10.1016/j.enbuild.2016.03.051. 6

[96] tecsis. Pt compact, pt compact plus. URL: http://www.tecsis.com/fileadmin/Content/tecsis/2_Files/3_Temperature/B_Electrical_Temperature_Measuring/de1127.pdf. 77

[97] Tesla Motors. Powerwall. URL: https://www.teslamotors.com/de_DE/powerwall. 24

[98] The Optimization Firm. Baron version 16.11.18. URL: http://www.minlp.com/home. 52

[99] A. N. Ünal, S. Ercan, and G. Kayakutlu. Optimisation studies on tri-generation: A review. *International Journal of Energy Research*, 39(10):1311–1334, 2015. doi:10.1002/er.3342. 3

[100] Y. Wang, X. Lin, M. Pedram, S. Park, and N. Chang. Optimal control of a grid-connected hybrid electrical energy storage system for homes. In *Design Automation and Test in Europe*, pages 881–886. doi:10.7873/DATE.2013.186. 8

[101] D. Wolf, A. Kanngießer, M. Budt, and C. Doetsch. Adiabatic compressed air energy storage co-located with wind energy—multifunctional storage commitment optimization for the german market using gomes. *Energy Systems*, 3(2):181–208, 2012. doi:10.1007/s12667-011-0044-7. 6

[102] X. Xia and A. M. Elaiw. Optimal dynamic economic dispatch of generation: A review. *Electric Power Systems Research*, 80(8):975–986, 2010. doi:10.1016/j.epsr.2009.12.012. 3

[103] L. Xie and M. D. Ilic. Model predictive dispatch in electric energy systems with intermittent resources. In *2008 IEEE International Conference on Systems, Man and Cybernetics (SMC)*, pages 42–47. doi:10.1109/ICSMC.2008.4811248. 5

[104] Y. Yoon and Y.-H. Kim. Effective scheduling of residential energy storage systems under dynamic pricing. *Renewable Energy*, 87:936–945, 2016. doi:10.1016/j.renene.2015.09.072. 8

[105] Yudong Ma, F. Borrelli, B. Hencey, B. Coffey, S. Bengea, and P. Haves. Model predictive control for the operation of building cooling systems. *IEEE Transactions on Control Systems Technology*, 20(3):796–803, 2012. doi:10.1109/TCST.2011.2124461. 7

[106] X. Zhang, G. Hug, J. Z. Kolter, and I. Harjunkoski. Model predictive control of industrial loads and energy storage for demand response. In *2016 IEEE Power and Energy Society General Meeting (PESGM)*, pages 1–5. doi:10.1109/PESGM.2016.7741228. 6

[107] Y. Zong, D. Kullmann, A. Thavlov, O. Gehrke, and H. W. Bindner. Application of model predictive control for active load management in a distributed power system with high wind penetration. *IEEE Transactions on Smart Grid*, 3(2):1055–1062, 2012. doi:10.1109/TSG.2011.2177282. 6